Chemistry–A European Journal

Supporting Information

GNPS-Guided Discovery of Madurastatin Siderophores from the Termite-Associated *Actinomadura* sp. RB99

Seoung Rak Lee, Felix Schalk, Jan W. Schwitalla, Huijuan Guo, Jae Sik Yu, Moonyong Song, Won Hee Jung, Z. Wilhelm de Beer, Christine Beemelmanns,* and Ki Hyun Kim*

Contents

1. General Experimental Procedures

Optical rotations were calculated using a Jasco P-1020 polarimeter (Jasco, Easton, MD, USA). Ultraviolet (UV) spectra were acquired on an Agilent 8453 UV-visible spectrophotometer (Agilent Technologies, Santa Clara, CA). Experimental ECD spectra in MeOH were acquired in a quartz cuvette of 1 mm optical path length on a JASCO J-1500 spectropolarimeter (Tokyo, Japan). NMR spectra, including ^{1}H-^{1}H COSY, HSQC, HMBC, and ROESY experiments, were carried out using a Varian UNITY INOVA 800 NMR spectrometer operating at 800 MHz (^{1}H) and 200 MHz (^{13}C), with chemical shifts given in ppm (δ). NMR spectra for **5** were recorded on a Varian UNITY INOVA 600 NMR spectrometer operating at 600 MHz (^{1}H) and 150 MHz (^{13}C), with chemical shifts given in ppm (δ).

Silica gel 60 (Merck, 230-400 mesh) and RP-C18 silica gel (Merck, 230-400 mesh) were used for column chromatography. Merck precoated silica gel F_{254} plates and RP-18 F_{254s} plates were used for thin layer chromatography (TLC). Spots were detected on TLC under UV light or by heating after spraying with anisaldehyde-sulfuric acid. Semi-preparative HPLC used a Shimadzu Prominence HPLC System with SPD-20A/20AV Series Prominence HPLC UV-Vis Detectors (Shimadzu, Tokyo, Japan). Preparative high-performance liquid chromatography (HPLC) utilized a Waters 1525 Binary HPLC pump with Waters 996 Photodiode Array Detector (Waters Corporation, Milford, CT, USA).

Low-resolution high-performance liquid chromatography-mass spectrometry (HPLC-MS) analysis was carried out on an Agilent 1200 Series HPLC system (Agilent Technologies, Santa Clara, CA, USA) equipped with a diode array detector and a 6130 Series ESI mass spectrometer by using an analytical Kinetex (4.6 × 100 mm, 3.5 µm). High-resolution (HR) HPLC-MS and HR-tandem HPLC-MS were carried out on an Agilent 6545 Accurate-Mass quadrupole time-of-flight (QTof)-HPLC-MS, consisting of a 1290 Infinity Series HPLC system, an automated liquid sampler, a diode array detector, a JetStream ESI source, and the 6545 Series QTof by using an Agilent EclipsePlus C18 column (2.1 mm × 50 mm, RRHD 1.8 µm, Agilent Technologies).

UHPLC-HESI-HRMS measurement was performed on a Dionex Ultimate3000 system combined with a Q-Exactive Plus mass spectrometer (Thermo Scientific) with a heated electrospray ion source (HESI). Metabolite separation was carried out by reverse phase liquid chromatography at 40 °C using a Luna Omega C18 column (100 × 2.1 mm, 1.6 µm, 100 Å, Phenomenex) preceded by a SecurityGuard™ ULTRA guard cartridge (2 × 2.1 mm, Phenomenex). Mobile phases were acidified with 0.1% formic acid and consisted of H_2O (A) and acetonitrile (B).

2. Cultivation and extraction of *Actinomadura* sp. RB99

Actinomadura sp. RB99 was cultivated in 25 mL liquid cultures in a shaker at 150 rpm and 28 °C for up to elven days and used as inoculum.

Table S1. Medium compositions

Compound	**Concentration**
ISP2 medium, pH 7.2	
Yeast extract	4 g/L
Malt extract	10 g/L
Glucose	4 g/L
ISP5 medium	
L-Asparagine * $1H_2O$	1.14 g/L
Glycerol	10 g/L
KH_2PO_4	1 g/L
Trace elements $FeSO_4$ * 7 H_2O	(1; 0.5; 0) µg/L for (standard; low Iron; no Iron)
Trace elements $MnCl_2$ * 4 H_2O	1 µg/L
Trace elements $ZnSO_4$ * 7 H_2O	1 µg/L
ISP5 sea salt medium with different iron concentrations, sea salt stock solution was autoclaved separately and added before inoculation	
L-Asparagine * $1H_2O$	1.14 g/L
Glycerol	10 g/L
KH_2PO_4	1 g/L
Sea salt solution (10% w/v)	16 ml/L
Trace elements $FeSO_4$ * 7 H_2O	($1_{standard}$; $0.5_{low\ iron}$; $0_{no\ iron}$) µg/L
Trace elements $MnCl_2$ * 4 H_2O	1 µg/L
Trace elements $ZnSO_4$ * 7 H_2O	1 µg/L

3. Co-Cultivation Studies

Table S2. Determination of inhibition zones during growth inhibition assay.

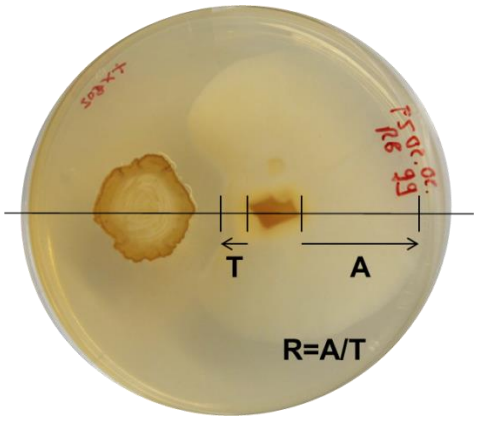

	9 days			12 days			14 days		
Strains	**T**	**A**	**R=A/T**	**T**	**A**	**R=A/T**	**T**	**A**	**R=A/T**
RB99 X187	150.50	330.00	2.19	177.60	536.40	3.02	126.00	483.00	3.83
RB99 X187#2	164.80	348.00	2.11	246.50	525.20	2.13	260.00	512.10	1.97
RB99 X187#3	194.00	280.00	1.44	282.00	480.80	1.70	268.80	511.30	1.90
RB99 X802	177.00	471.00	2.66	192.00	858.10	4.47	153.00	807.10	5.28
RB99 X802#2	180.20	585.00	3.25	182.50	836.50	4.58	146.30	858.10	5.87
RB99 X802#3	385.20	621.10	1.61	387.10	867.00	2.24	336.10	878.20	2.61
X187 [control]	433.00	435.00	1.00	517.00	523.30	1.01	681.50	683.70	1.00
X802 [control]	401.60	415.90	1.04	575.20	538.60	0.94	687.00	666.00	0.97

Table S3. Fungus-bacterium co-culture (*Actinomadura* sp. RB99 versus *Pseudoxylaria* sp. X802) grown on PDA agar plates showing inhibition of fungal growth towards the bacterial colony.

Days	***Actinomadura* sp. RB99 versus *Pseudoxylaria* sp. X802**	***Actinomadura* sp. RB99 versus *Pseudoxylaria* sp. X187**
0	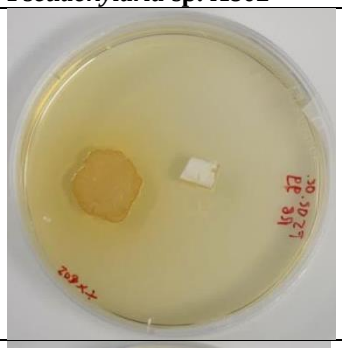	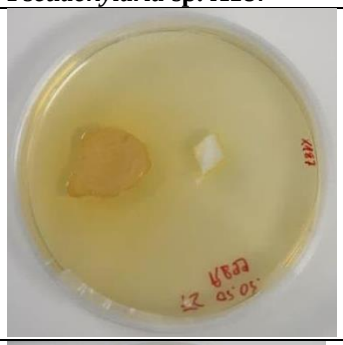
2		
5		
7		
9		

12		
14	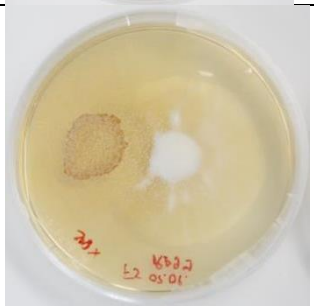	

Table S3-1. Fungus-bacterium co-culture (*Actinomadura* sp. RB99 versus *Termitomyces* sp. T153) grown on PDA agar plates showing inhibition of fungal growth towards the bacterial colony.

Days	***Actinomadura* sp. RB99 versus *Termitomyces* sp. T153 (top or bottom view)**	***Days***	***Actinomadura* sp. RB99 versus *Termitomyces* sp. T153 (top or bottom view)**
0	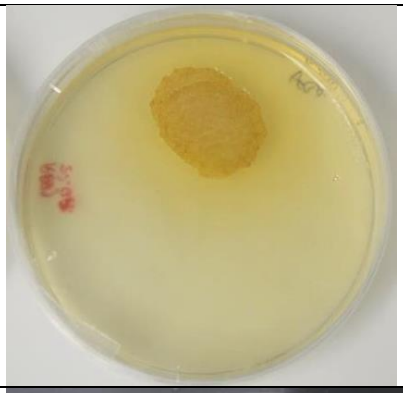	9	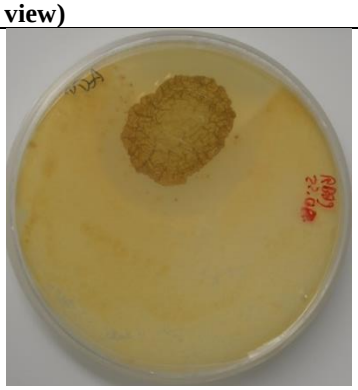
7	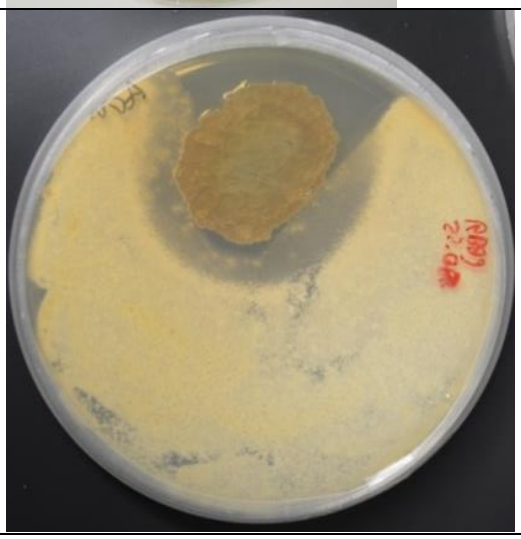	13	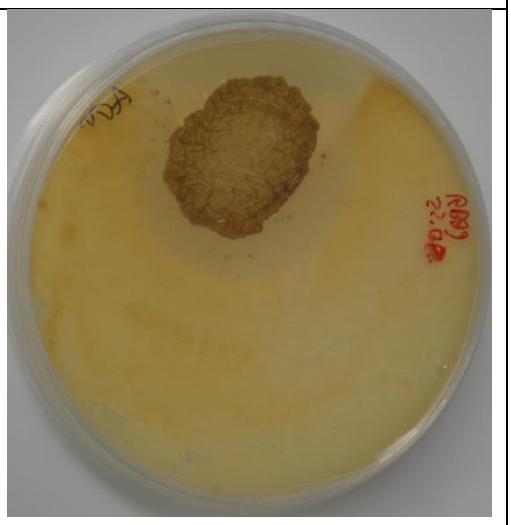

4. CAS Activity test

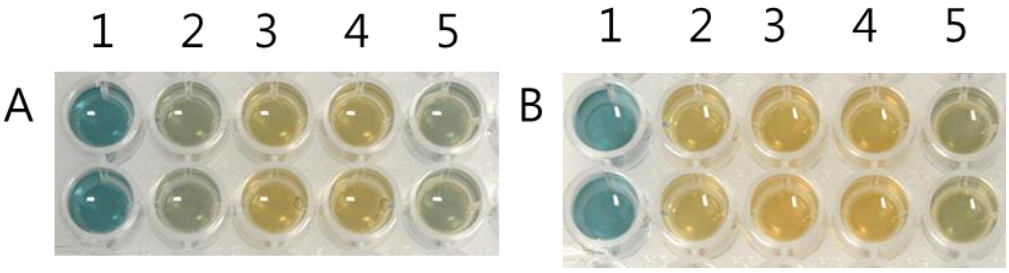

Figure S1. Exemplary CAS siderophore assay of bacterial extracts (1 mg/mL). Measurement of duplicates of: (1) MeOH (negative control), (2) 1 mM EDTA (positive control), (3-5) extracts derived from cultures grown on (3) ISP5 sea salt, (4) ISP5 sea salt with low Fe-content, and (5) ISP5 sea salt depleted of Fe. A) after 45 min and B) after 90 min. Orange color indicates iron binding activity. Screening was performed in duplicates, n= 2.

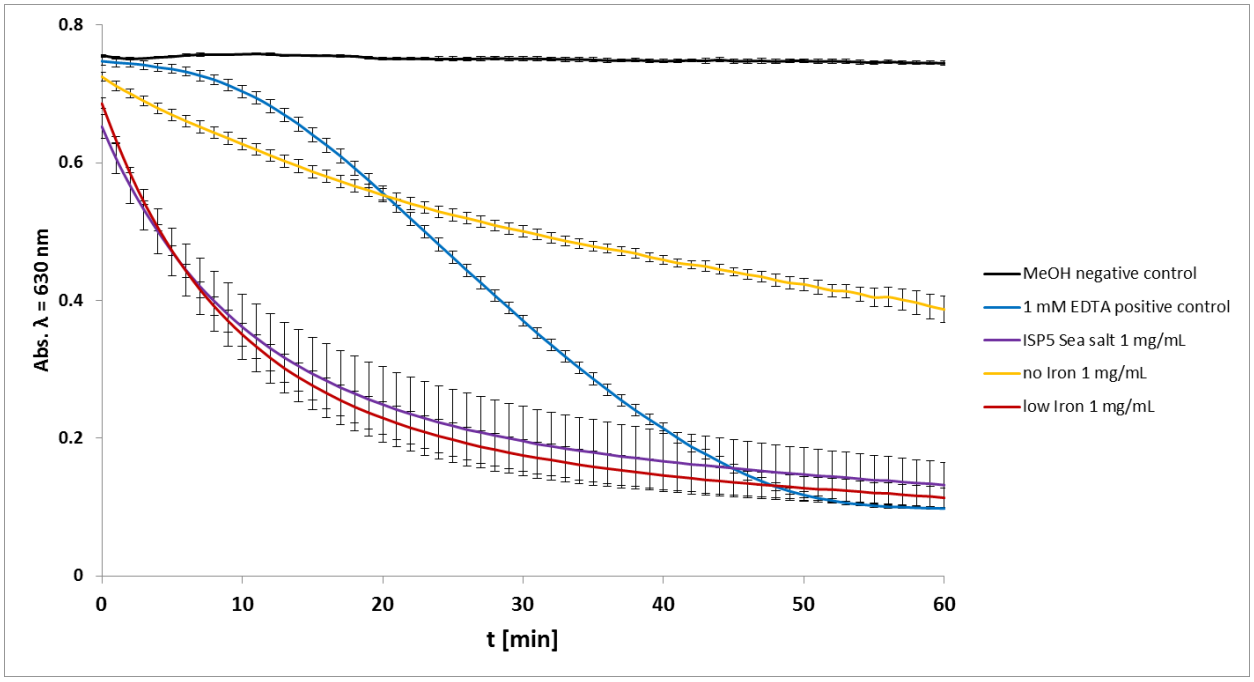

Figure S2. CAS siderophore assay of methanolic extracts obtained from bacterial cultures grown under different iron conditions. MeOH was used as negative control and 1 mM EDTA was used as positive control. Error bars indicate ± 0.5 standard deviation, n = 2.

5. Analytical procedures

General extraction procedure: C_{18}-ec SPE cartridges (6 mL, 1 g, Macherey-Nagel) were washed and prepared for extraction according to the manufacturer's manual. Cartridges were equilibrated with 5 % MeOH in ddH_2O. Cell free culture supernatant (20 mL, 5 % MeOH) was loaded onto the cartridge. The samples were washed with one column volume 10% MeOH followed by one column volume 20 % MeOH. Subsequently, analytes of interest were eluted with 10 mL 50 % MeOH followed by 10 mL 100 % MeOH. Eluates were combined in weighed glass vials and dried *in vacuo*. Residues were weighed and resuspended in MeOH (1 mg/mL) using ultra-sonication. Concentrated samples were stored in the dark at -20 °C for up to one week. Analytic sub-samples were cleaned from particles *via* centrifugation for 15 min, 13.000 rpm, diluted to a final concentration of 75 µg/mL with MeOH and submitted to UPLC-HRMS based analysis.

MS^2 and GNPS-based discovery of madurastatin congeners

A molecular network was created using the online workflow (https://ccms-ucsd.github.io/GNPSDocumentation) on the GNPS website (http://gnps.ucsd.edu). The data was filtered by removing all MS/MS fragment ions within +/- 17 Da of the precursor m/z. MS/MS spectra were window filtered by choosing only the top 6 fragment ions in the +/- 50Da window throughout the spectrum. The precursor ion mass tolerance was set to 0.02 Da and a MS/MS fragment ion tolerance of 0.02 Da. A network was then created where edges were filtered to have a cosine score above 0.7 and more than 6 matched peaks. Further, edges between two nodes were kept in the network if and only if each of the nodes appeared in each other's respective top 10 most similar nodes. Finally, the maximum size of a molecular family was set to 100, and the lowest scoring edges were removed from molecular families until the molecular family size was below this threshold. The spectra in the network were then searched against GNPS' spectral libraries. The library spectra were filtered in the same manner as the input data. All matches kept between network spectra and library spectra were required to have a score above 0.7 and at least 6 matched peaks.

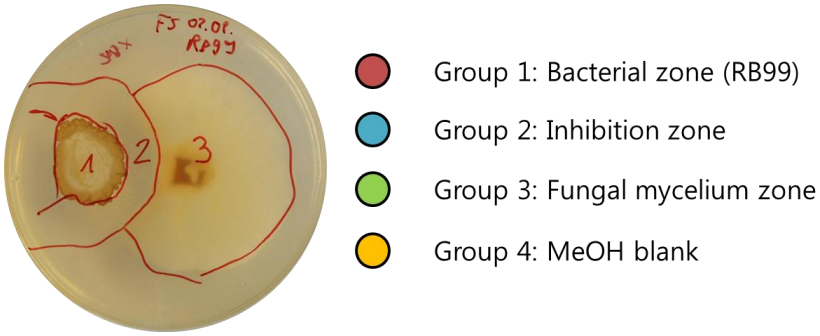

Figure S3. Exemplary co-culture analysis and section of zones used for metabolite extraction and analysis.

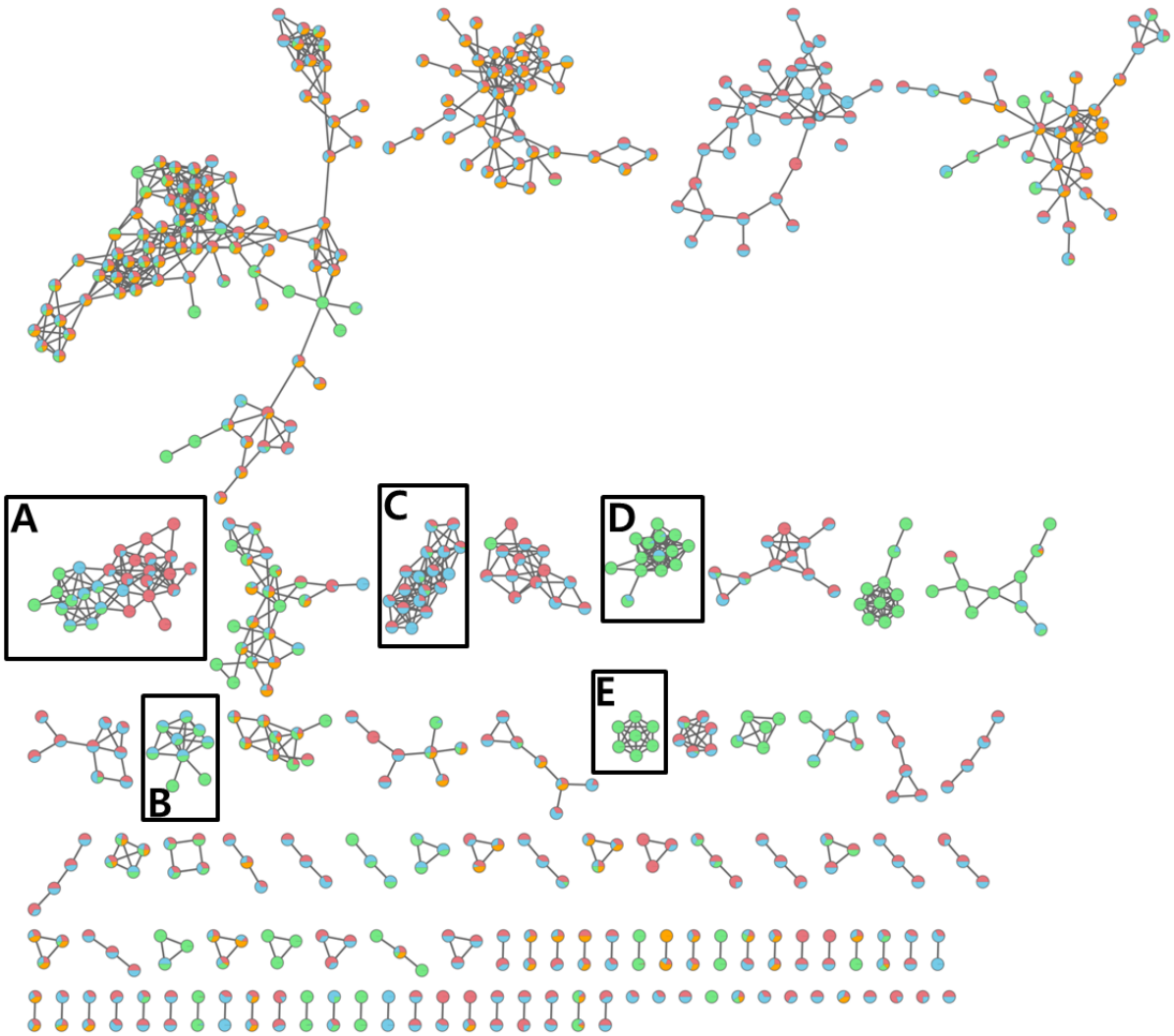

Figure S4. Exemplary analysis of co-culture sample (*Actinomadura* sp. RB99 versus *Pseudoxylaria* sp. X802) using network cluster analysis via GNPS platform and visualized by Cytoscape (red: bacterial zone, blue inhibition zone, green: fungal mycelium, yellow: methanol blank, see **Figure S3**). Dereplicated GNPS clusters: A) phosphoethanolamines, B) phosphocholines, C) oligosaccharides, D) pseudoxylallemycins, and E) cytochalasins.

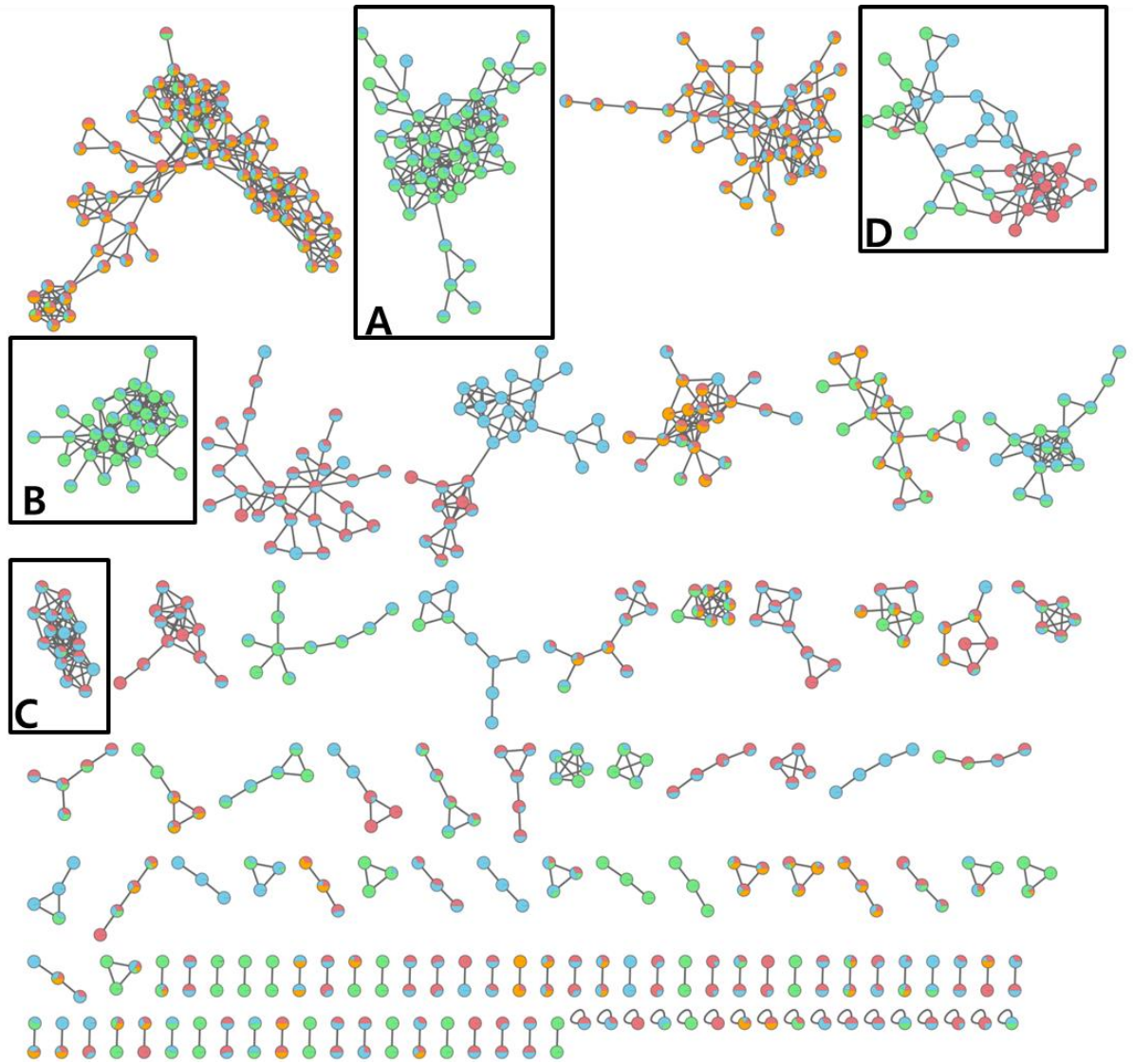

Figure S5. Exemplary analysis of co-culture sample (*Actinomadura* sp. RB99 versus *Pseudoxylaria* sp. 187) using network cluster analysis via GNPS platform and visualized using Cytoscape (red: bacterial zone, blue inhibition zone, green: fungal mycelium, yellow: methanol blank, see Figure S3. Dereplicated GNPS clusters: A) xylacremolide, B) pseudoxylaramide, C) oligosaccharides, D) phospholipids (phosphoethanolamines).

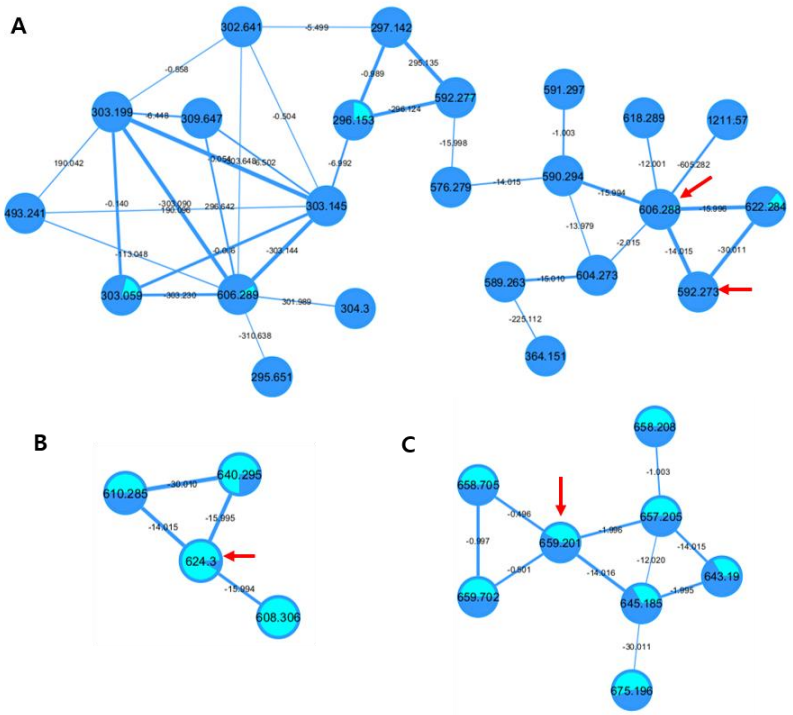

Figure S6. GNPS cluster from SPE fraction eluted by 40% MeOH and 60% MeOH. Cyan nodes represent the 40% MeOH fraction, and blue nodes represent the 60% MeOH fraction. A) 'oxazoline' containing subcluster (*m/z* 606.288: madurastatin A1; *m/z* 592.277: madurastatin C1); B) 'serine' containing subcluster (*m/z* 624.3: madurastatin A2; C) Fe-adducts of 'oxazoline' containing subcluster: *m/z* 659.201: Fe-madurastatin A1)

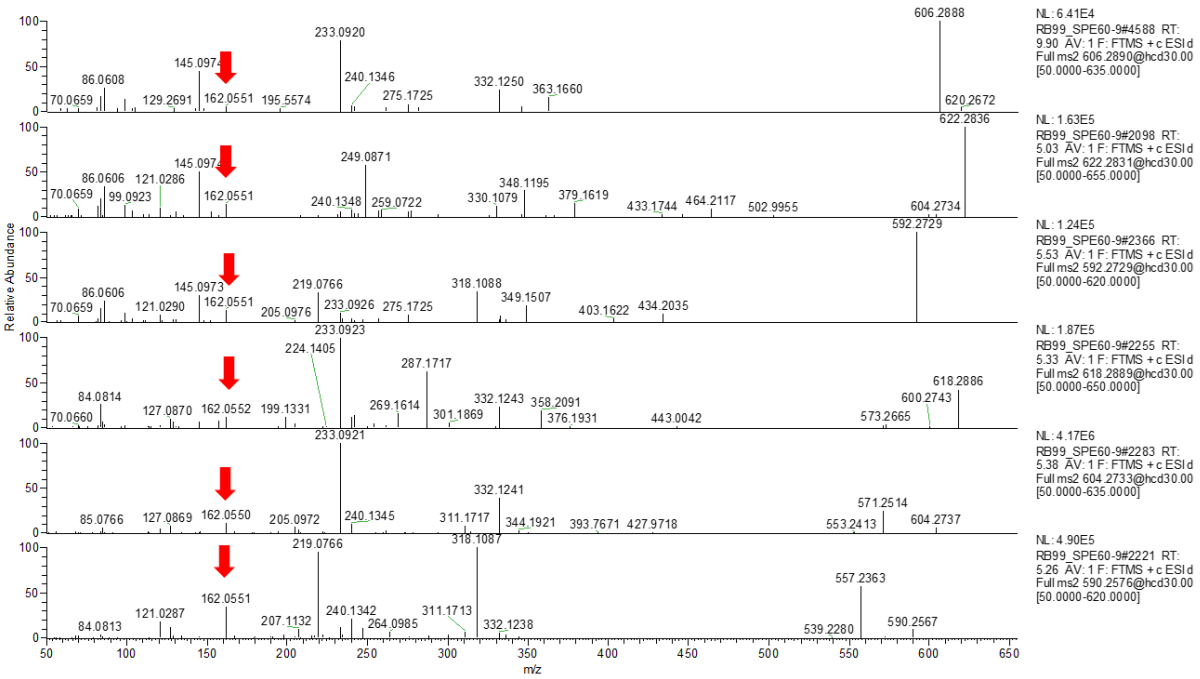

Figure S7. LCMS/MS spectra of oxazoline containing derivatives. Red arrow highlights the diagnostic fragment ion at *m/z* 162.0551.

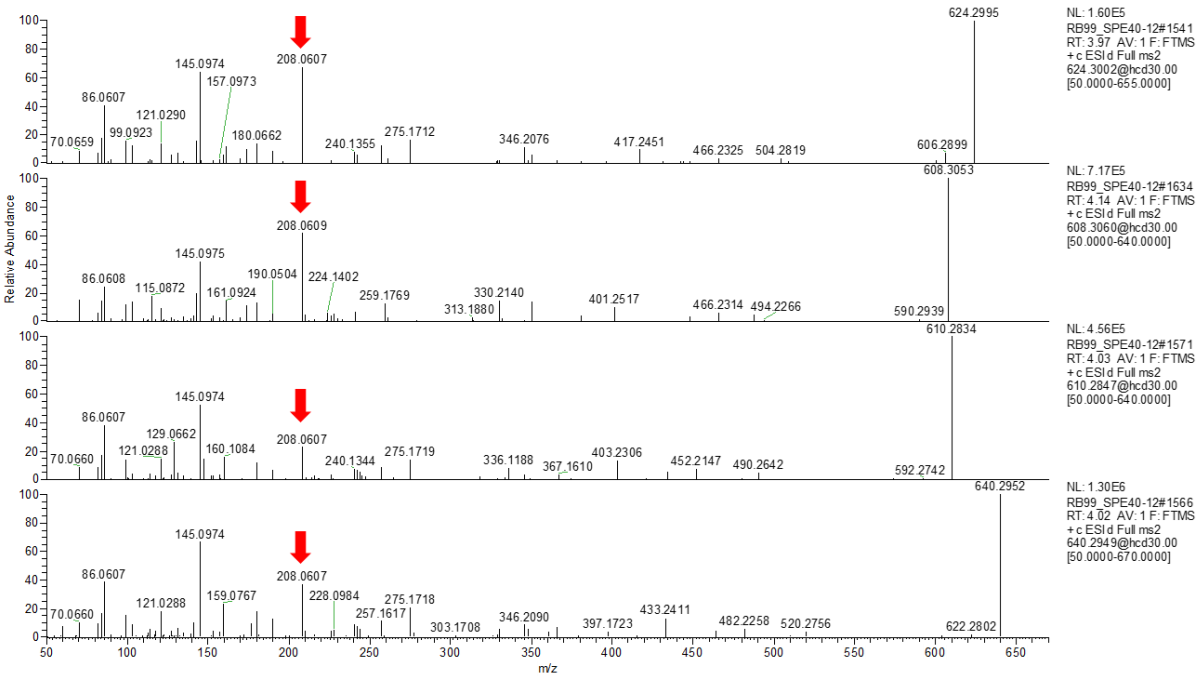

Figure S8. LCMS/MS spectra of serine containing derivatives. Red arrow highlights the diagnostic fragment ion at *m/z* 208.0607.

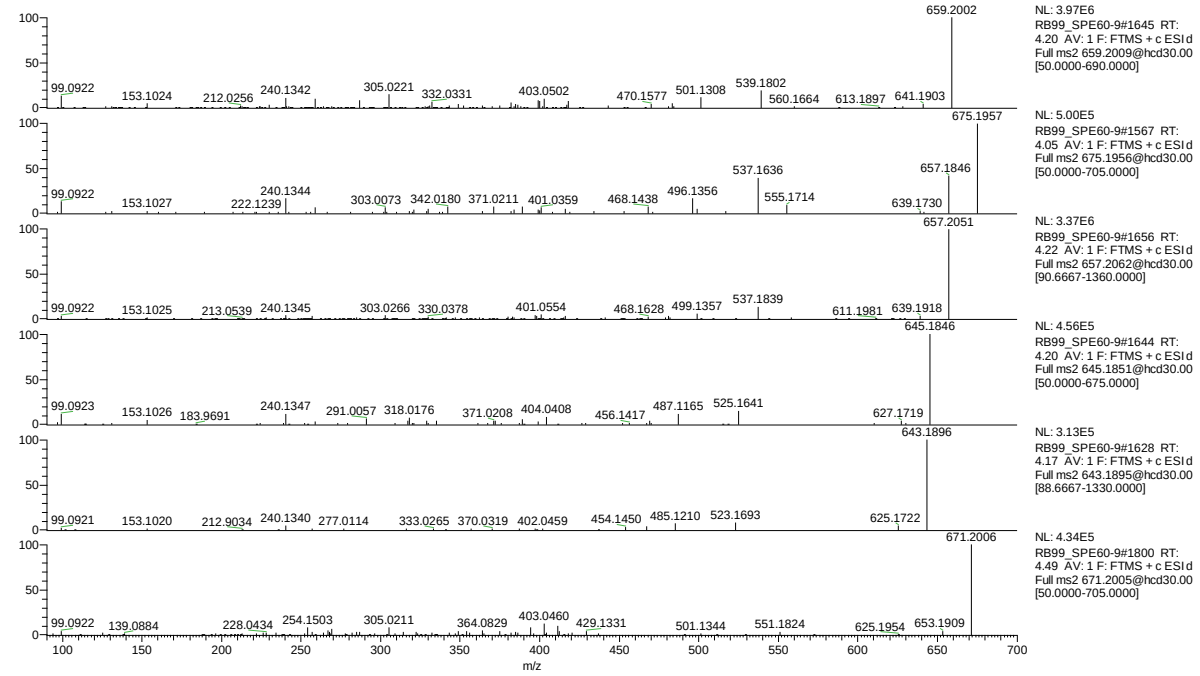

Figure S9. LCMS/MS spectra of Fe adduct of oxazoline containing derivatives.

6. Time-resolved analysis of siderophore production in different media

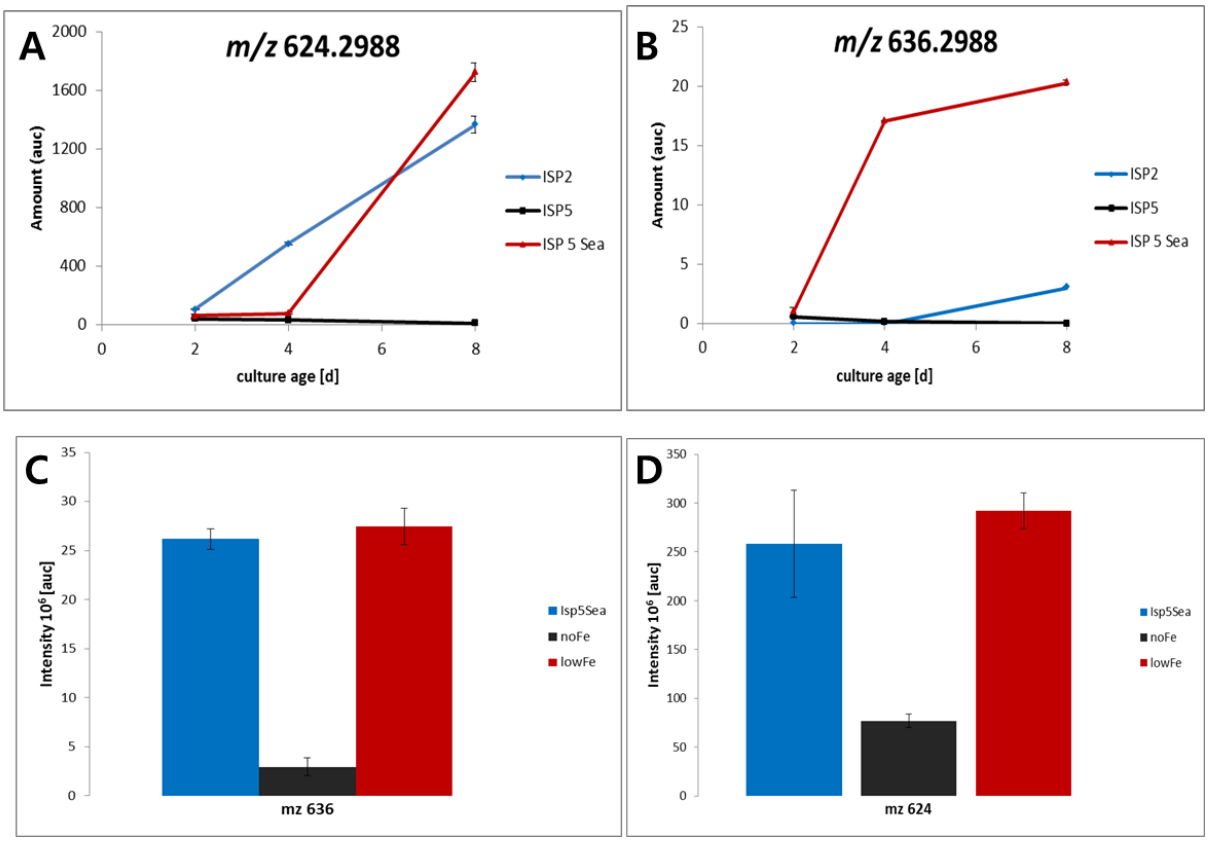

Figure S10. Quantification of siderophore production by *Actinomadura* sp. RB99 A) **1** *m/z* $[M+H]^+$ 624.2988, and B) **2** *m/z* $[M+H]^+$ 636.2988 after two, four and eight days of cultivation in different media. Intensity units at 10^6 auc. Error bars indicate ± 0.5 standard deviation, duplicates n=2. C-D) Determination of production tiers for *m/z* $[M+H]^+$ 624.2988 and *m/z* $[M+H]^+$ 624.2988 after eight days when cultivated in media containing different iron concentrations. Error bars indicate ± 0.5 standard deviation, triplicates n=3.

7. Extraction and Isolation of Compounds

Actinomadura sp. RB99 was grown in 50 mL ISP-2 broth for seven days at 30°C (pre-culture) and used to inoculate 100 ISP-2 agar plates. Plates were incubated for 10 days at 30°C, cut into small pieces, consolidated, and immersed overnight in MeOH. The MeOH phase was filtered and evaporated *in vacuo*. The resultant MeOH extract (11 g) was dissolved in distilled water (700 mL) and then solvent-partitioned with EtOAc (700 mL) three times, providing 4.5 g of residue. The EtOAc-soluble fraction (4.5 g) was loaded onto a silica gel column for open column chromatography and fractionated with a gradient solvent system of CH_2Cl_2-MeOH (50:1 to 0:1, *v*/*v*) to afford seven fractions (A-G). Fraction E (110 mg) was subjected to preparative reversed-phase HPLC (Phenomenex Luna C18, 250 × 21.2 mm i.d., 5 μm) using MeOH-H_2O (1:9–1:0, v/v, gradient system, flow rate: 5 mL/min) to give four subfractions (E1-E4). Compound **4** (2.0 mg, t_R = 29.0 min) was purified from subfraction E3 (20 mg) by semi-preparative reversed-phase HPLC eluting 28% MeOH/H_2O (isocratic system, flow rate: 2 mL/min). Fraction F (490 mg) was separated by using preparative reversed-phase HPLC (Phenomenex Luna C18, 250 × 21.2 mm i.d., 5 μm) using CH_3CN-H_2O (0.5:9.5–1:0, v/v, gradient system, flow rate: 5 mL/min) to give four subfractions (F1-F4). Subfraction F3 (50 mg) was isolated by semi-preparative reversed-phase HPLC eluting 30% MeOH/H_2O (isocratic system, flow rate: 2 mL/min), affording compounds **2** (2.3 mg, t_R = 50.0 min) and **3** (1.4 mg, t_R = 55.0 min). Five subfractions (G1-G5) were acquired from fraction G (300 mg) using preparative reversed-phase HPLC (Phenomenex Luna C18, 250 × 21.2 mm i.d., 5 μm) using CH_3CN -H_2O (1:9–1:0, v/v, gradient system, flow rate: 5 mL/min). Compound **1** (4.3 mg, t_R = 15.0 min) was isolated from subfraction G2 (45 mg) by semi-preparative reversed-phase HPLC eluting 19% MeOH/H_2O (isocratic system, flow rate: 2 mL/min).

For isolation of Fe-siderophore complex of 5

The resultant MeOH extract was dissolved in 10% MeOH/90% H_2O and loaded on a conditioned SPE-C18 cartridge (5 g/45 mL), and then fractioned by step-gradient of MeOH and H_2O mixture (20 mL/fraction). The resultant fractions were concentrated under reduced pressure and submitted to LCMS analysis. The fraction eluted at 40% MeOH contained the apo-siderophore (**1**) with the *m*/*z* at 624.2977 $[M+H]^+$ as well as a Fe-siderophore complex with an *m*/*z* of 659.1983 $[M+H]^+$. Then, the 40% MeOH fraction was subjected to Sephadex LH20 purification and metabolites eluted using 50% MeOH. MS-guided analysis indicated that the Fe-siderophore complex was enriched in Fr. 12. This fraction was titrated with a 100 mM $Ga(NO_3)_3$ aq. solution to exchange Fe^{3+} with Ga^{3+} yielding a siderophore complex with an *m*/*z* of 672.1894 $[M+H]^+$. The complex was separated by semipreparative HPLC (Phenomenex Synergi-HydroRP, 250 × 10 mm i.d., 5 μm) using CH_3CN/0.1% FA gradient (0-5 min, 10% CH_3CN/90% H_2O (0.1% FA); 5-40 min, 10% CH_3CN/90% H_2O (0.1% FA)-28% CH_3CN/72% H_2O (0.1% FA), flow rate at 2 mL/min), affording compound **5** (1.0 mg; t_R = 20.0 min).

8. Structure Elucidation of Isolated Compounds

Structure elucidation of 1

Compound **1** was obtained as an amorphous powder and its molecular formula was determined to be $C_{27}H_{41}N_7O_{10}$ on the basis of the positive-ion mode HR-ESIMS data, which exhibited a protonated ion peak at *m/z* 624.3022 $[M+H]^+$ (Calcd. for $C_{27}H_{42}N_7O_{10}^+$, 624.2993). The ^{1}H NMR data (**Table S4**) of **1** showed two methyls [δ_H 1.38 (3H, d, *J* = 7.0 Hz, H-12) and 2.55 (3H, s, H-1')], nine methylenes [δ_H 1.75 (2H, m, H-18), 1.77 (2H, m, H-19), 1.84 (1H, m, H-24a), 1.98 (1H, m, H-25a), 2.03 (1H, m, H-25b), 2.07 (1H, m, H-24b), 2.54 (2H, m, H-15), 3.43 (1H, m, H-14a), 3.49 (1H, m, H-14b), 3.59 (1H, m, H-26a), 3.61 (2H, m, H-17), 3.64 (1H, m, H-26b), 3.90 (1H, dd, *J* = 11.0, 4.5 Hz, H-9a), and 3.95 (1H, dd, *J* = 11.0, 5.0 Hz, H-9b)], four methines [δ_H 3.56 (1H, m, H-20), 4.32 (1H, q, *J* = 7.0 Hz, H-11), 4.50 (1H, m, H-23), and 4.59 (1H, dd, *J* = 5.0, 4.5 Hz, H-8)], and four aromatic protons [δ_H 6.92 (1H, t, *J* = 7.5 Hz, H-2), 6.93 (1H, dd, *J* = 7.5, 1.0 Hz, H-4), 7.39 (1H, t, *J* = 7.5 Hz, H-3), and 7.91 (1H, dd, *J* = 7.5, 1.0 Hz, H-1)]. The ^{13}C NMR spectrum displayed a total of 27 carbon signals, including two methyls (δ_C 17.4 and 32.6), nine methylenes (δ_C 21.4, 22.6, 28.1, 28.9, 36.1, 32.6, 47.7, 52.2, and 62.5), four methines (δ_C 50.5, 51.2, 57.1, and 62.8), four aromatic carbons (δ_C 117.8, 120.1, 130.1, and 134.6), two non-protonated aromatic carbons (δ_C 110.9 and 160.1), and six carbonyl carbons (δ_C 165.5, 170.1, 172.7, 173.9, 174.1, and 174.7). 1D and 2D NMR (^{1}H-^{1}H COSY, HSQC, and HMBC data) analysis of **1** revealed five amino acid spin systems, namely, serine, α-alanine, β-alanine, and two modified ornithines, along with salicylic acid unit, coupling structure of which was same to madurastatin A2, identified from the culture broth of a pathogenic *Actinomadura madurae* IFM 0745 strain.[1] HRESI-MS/MS[2] analysis of **1** showed distinctive fragment ions at *m/z* 121.0286, 131.0817, 161,0921, 208.0604, 275.1712, 346.2085, 350.1350, 417.2457 and 504.2777 due to the sequential cleavage of amide bonds of a linear peptide. The structure was also confirmed by the comparison of the experimental HRESI-MS/MS spectrum of **1** with its predicted HRESI-MS/MS spectrum obtained from Competitive Fragmentation Modeling-ID (CFM-ID) 3.0. The detected fragment ions in the experimental HRESI-MS/MS spectrum of **1** matched to corresponding ions in the predicted HRESI-MS/MS spectrum from CFM-ID 3.0. To verify the absolute configurations of **1**, acidic hydrolysis followed by advanced Marfey's method was employed. The acid hydrolysates of **1** and standard amino acids (L/D-Ala, Ser, and Orn, and *N*-methyl-L-Orn) were derivatized with 1-fluoro-2,4-dinitrophenyl-5-L-alanineamide (L-FDAA), and the resultants were analyzed by LC/MS, which showed that the absolute configurations of Ala, Orn, and *N*-methyl-Orn moieties are L-forms while Ser has the absolute configuration of D-form.

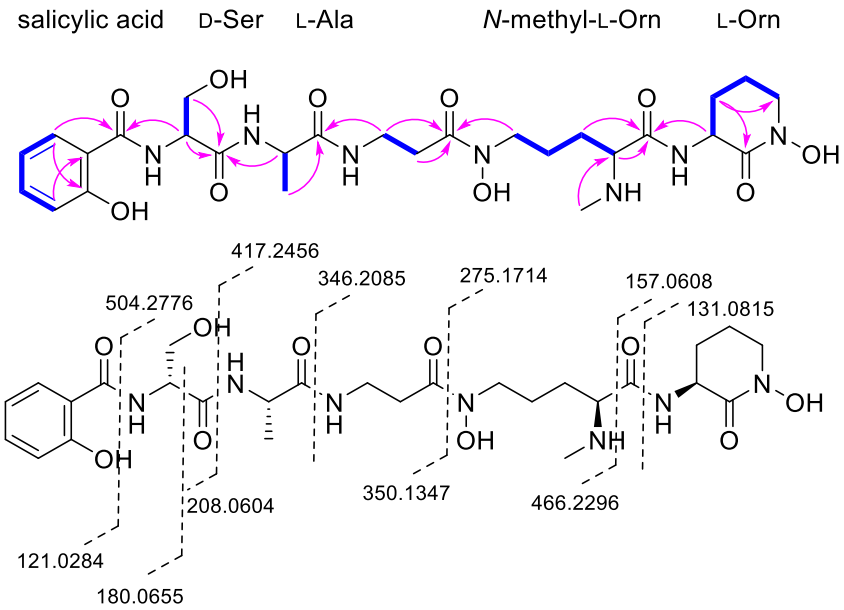

Figure S11. Chemical structures of **1** and 2D NMR data and MS/MS fragment ions of **1**. The dashed lines show the fragments obtained in a tandem MS experiment. Blue bonds indicate ^{1}H-^{1}H COSY correlations and pink arrows indicated HMBC correlations. The depicted numbers indicate the corresponding *m/z* values.

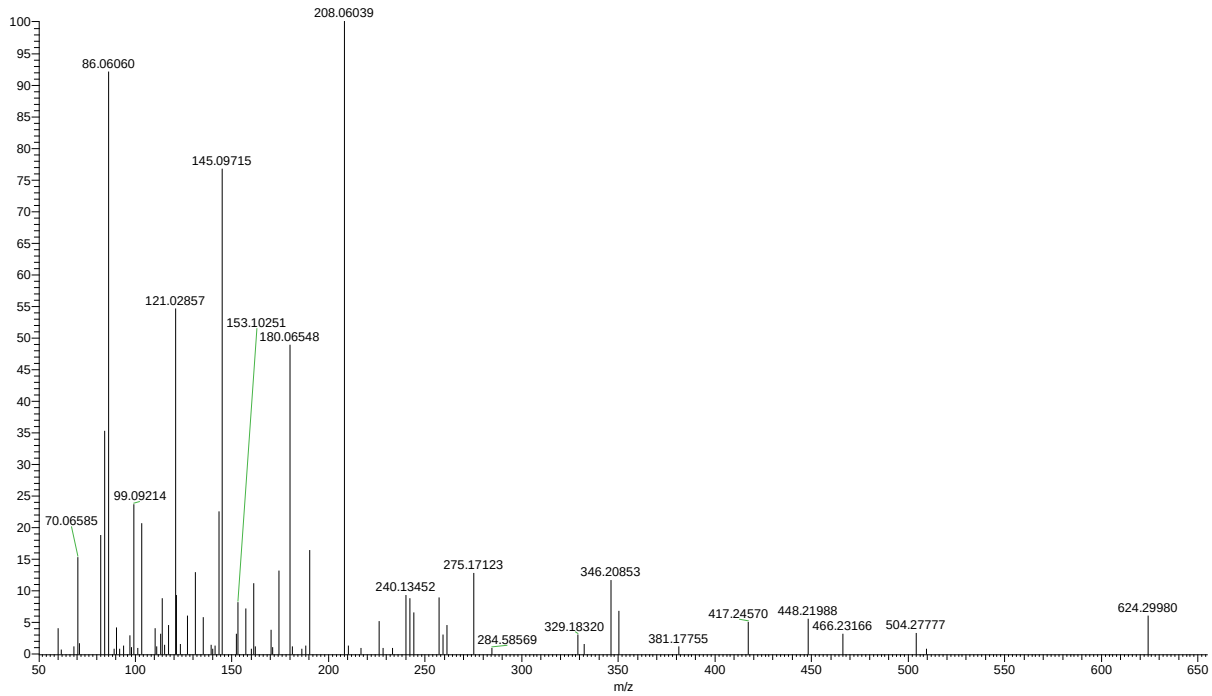

Figure S12. MS^{2} spectrum of **1** at *m/z* 624.2998 $[M+H]^{+}$ ($C_{27}H_{42}N_{7}O_{10}^{+}$, calcd. 624.2993).

Structure elucidation of Ga-Complex of 5

The molecular formula of **5** was deduced from HRESI-MS analysis with the observation of pseudomolecular ion peak at *m/z* 672.1891 $[M+H]^+$ (Calcd. for $C_{27}H_{37}N_7O_9Ga$, 672.1909), and isotope distribution of Ga (^{69}Ga:^{71}Ga 5:3). LC-HRMS analysis showed very closed minor peaks at *m/z* 659.1984 $[M+H]^+$ (Calcd. for $C_{27}H_{37}N_7O_9Fe$, 659.1997), with the isotope distribution of Fe (^{54}Fe:^{56}Fe 6:100). This led to the prediction of apo-siderophore of compound **5** with the molecular formula of $C_{27}H_{36}N_7O_9$. Detailed analysis of HPLC fraction containing major compound **5** allowed to detect trace amount of apo-siderophore of **5** at *m/z* 606.2866 $[M+H]^+$ (Calcd. for $C_{27}H_{40}N_7O_9^+$, 606.2882). Detailed analysis of HRMS/MS of apo-siderophore at showed high similarity with compound **1**. The major difference between compound **5** and compound **1** was the absence of fragment ions at *m/z* 180.0655 and 208.0604 from **1** and the presence of fragment ions at *m/z* 162.0551, 233.0921, 261.0871 and 332.1241 from **5**. This led to the hypothesis that apo-siderophore **5** was present as oxazoline form, by losing water molecule from the serine moiety of compound **1**. ^1H NMR spectrum indicated the two sets of proton signals, represent the major Ga adduct and minor Fe adduct. Overall, the ^1H NMR spectrum exhibited very similar signals with compound **1**, and the presence of cyclic oxazoline was proved by the observation of HMBC correlation of H_2-9 (δ_H 4.69 and 4.43) to C-7 (δ_C 170.46).

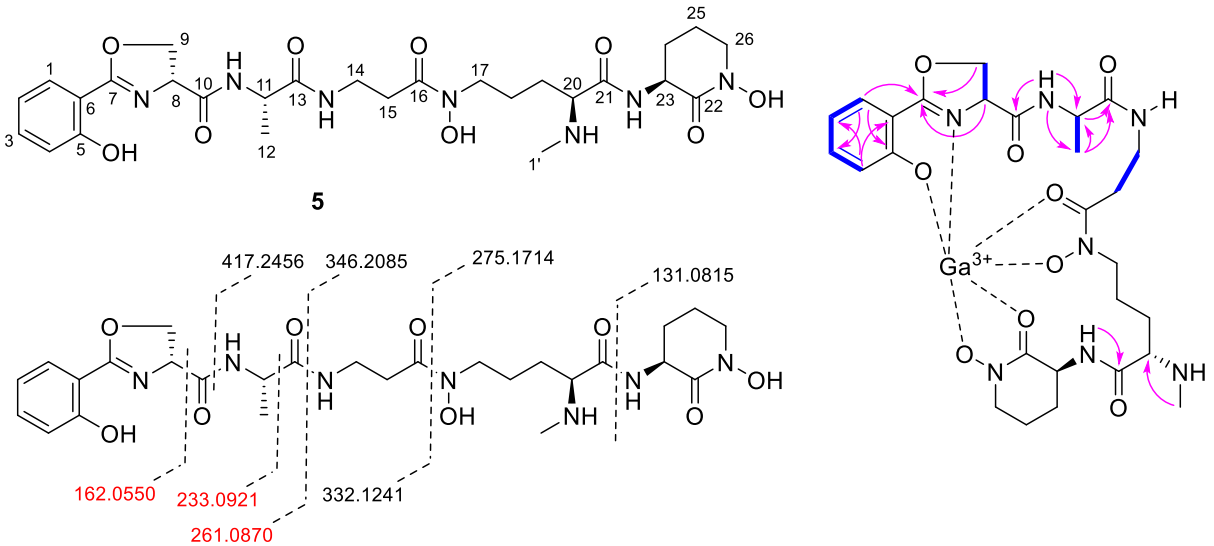

Figure S13. Chemical structure of madurastatin A1 (**5**) and 2D NMR data of **5** (Ga complex) and MS/MS fragment ions of **5** (apo form). Blue bonds indicate ^1H-^1H COSY correlations and pink arrows indicated HMBC correlations.

Structure elucidation of 2

Compound **2** was isolated as an amorphous powder and its molecular formula of $C_{28}H_{41}N_7O_{10}$ was suggested by the positive-ion mode HRESI-MS data at *m/z* 636.3017 $[M+H]^+$ (Calcd. for $C_{28}H_{42}N_7O_{10}^+$, 636.2993). Detailed analysis of 1D and 2D NMR spectra revealed that spectroscopic values of **2** were almost identical of those of **1**, except for the presence of an additional methylene [δ_H 3.77 (1H, d, J = 4.0 Hz, H-2'a) and 4.34 (1H, d, J = 4.0 Hz, H-2'b); δ_C 68.0]. The HMBC correlations of H_3-1'/C-20, H_3-1'/C-2', H-2'/C-20, H-2'/C-21, H-23/C-2', and H-23/C-21 afforded the construction of 4-imidazolidinone conjugated to *N*-methyl-L-Orn moiety. The analysis of HRESI-MS/MS data of **2** verified the NMR-based structural characterization, which was also supported by comparison with its predicted HRESI-MS/MS spectrum proposed from CFM-ID 3.0.

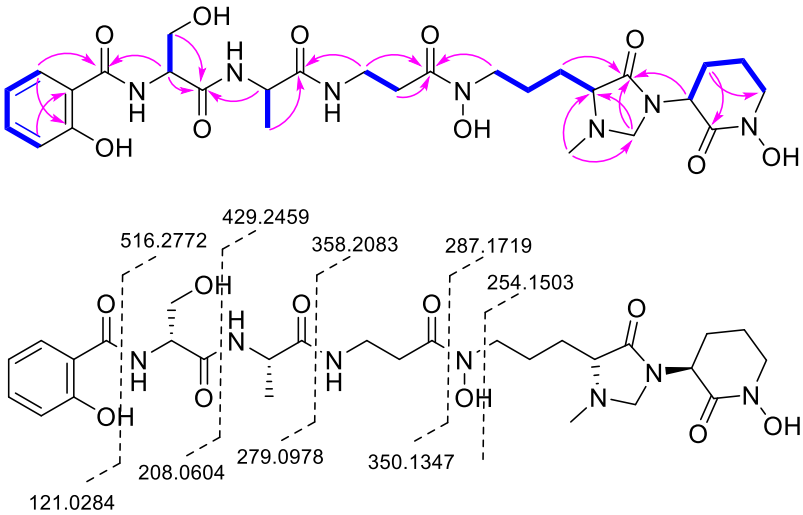

2

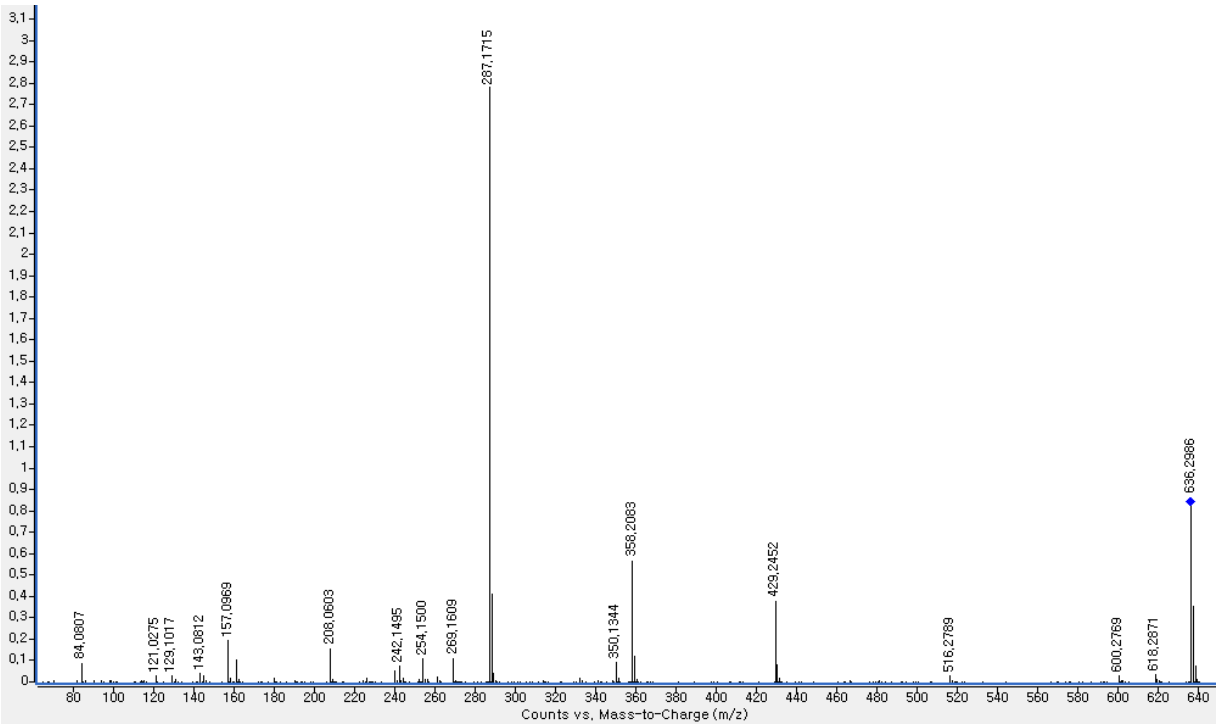

Figure S14. 2D NMR data and MS/MS fragment ion pattern of **2**. Blue bonds indicate ^1H-^1H COSY

correlations and pink arrows indicated HMBC correlations.

Structure elucidation of 3

The molecular formula of compound **3** was determined to be $C_{27}H_{38}N_6O_{10}$ based on the deprotonated ion peak at *m/z* 605.2568 $[M-H]^-$ (Calcd. for $C_{27}H_{37}N_6O_{10}^-$, 605.2571) in the negative-ion mode HR-ESIMS. Inspection of ^1H and ^{13}C NMR spectra of **3** indicated that the NMR data of **3** was similar with that of **1** except for some discrepancies. The major difference was that the *N*-methyl group in **2** was absent at C-20 (δ_C 36.7) in **3**. The $^3J_{HH}$ vicinal correlations from H_2-17 to H_2-20 in ^1H-^1H-COSY as well as HMBC correlations of H_2-19/C-21 and H-23/C-21 supported the converted substructure in **3.** In addition, HMBC correlations from H_3-1' (δ_H 2.94) to C-21 and C-23 led to the confirmation of *N*-methylation at nitrogen between C-21 and C-23. Another difference was present in the terminal ornithine moiety; an interesting oxygenated methine [δ_H 5.75 (1H, brs); δ_C 82.0] was assigned at C-26 by COSY correlations from H-23 to H-26 as well as a HMBC correlation from H_2-24 to C-26. According to the molecular formula of **3**, $C_{27}H_{38}N_6O_{10}$, 12 unsaturation degrees of **3** was deduced, which suggested one additional unsaturation degree in the terminal ornithine moiety of **3**. To allocate one unsaturation degree in the terminal ornithine moiety, the presence of epoxide ring was deduced between C-26 and nitrogen atom, affording the elucidation of novel structural moiety, 7-oxa-1-azabicyclo[4.1.0]heptan-2-one, which has rarely been reported. The proposed substructure was also verified by the analysis of its HRESI-MS/MS fragmentation data where detection of the characteristic ion at *m/z* 143.0814 confirmed the assignment of 7-oxa-1-azabicyclo[4.1.0]heptan-2-one residue, which was also supported by comparison with its predicted HRESI-MS/MS spectrum proposed from CFM-ID 3.0. The stereochemistry of **3** at C-8, C-11, and C-23 was determined as same to compound **2** by the consideration of spectroscopic data patterns and deduced from the same biosynthetic logic.

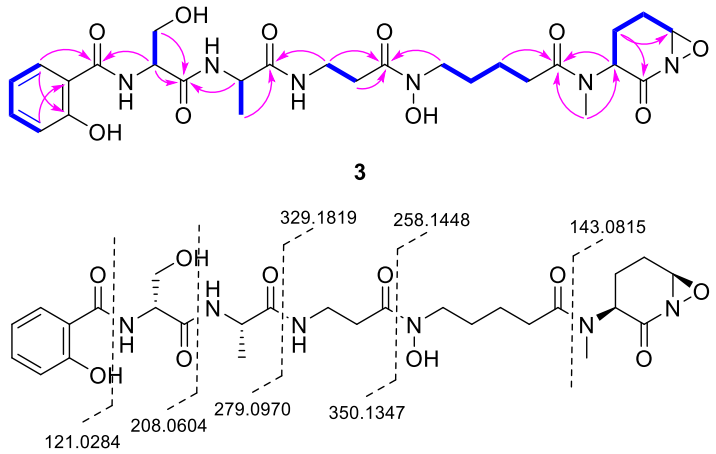

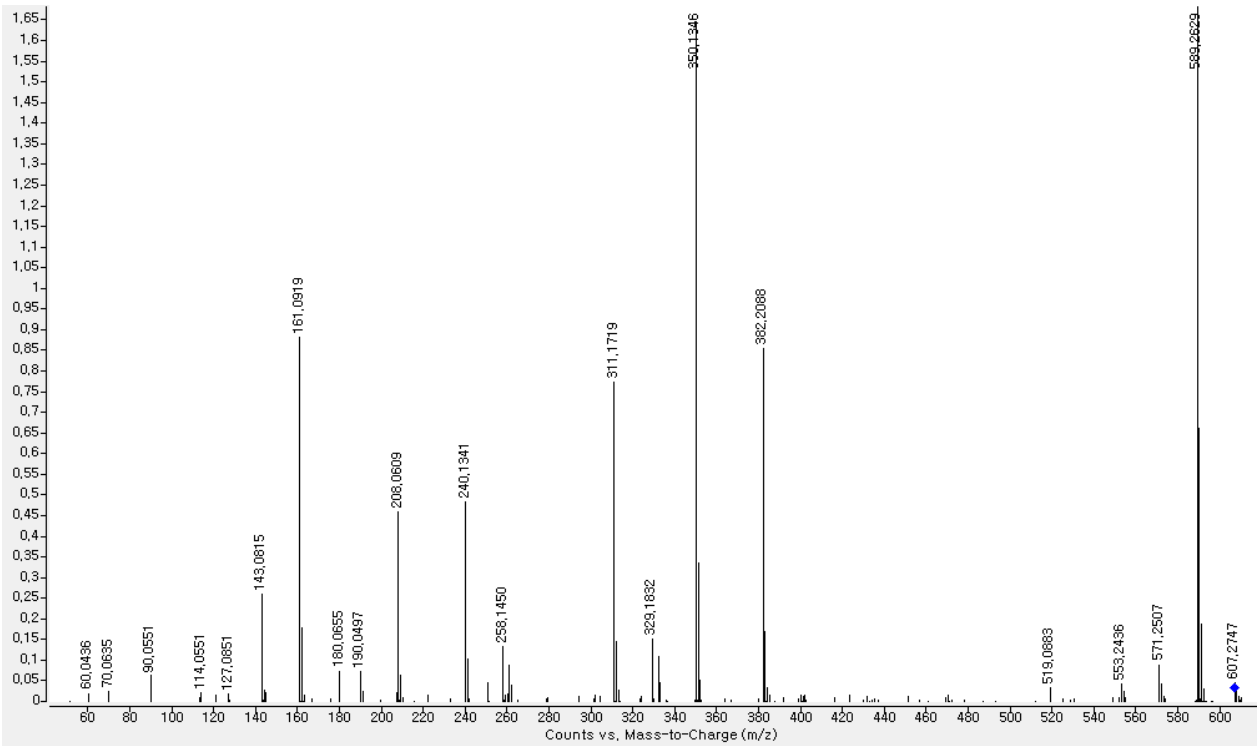

Figure S15. 2D NMR data and MS/MS fragment ion pattern of **3**. Blue bonds indicate ^{1}H-^{1}H COSY correlations and pink arrows indicated HMBC correlations.

Structure elucidation of 4

HRESI-MS analysis of **4** suggested a molecular formula of $C_{16}H_{21}N_3O_7$ from a pseudomolecular ion peak at *m/z* 368.1451 $[M+H]^+$ ($C_{16}H_{22}N_3O_7^+$,calcd. 368.1458). Comparison of spectra obtained for **4** and **1** proposed that the structure of **4** shares the salicylic acid, serine, α-alanine, and β-alanine units of **1**. This deduction was verified by 2D NMR (^{1}H-^{1}H COSY, HSQC, and HMBC data) of **4** especially, not only $^3J_{HH}$ vicinal correlations between H_2-14 and H_2-15 in ^{1}H-^{1}H COSY but also HMBC correlations of H_2-14/C-13, H_2-14/C-16, and H_2-15/C-16. In addition, distinctive fragment ions observed in HRESI-MS/MS data clearly supported the amino acid sequence of **4**.

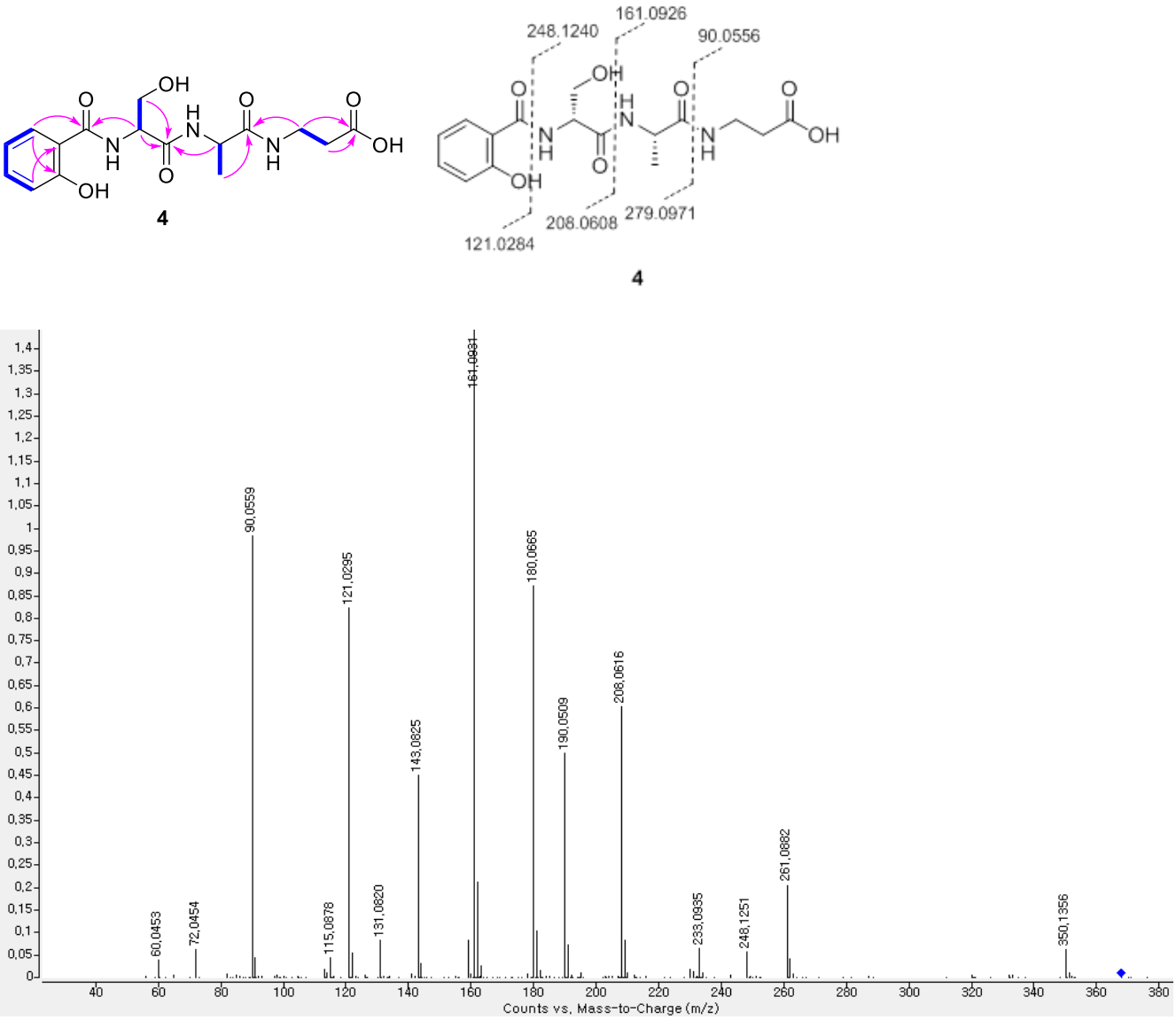

Figure S16. 2D NMR data and MS/MS fragment ion pattern of **4**. Blue bonds indicate ^{1}H-^{1}H COSY correlations and pink arrows indicated HMBC correlations.

Structure prediction of derivative 6 with an *m/z* 610.2831

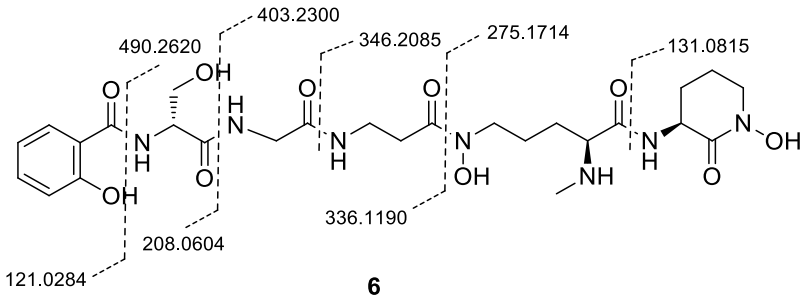

Figure S17. Proposed structure of **6** based on MS^2 fragmentation.

Derivative **6** (*m/z* 610.2829) was assigned the molecular formula $C_{26}H_{39}N_7O_{10}$, corresponding to loss of a CH_2 unit (Δ *m/z* = 14.016) compared to **1** ($[M+H]^+$ $C_{27}H_{42}N_7O_{10}^+$,calcd. 624.2993). Identical fragments with *m/z* 121.0286, *m/z* 180.0656 and *m/z* 208.0606 confirm the link between salicylic acid and serine unit like in **1**. Fragment *m/z* 275.1714 confirms no changes on the double ornithine part on the right side of the molecule. Other fragments for **6** that occur either during neutral loss of salicylic acid and the first serine moiety (*m/z* 490.254 and *m/z* 403.2291), or during fragment loss of the ornithine moieties (*m/z* 452.2114 and *m/z* 336.1194) are replaced and shifted by Δ *m/z* = 14.016 compared to their counterparts in **1**. This corresponds to loss of a CH_2 unit which was localized as a substitution of glycine instead of alanine. The presence of β-alanine can be confirmed by a small fragment formed from β-alanine and ornithine (*m/z* 145.0972) residues, which exists for MS/MS spectra of both **1** and **6**. Alanine however, is replaced by glycine which is indicated by a very dominant key fragment (*m/z* 129.0659) that only occurs during fragmentation of **6** but not for **1**. *Vice versa*, the corresponding alanine fragment (*m/z* 143.0815) can only be detected during fragmentation of **1** but not for **6**.

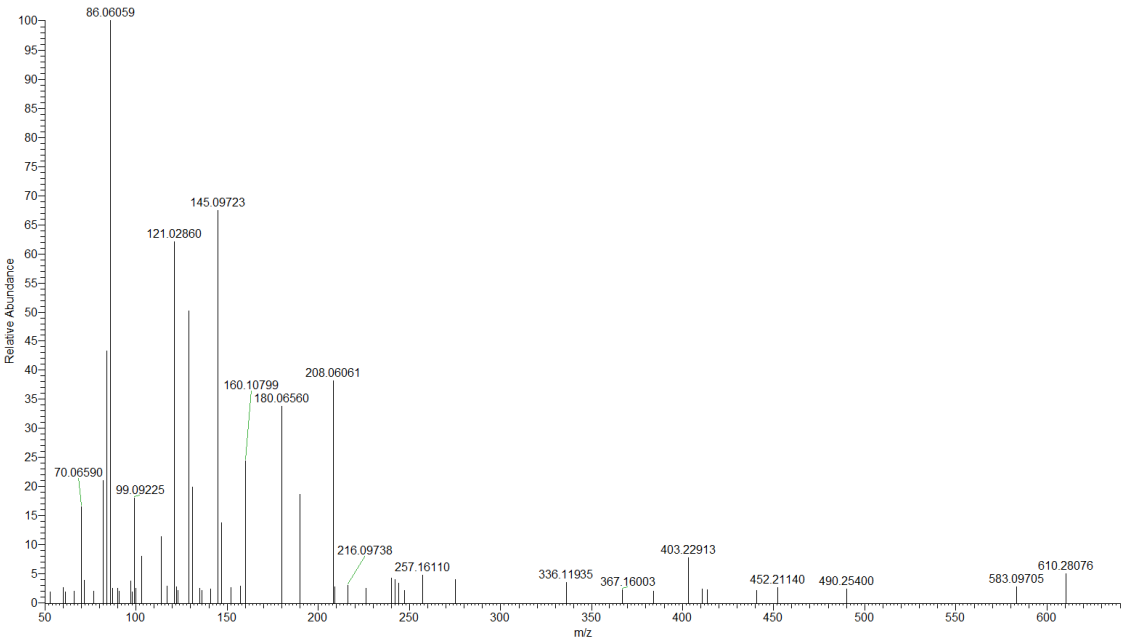

Figure S18. MS^2 spectrum of **6** at *m/z* 610.2829 $[M+H]^+$ ($C_{26}H_{40}N_7O_{10}^+$, calcd. 610.2831).

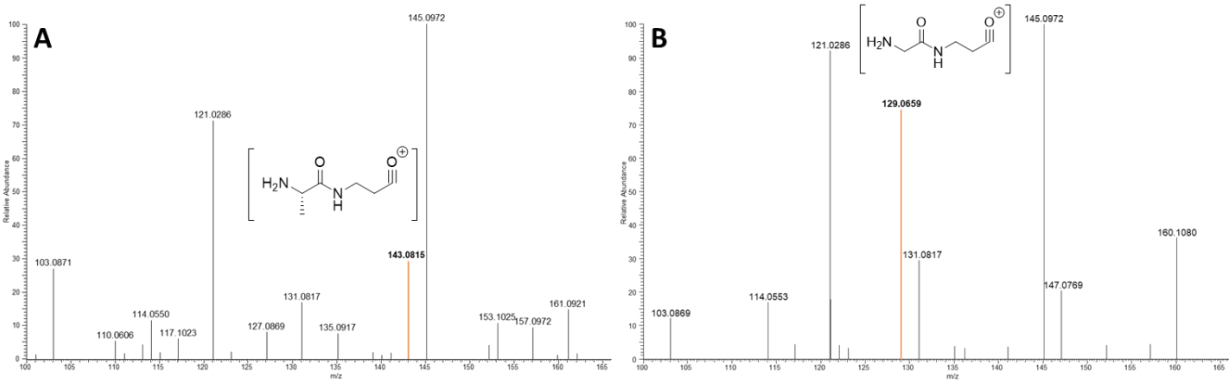

Figure S19. Comparison of partial MS^2 of **1** (**A**) and **6** (**B**) used for confirmation of an alanine to glycine substitution. Corresponding unique key fragments *m/z* 143.0815 (**1, A**) and *m/z* 129.0659 (**6, B**) are highlighted in red.

Structure prediction of derivative 7 with an *m/z* 640.2933

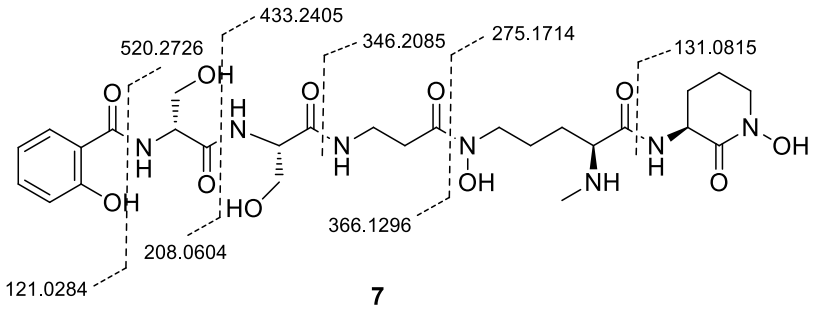

Figure S20. Proposed structure of **7** based on MS^2 fragmentation.

Compound **7** with HRESI-MS *m/z* $[M+H]^+$ 640.2947 is assigned the chemical formula $C_{27}H_{41}N_7O_{11}$, ($C_{27}H_{42}N_7O_{11}^+$,calcd. 640.2937). Fragments with *m/z* 121.0286, 180.0654 and 208.0604 occur in MS/MS spectra for both compounds (**7** and **1**) and confirm the intact salicylic acid and first serine moiety. Fragments found in both spectra with *m/z* 346.2085 and 275.1712 represent moieties carrying hydroxylated ornithine, *N*-methyl ornithine and β-alanine, respectively. In contrast to the spectra of **1**, the MS/MS spectra of **7** features new fragments corresponding to parts of the parent ion containing an additional serine moiety in place of alanine. Accordingly, those fragments are consequently shifted by Δ *m/z* = 15.995 (Oxygen) compared to their counterparts found in **1** (e.g. *m/z* 504.2777→520.2690, 417.2457→433.2440, 448.2199→464.2101 and 143.0815→159.0765). The location of oxygen changing the alanine (**1**) into a serine (**7**) was determined based on comparison of key fragments *m/z* 161.0921 unique for MS/MS of **1** and *m/z* 177.0865 unique for MS/MS of **7**.

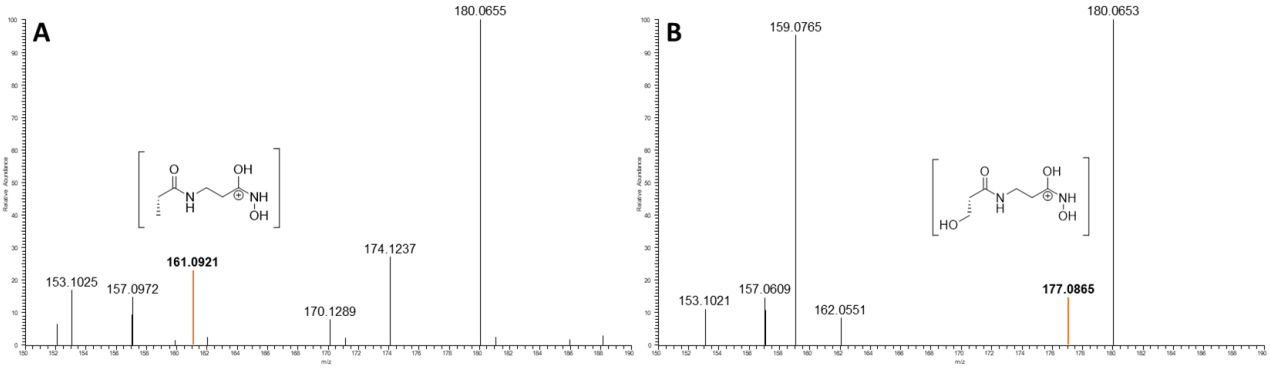

Figure S21. Comparison of partial MS^2 of **1** (**A**) and **7** (**B**) used for confirmation of an alanine to serine substitution. Corresponding unique key fragments *m/z* 161.0921 (**1, A**) and *m/z* 177.0865 (**7, B**) are highlighted in red.

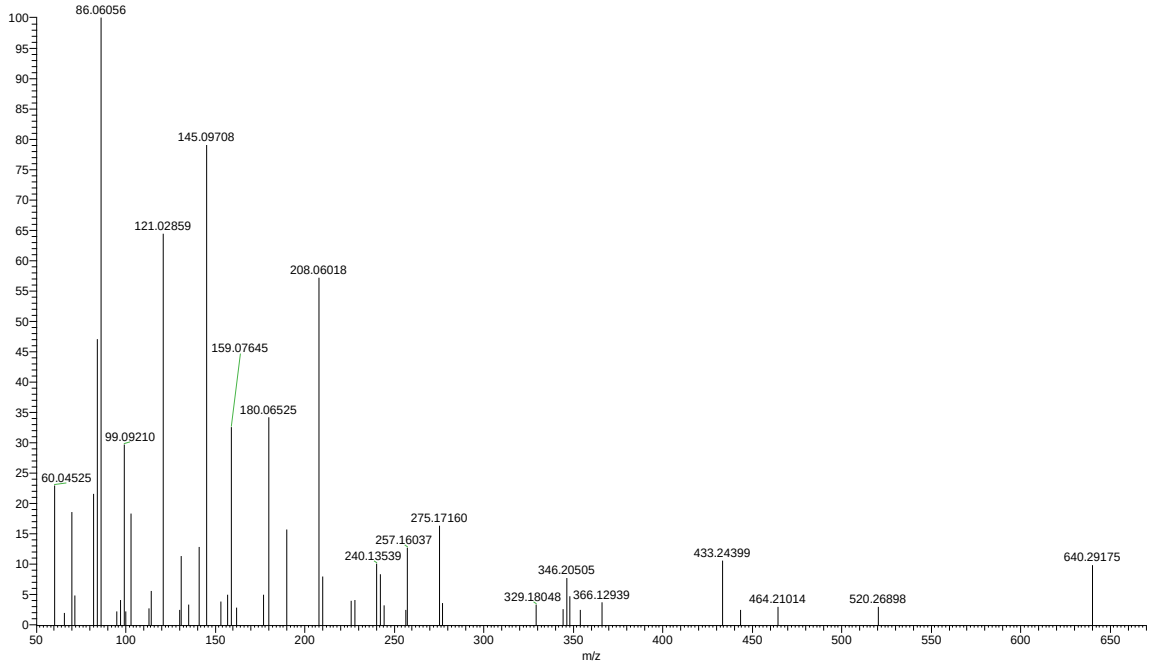

Figure S22. MS^2 spectrum of **7** at *m/z* 640.2947 $[M+H]^+$ ($C_{27}H_{42}N_7O_{11}^+$, calcd. 640.2937).

9. Marfey`s analysis

Determination of the absolute configuration of amino acids of compound 1 (Marfey's Derivatization Reaction).

Compound **1** (0.3 mg) was hydrolyzed with 6 N HCl (500 µL) for 1 h at 110 °C. After cooling to room temperature, the hydrolysate of **1** was evaporated *in vacuo* to eliminate traces of HCl. Distilled water (400 µL) was added to the hydrolysate mixture and then evaporated to remove traces of HCl; this procedure was carried out three times. The dried hydrolysate mixture of **1**, as well as the standard amino acids (L/D-Ala, Orn, and Ser, and *N*-Me-L-Orn), were dissolved in 1 N $NaHCO_3$ (100 µL) and then reacted with 50 µL of L-FDAA (10 mg/mL in acetone). Each hydrolysate was heated for 10 min at 80°C. Each mixture was quenched with 2 N HCl (50 µL) and evaporated *in vacuo*. The residue was dissolved in 200 µL of MeOH. Each aliquot (5 µL) acquired from the hydrolysate mixtures was directly injected onto the LC/MS (Phenomenex Luna C18, 4.6 × 100 mm, 3.5 µm, flow rate: 0.3 mL/min), and a full scan in negative ion mode (scan range from *m*/*z* 100 to 1200) was applied to confirm the retention times of the L-FDAA-derivatized amino acids. The mobile phase, consisting of formic acid in distilled water (0.1% *v*/*v*) (A) and acetonitrile (B), was performed with a gradient solvent system as follows: 20–40% (B) for 10 min, 100% (B) isocratic for 5 min, and then 20% (B) isocratic for 5 min, to conduct a post-run washing procedure for the column. The retention times of the L-FDAA derivatized amino acids used as standards were 18.2 min (L-Ala, *m*/*z* 340 $[M-H]^-$), 20.2 min (D-Ala, *m*/*z* 340 $[M-H]^-$), 25.4 min (L-Orn, *m*/*z* 635 $[M-H]^-$), 24.0 min (D-Orn, *m*/*z* 635 $[M-H]^-$), 14.9 min (L-Ser, *m*/*z* 357 $[M-H]^-$), 20.7 min (D-Ser, *m*/*z* 357 $[M-H]^-$), and 25.8 min (*N*-Me-L-Orn, *m*/*z* 649 $[M-H]^-$), The retention times of the derivatized hydrolysate of **1** were L-Ala (18.2 min), L-Orn (25.4 min), D-Ser (20.7 min), and *N*-Me-L-Orn (25.8 min).

Determination of the Absolute Configuration of Amino Acids in 5 (Marfey's Derivatization Reaction).

Ga-complex of **5** (0.1 mg) was hydrolyzed in 6N HCl (500 µL) for 5 h at 90 ºC. After cool down at room temperature, the hydrolysate mixture was diluted by H_2O (5 mL) and residue HCl was removed under reduced pressure. The trace HCl was removed by repeated the procedure (5 mL of H_2O) for three times. Afterwards, the hydrolysate was lyophilized for 30 min. Marfey's reaction was performed by adding 100 µL of 1 M of $NaHCO_3$ aq. solution, as well as 50 µL of L-FDAA in acetone as 10 mg/mL (fresh preparation), and the mixture was heated at 50 ºC for 45 min under shaking at 600 rpm. The reaction was quenched by adding 40 µL of 2 N HCl aq. solution, adjust the pH at 7. Neutralized reaction mixture was diluted by 1:1 v/v of 50% MeCN/H_2O (LCMS grade). The final mixture was diluted with 1:100 in 50% MeCN/H_2O and ready for LC-HRMS analysis. 0.1 mg of standard amino acids: L-serine, D-serine, L-alanine, D-alanine, ß-alanine, L-ornithine, D-ornithine were subjected to Marfey's reaction by the same procedure as described above.

LC-ESI-HRMS were performed on a Dionex Ultimate3000 system coupled with a Luna Omega C18 column (100 × 2.1 mm, particle size 1.6 µm, pore diameter 100 Å, Phenomenex) combined with Q-Exactive Plus mass spectrometer (Thermo Scientific) equipped with an electrospray ion (HESI) source.

Column oven was set to 40 °C; scan range of full MS was set to *m/z* 150 to 2,000 with resolution of 70,000 and AGC target 3e6 and maximum IT 100 ms under positive and negative mode with centroid data type. MS^2 was performed to choose top10 intensive ions under positive mode with resolution of 17,500 and AGC target 1e5 and maximum IT 50 ms and (N)CE 28 with centroid data type. The spray voltage (+) was set to 4000 Volt, and (–) was set to 3300 Volt. The capillary temperature (+/–) was set to 340 °C and probe heater temperature (+/–) was set to 200 °C. The sheath gas flow (+–) was set to 35 L/min and Aux gas flow (+/–) to 5 L/min. Max spray current (+) and (–) was set to 100 Volt. S-Lens RF level was set to 50. The FDAA derivatives were separated under the gradient: 0 – 0.5 min, 5% B; 0.5 – 9 min, 5% – 97% B; 9 – 12 min, 97% B; 12 – 13 min, 97% – 5% B; 13 – 18 min, 5% B (A: 0.1% FA; B: MeCN with 0.1% FA), with flow rate of 0.3 mL/min and injection volume is 5 µL. The retention times of the L-FDAA derivatized amino acids used as standards were 5.94 min (L-Ala, *m/z* 342.1038 $[M+H]^+$), 6.23 min (D-Ala, *m/z* 342.1038 $[M+H]^+$), 5,91 min (ß-Ala, *m/z* 342.1038 $[M+H]^+$), 4.72 min/4.89 min (L-Orn, *m/z* 385.1461 $[M+H]^+$), 4.58 min/4.89 min (D-Orn, *m/z* 385.1461 $[M+H]^+$), 5.36 min (L-Ser, *m/z* 358.0987 $[M+H]^+$), 5.42 min (D-Ser, *m/z* 358.0987 $[M+H]^+$). The retention times of the derivatized hydrolysate of **5** were L-Ala (5.94 min), ß-Ala (5.91 min), L-Orn (4.72 min), D-Ser (5.42 min).

10. Physical data of isolated compounds

Madurastatin A2 (**1**). Amorphous powder; $[\alpha]^{25,D}$ -12.1 (*c* 0.05, MeOH); UV (MeOH) λ_{max} (log ε) 202 (4.23), 238 (1.31), 299 (0.76) nm; ^{1}H (800 MHz) and ^{13}C NMR (200 MHz), see Table S4 and Table S5, respectively; positive-mode HR-ESI-MS *m/z* 624.3022 $[M+H]^+$ (Calcd. for $C_{27}H_{42}N_7O_{10}^+$, 624.2993).

Madurastatin E1 (**2**). Amorphous powder; $[\alpha]^{25,D}$ -8.6 (*c* 0.04, MeOH); UV (MeOH) λ_{max} (log ε) 202 (4.20), 238 (1.25), 299 (0.73) nm; ^{1}H (800 MHz) and ^{13}C NMR (200 MHz), see Table S4 and Table S5, respectively; positive-mode HR-ESI-MS *m/z* 636.3017 $[M+H]^+$ (Calcd. for $C_{28}H_{42}N_7O_{10}^+$, 636.2993).

Madurastatin F (**3**). Amorphous powder; $[\alpha]^{25,D}$ -6.4 (*c* 0.03, MeOH); UV (MeOH) λ_{max} (log ε) 202 (4.25), 239 (1.24), 298 (0.76) nm; ^{1}H (800 MHz) and ^{13}C NMR (200 MHz), see Table S4 and Table S5, respectively; negative-mode HR-ESI-MS *m/z* 605.2568 $[M-H]^-$ (Calcd. for $C_{27}H_{37}N_6O_{10}^-$, 605.2571).

Madurastatin G1 (**4**). Amorphous powder; $[\alpha]^{25,D}$ -7.7 (*c* 0.03, MeOH); UV (MeOH) λ_{max} (log ε) 202 (4.09), 239 (1.15), 298 (0.74) nm; ^{1}H (800 MHz) and ^{13}C NMR (200 MHz), see Table S4 and Table S5, respectively; positive-mode HR-ESI-MS *m/z* 368.1451 $[M+H]^+$ (Calcd. for $C_{16}H_{22}N_3O_7^+$, 368.1458).

Madurastatin A1 (**5**, Ga^{3+}-complex). Orange powder; $[\alpha]^{25,D}$ 269.2 (*c* 0.01, 50% MeOH); UV (MeOH) λ_{max} (log ε) 202, 239, 298 nm; ^{1}H (600 MHz) and ^{13}C NMR (150 MHz), see Table S6; positive-mode HR-ESI-MS *m/z* 672.1891 $[M+H]^+$ (Calcd. for $C_{27}H_{37}N_7O_9Ga^+$, 672.1909).

11. Analytical Data

Table S4. ^{1}H NMR (800 MHz) data of compounds **1–4** in MeOH-d_4.[a]

Position	**1**	**2**	**3**	**4**
	δ_H	δ_H	δ_H	δ_H
1	7.91 dd (7.5, 1.0)	7.90 dd (7.5, 1.0)	7.90 dd (7.5, 1.0)	7.90 dd (7.5, 1.0)
2	6.92 t (7.5)	6.92 t (7.5)	6.92 t (7.5)	6.92 t (7.5)
3	7.39 t (7.5)	7.39 t (7.5)	7.39 t (7.5)	7.39 t (7.5)
4	6.93 dd (7.5, 1.0)	6.93 dd (7.5, 1.0)	6.93 dd (7.5, 1.0)	6.93 dd (7.5, 1.0)
8	4.59 dd (5.0, 4.5)	4.59 dd (5.0, 4.5)	4.59 dd (5.0, 4.5)	4.58 dd (5.0, 4.5)
9	3.90 dd (11.0, 4.5), 3.95 dd (11.0, 5.0)	3.89 dd (11.0, 4.5), 3.94 dd (11.0, 5.0)	3.88 dd (11.0, 4.5), 3.92 dd (11.0, 5.0)	3.90 dd (11.0, 4.5), 3.95 dd (11.0, 5.0)
11	4.32 q (7.0)	4.33 q (7.0)	4.34 q (7.0)	4.36 q (7.0)
12	1.38 d (7.0)	1.37 d (7.0)	1.37 d (7.0)	1.36 d (7.0)
14	3.43 m, 3.49 m	3.45 m	3.45 m	3.40 m, 3.43 m
15	2.54 m	2.70 m	2.69 m	2.46 t (6.5)
17	3.61 m	3.57 m, 3.61 m	3.54 m, 3.59 m	
18	1.75 m	1.78 m	1.37 m, 1.42 m	
19	1.77 m	1.96 m	1.59 m	
20	3.56 m	3.05 m	2.21 m	
23	4.50 m	4.66 m	4.21 m	
24	1.84 m. 2.07 m	1.93 m, 2.32 m	1.96 m, 2.11 m	
25	1.98 m, 2.03 m	2.02 m, 2.06 m	1.76 m, 2.37 m	
26	3.59 m, 3.64 m	3.58 m, 3.65 m	5.75 brs	
1'	2.55 s	2.41 s	2.94 s	
2'		3.77 d (4.0), 4.34 d (4.0)		

[a] Coupling constants (in parentheses) are in Hz.

Table S5. ^{13}C NMR (200 MHz) data of compounds **1**–**4** in MeOH-d_4.[a]

Position	**1**	**2**	**3**	**4**
	Δc	δc	δc	δc
1	130.1 d	130.0 d	130.1 d	130.0 d
2	120.1 d	120.1 d	120.1 d	120.1 d
3	134.6 d	134.6 d	134.7 d	134.7 d
4	117.8 d	117.9 d	118.0 d	117.9 d
5	160.1 s	159.9 s	160.1 s	160.0 s
6	117.5 s	117.6 s	117.6 s	117.5 s
7	170.1 s	169.9 s	170.0 s	170.1 s
8	57.1 d	57.1 d	57.1 d	57.2 d
9	62.5 t	62.6 t	62.7 t	62.7 t
10	172.7 s	172.5 s	172.7 s	172.4 s
11	50.5 d	50.5 d	50.5 d	50.4 d
12	17.4 q	17.4 q	17.5 q	17.6 q
13	174.7 s	174.5 s	174.7 s	174.6 s
14	36.1 t	36.1 t	36.2 t	36.6 t
15	32.6 t	32.6 t	32.7 t	35.5 t
16	173.9 s	173.3 s	173.7 s	176.6 s
17	47.7 t	48.4 t	48.1 t	
18	22.6 t	22.8 t	21.3 t	
19	28.9 t	25.8 t	26.6 t	
20	62.8 d	67.1 d	36.7 t	
21	174.1 s	175.6 s	168.9 s	
22	165.5 s	164.7 s	165.1 s	
23	51.2 d	52.4 d	62.2 d	
24	28.1 t	29.1 t	27.3 t	
25	21.4 t	21.7 t	29.5 t	
26	52.2 t	52.0 t	82.0 d	
1'	32.6 q	39.8 q	31.2 q	
2'		68.0 t		

[a] ^{13}C NMR data extracted from HSQC and HMBC data.

Table S6. NMR Data (DMSO-d_6, at 300 K) for madurastatin A1 (**5**, Ga^{3+}-complex).[a]

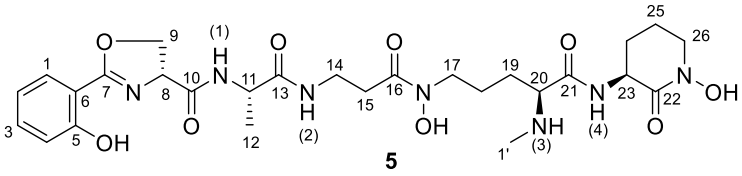

5

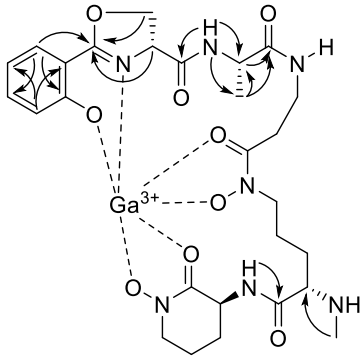

	Madurastatin A1 (**5**, Ga-complex)			
Position	δ_C, mult.[b]	δ_H, mult. (*J* in Hz)	COSY	HMBC
1	129.37, CH	7.55, d (8.51)	2	5, 3, 7
2	114.69, CH	6.56, t (8.17)	3, 5	4, 6
3	135.61, CH	7.32, t (6.77)	2, 4	1
4	122.35, CH	6.62, d (8.83)	3	2, 6
5	167.73, qC			
6	108.44, qC			
7	170.46, qC			
8	64.75, CH	4.98, dd (10.69, 6.90)	9a, 9b	7
9	71.12, CH_2	4.69, d (9.03)	8, 9b	7
		4.43, dd (8.72, 6.54)	8, 9a	7
10	171.61, qC			
11	47.67, CH	4.29, t (7.22)	12, *N*H(1)	13
12	13.81, CH_3	1.13, d (7.27)	11	11, 13
13	172.88, qC			
14	35.74, CH_2	3.42, m	14b, *N*H(2)	
		3.10, m	14a, 15	
15		2.17, m	14b	
16				
17				
18				
19	29.70, CH_2	1.17, m		
20	62.32, CH	2.96, m	19, *N*H(3)	
21	172.25, qC			
22				
23	46.19, CH	4.50, m	24a, *N*H(4)	
24	25.30, m	1.95, m	23	
25		1.67, m		
26				
1’	33.14, CH_3	2.27, s	*N*H(3)	20
*N*H(1)		8.70, d (7.38)	11	10, 11, 12
*N*H(2)		7.40, brt (5.38)	14a	
*N*H(3)		7.22, t (5.55)	1’	
*N*H(4)		8.17, d (9.15)	23	21

[a] 600 MHz for ^{1}H NMR and 150 MHz for ^{13}C NMR

[b] numbers of attached protons were determined by analysis of 2D spectra.

Table S7. NMR Data (CD_3OD, at 300 K) for synthetic salicyl-D-Ser-Ala-ßAla-OH (**4a**) and salicyl-L-Ser-Ala-ßAla-OH (**4b**) [a,b, c]

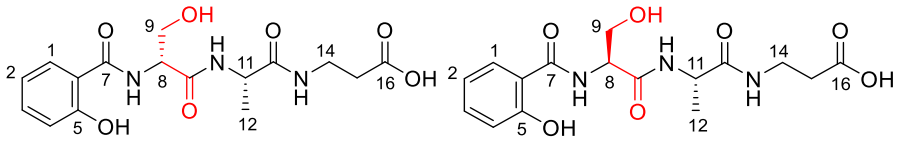

Salicyl-D-Ser-Ala-ßAla-OH (**4a**) Salicyl-L-Ser-Ala-ßAla-OH (**4b**)

	Salicyl-D-Ser-Ala-ßAla-OH (**4a**)				Isolated compound **4**		Salicyl-L-Ser-Ala-ßAla-OH (**4b**)	
position	δ_C, mult.[b]	δ_H, mult. (*J* in Hz)	COSY	HMBC	δ_C, mult.	δ_H, mult. (*J* in Hz)	δ_C, mult.[b]	δ_H, mult. (*J* in Hz)
1	130.24, CH	7.90, dd (8.22, 1.71)	2	3, 5, 7	130.0 d	7.90 dd (7.5, 1.0)	130.31, CH	7.90, dd (8.21, 1.63)
2	118.14, CH	6.93, t (8.25)	1, 3	4	120.1 d	6.92 t (7.5)	118.10, CH	6.93, t (8.25)
3	134.93, CH	7.39, td (8.25, 1.71)	2, 4	1, 5	134.7 d	7.39 t (7.5)	134.89, CH	7.39, td (8.25, 1.71)
4	120.43, CH	6.93, d (8.25)	3	2	117.9 d	6.93 dd (7.5, 1.0)	120.43, CH	6.93, d (8.25)
5	160.14, qC				160.0 s		160.06, qC	
6	117.69, qC				117.5 s		117.74, qC	
7	170.25, qC				170.1 s		169.96, qC	
8	57.50, CH	4.58, t (5.29)	9a	9, 10	57.2 d	4.58 dd (5.0, 4.5)	56.83, CH	4.66, t (5.85)
9	62.92, CH_2	3.94, dd (11.15, 5.37)	8	10	62.7 t	3.95 dd (11.0, 5.0)	63.27, CH_2	3.98, dd (10.98, 5.40)
		3.89, dd (11.15, 5.18)		10		3.90 dd (11.0, 4.5),		3.84, dd (10.88, 6.18)
10	172.68, qC				172.4 s		172.53, qC	
11	50.73, CH	4.35, q (7.23)	12	12, 13	50.4 d	4.36 q (7.0)	50.67, CH	4.38, q (7.23)
12	17.89, CH_3	1.37, d (7.27)	11	13	17.6 q	1.36 d (7.0)	17.81, CH_3	1.38, d (7.19)
13	174.94, qC				174.6 s		174.94, qC	
14	36.49, CH_2	3.42-3.45, m	15	15, 16	36.6 t	3.40 m, 3.43 m	36.51, CH_2	3.42, t (6.96)
15	34.52, CH_2	2.52, t (7.00)	14	16	35.5 t	2.46 t (6.5)	34.54, CH_2	2.51, t (6.90)
16	175.21, qC				176.6 s		175.27, qC	

[a] 600 MHz for ^1H NMR and 150 MHz for ^{13}C NMR. [b] numbers of attached protons were determined by analysis of 2D spectra.

[C] synthesized by BIOSYNTAN GmbH (Robert-Rössle-Str. 10, D-13125 Berlin

.

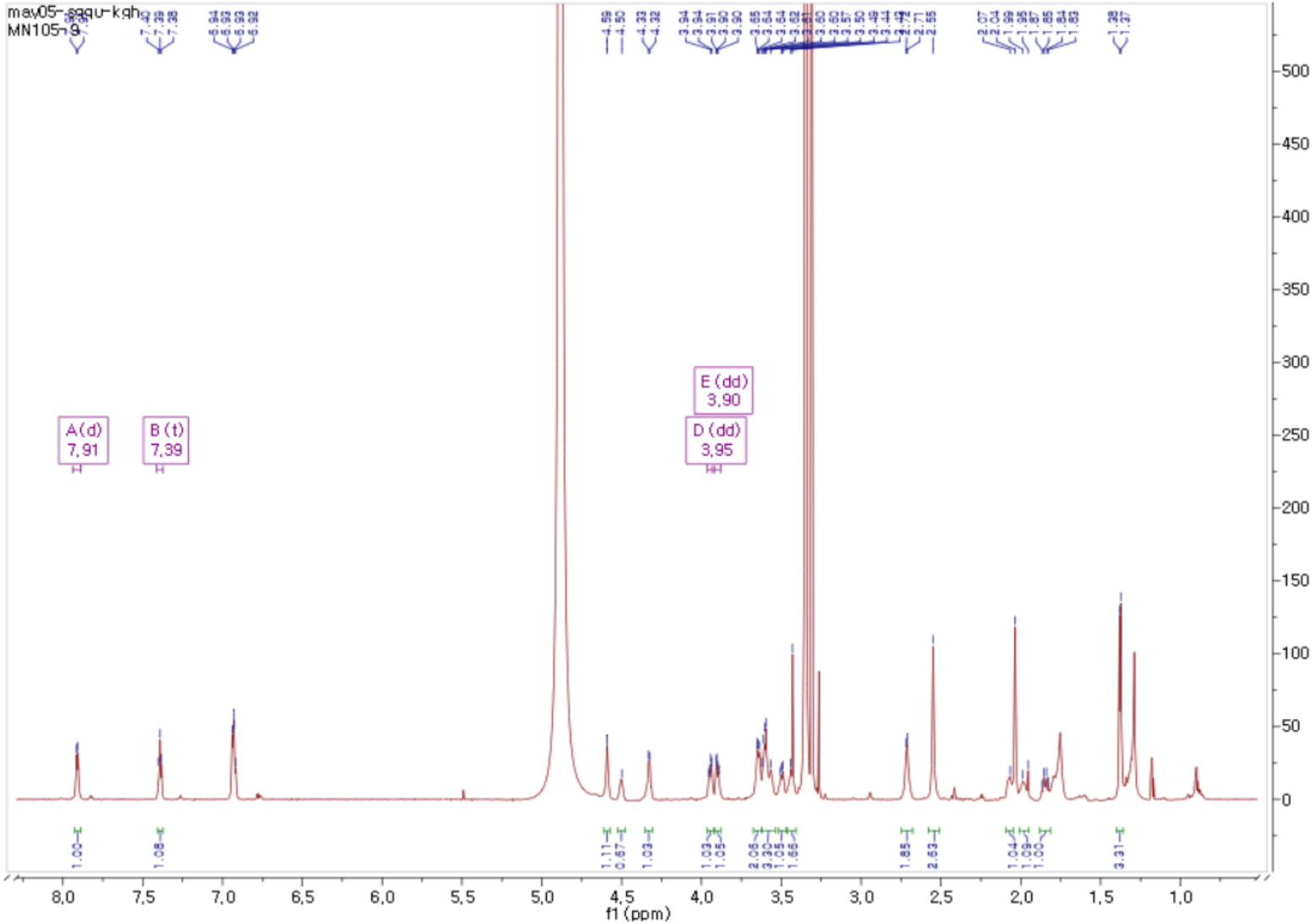

Figure 23. ^{1}H NMR spectrum of madurastatin A2 (**1**) (CD_3OD, 800 MHz)

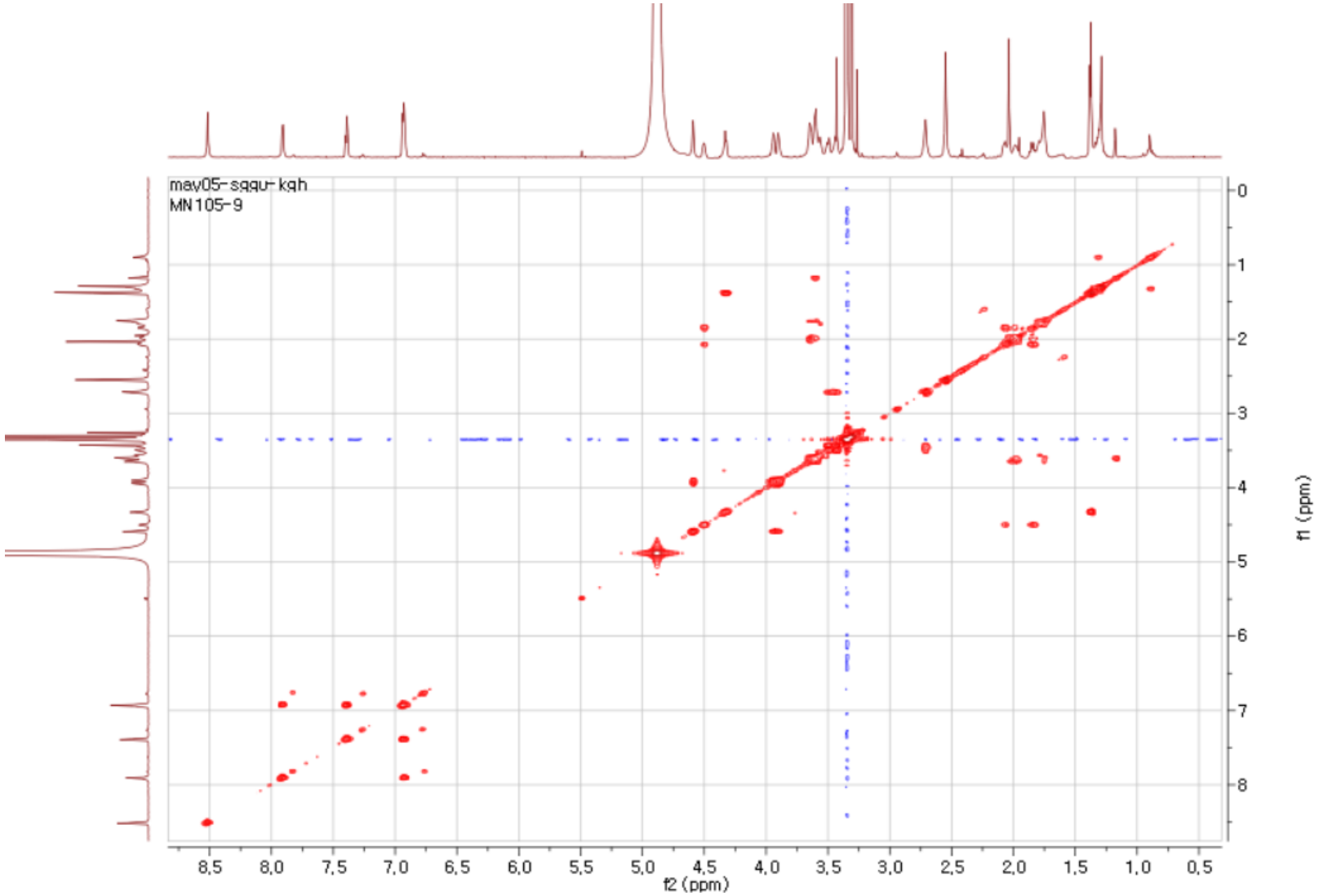

Figure S24. ^{1}H-^{1}H COSY spectrum of madurastatin A2 (**1**) (CD_3OD, 800 MHz)

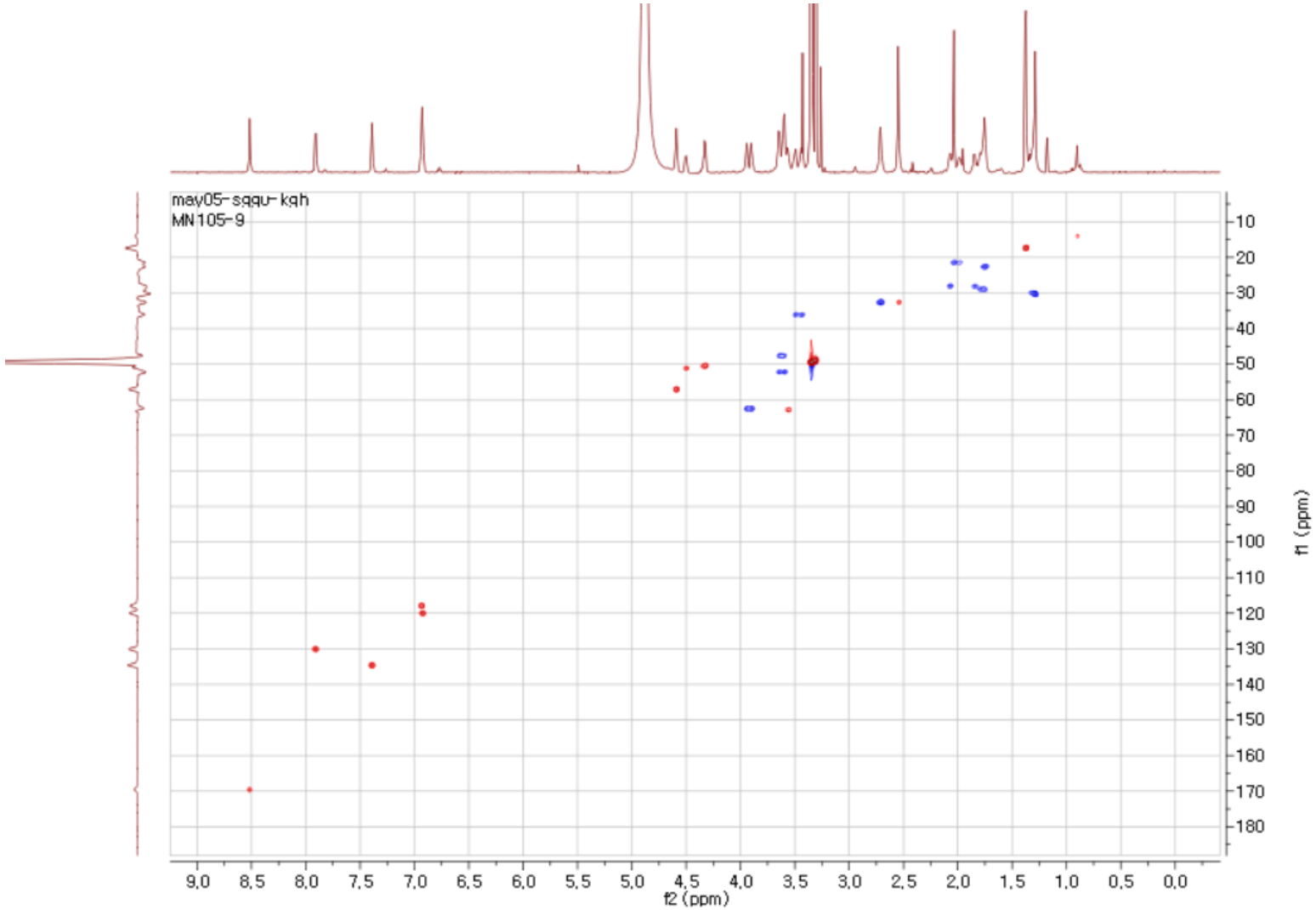

Figure S25. HSQC spectrum of madurastatin A2 (**1**) (CD_3OD, 800 MHz)

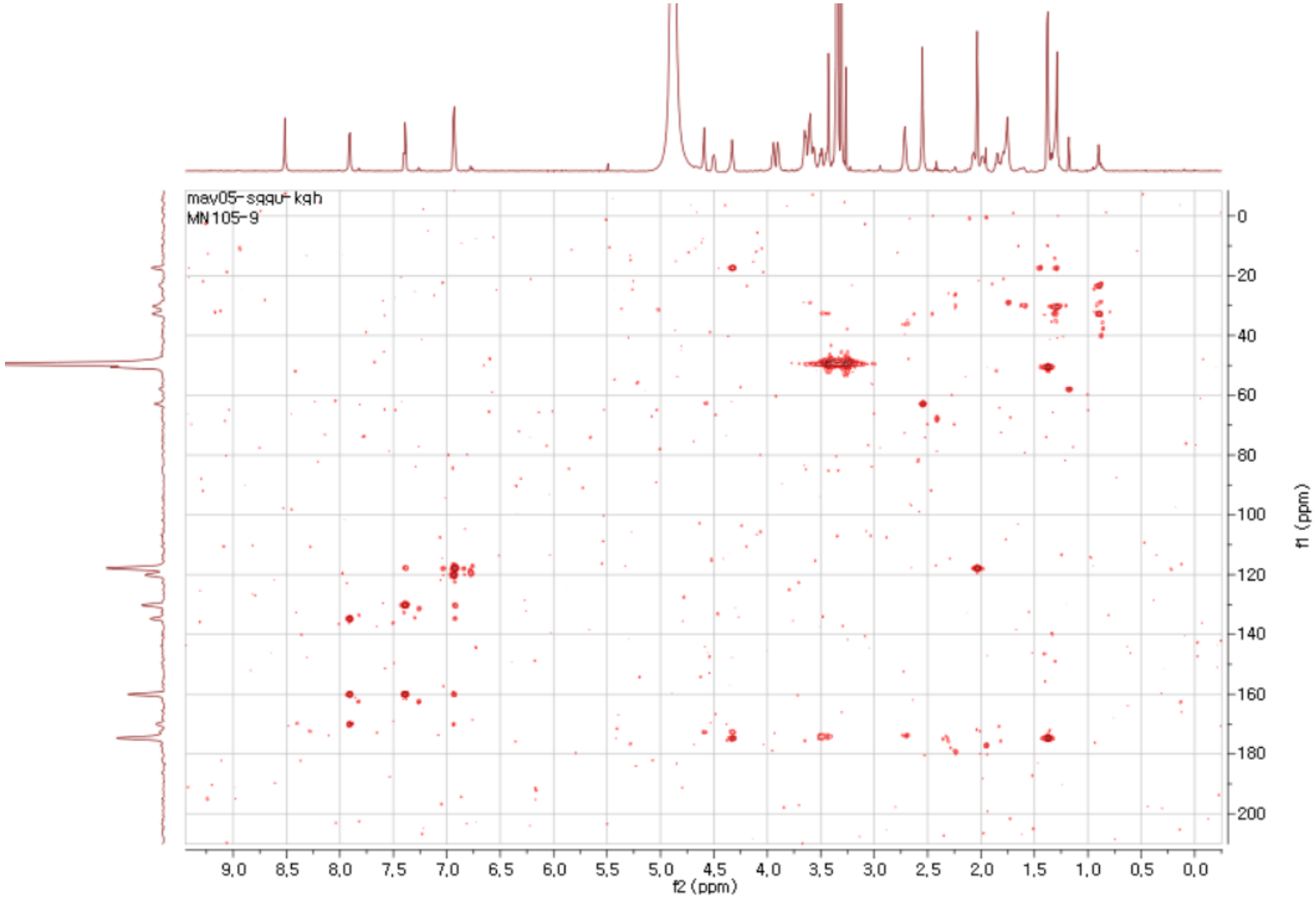

Figure S26. HMBC spectrum of madurastatin A2 (**1**) (CD_3OD, 800 MHz)

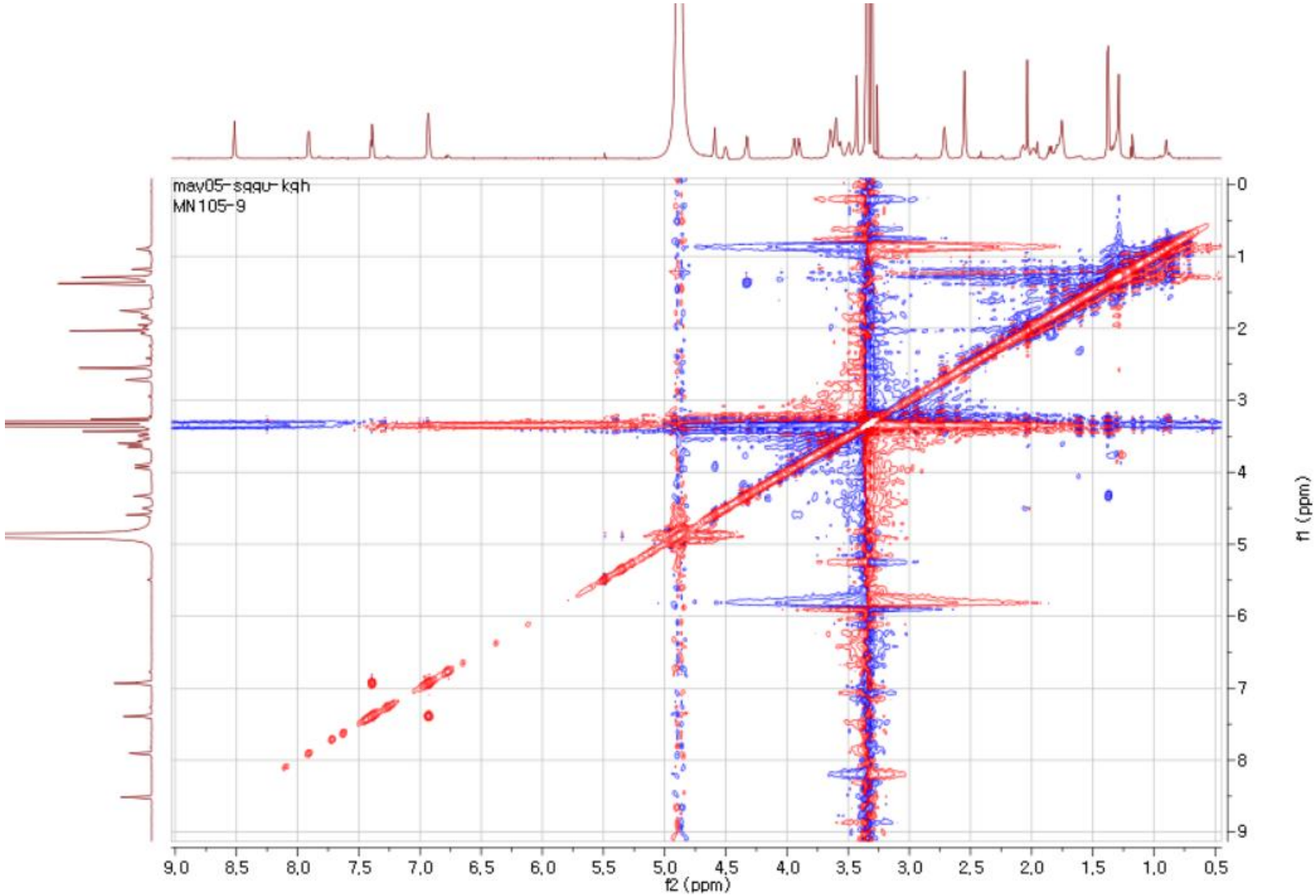

Figure S27. ROESY spectrum of madurastatin A2 (**1**) (CD_3OD, 800 MHz)

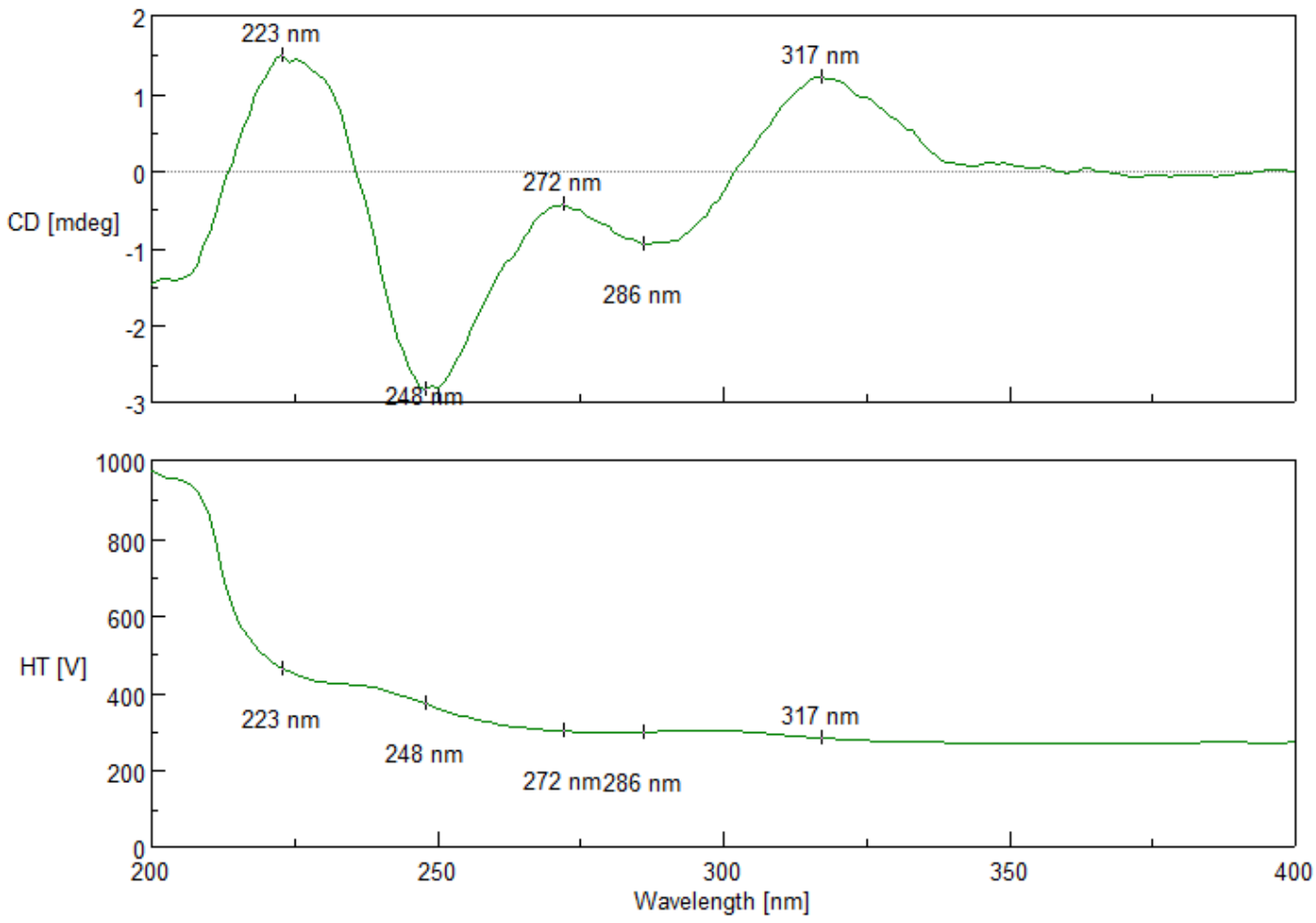

Figure 28. ECD spectrum of madurastatin A2 (**1**) (MeOH)

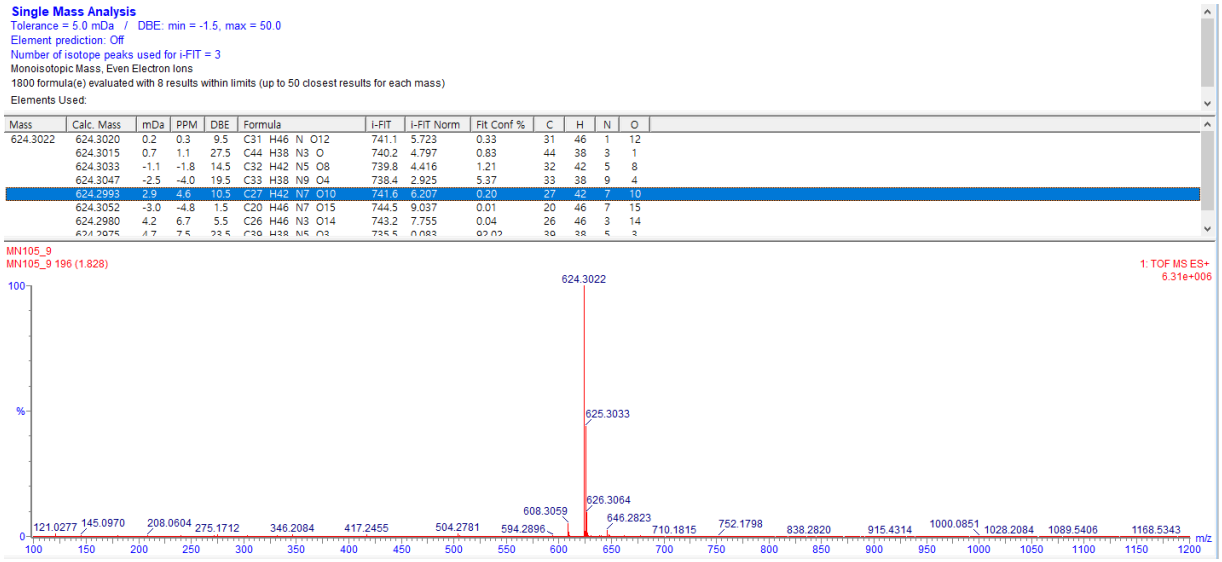

Figure S29. HR-ESIMS spectrum of madurastatin A2 (**1**)

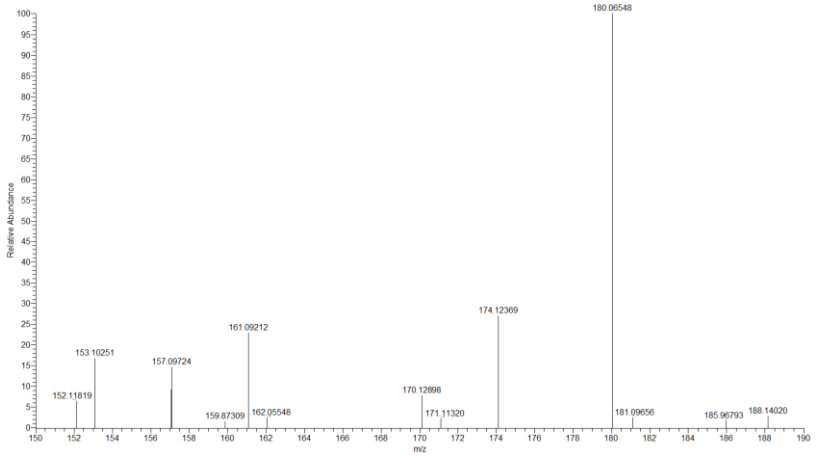

Figure S30. Partial MS^2-spectrum of **1** showing the presence of diagnostic key fragment *m/z* 161.09212 and absence of key fragment *m/z* 177.08647.

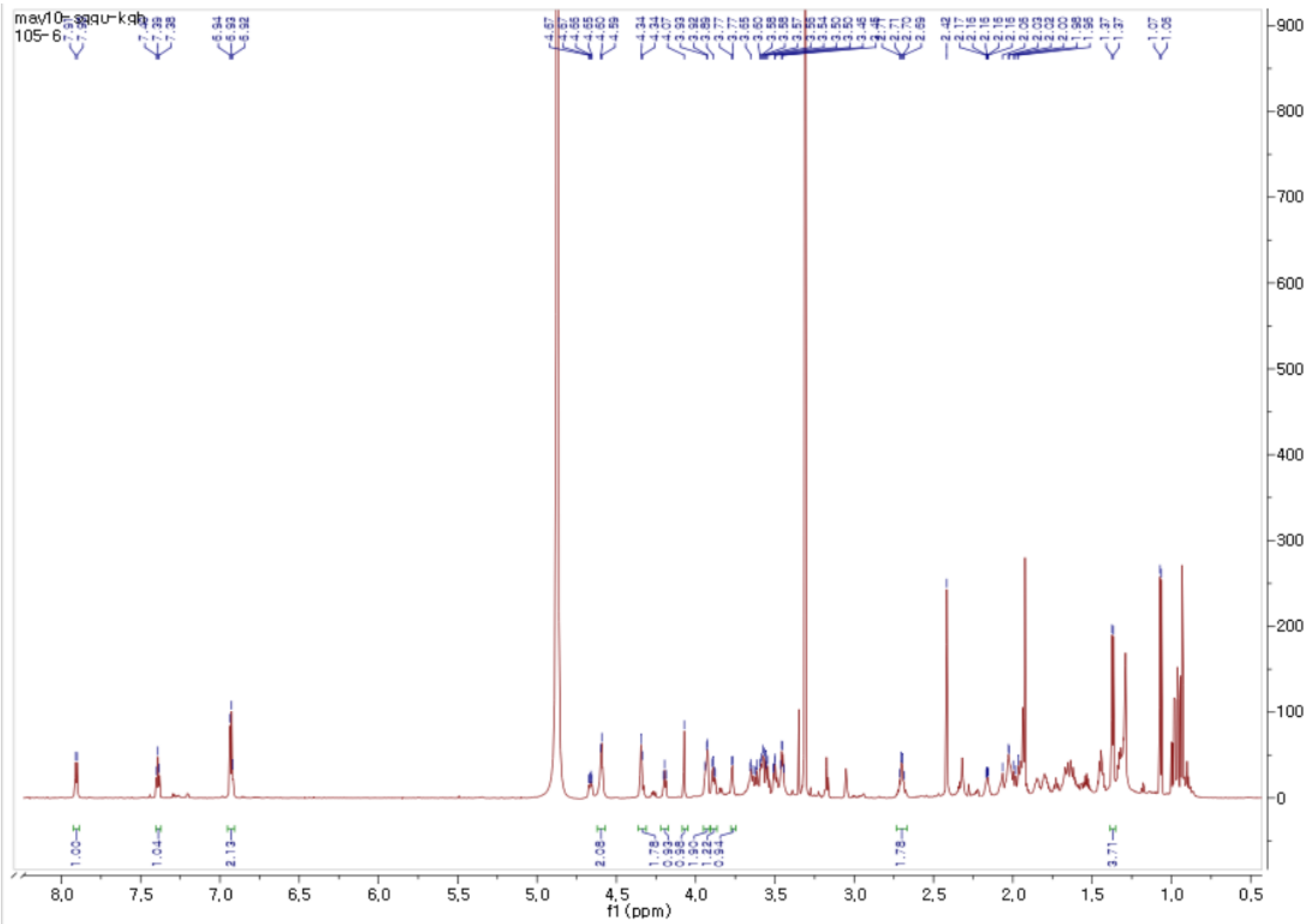

Figure S31. ^{1}H NMR spectrum of madurastatin E1 (**2**) (CD_3OD, 800 MHz)

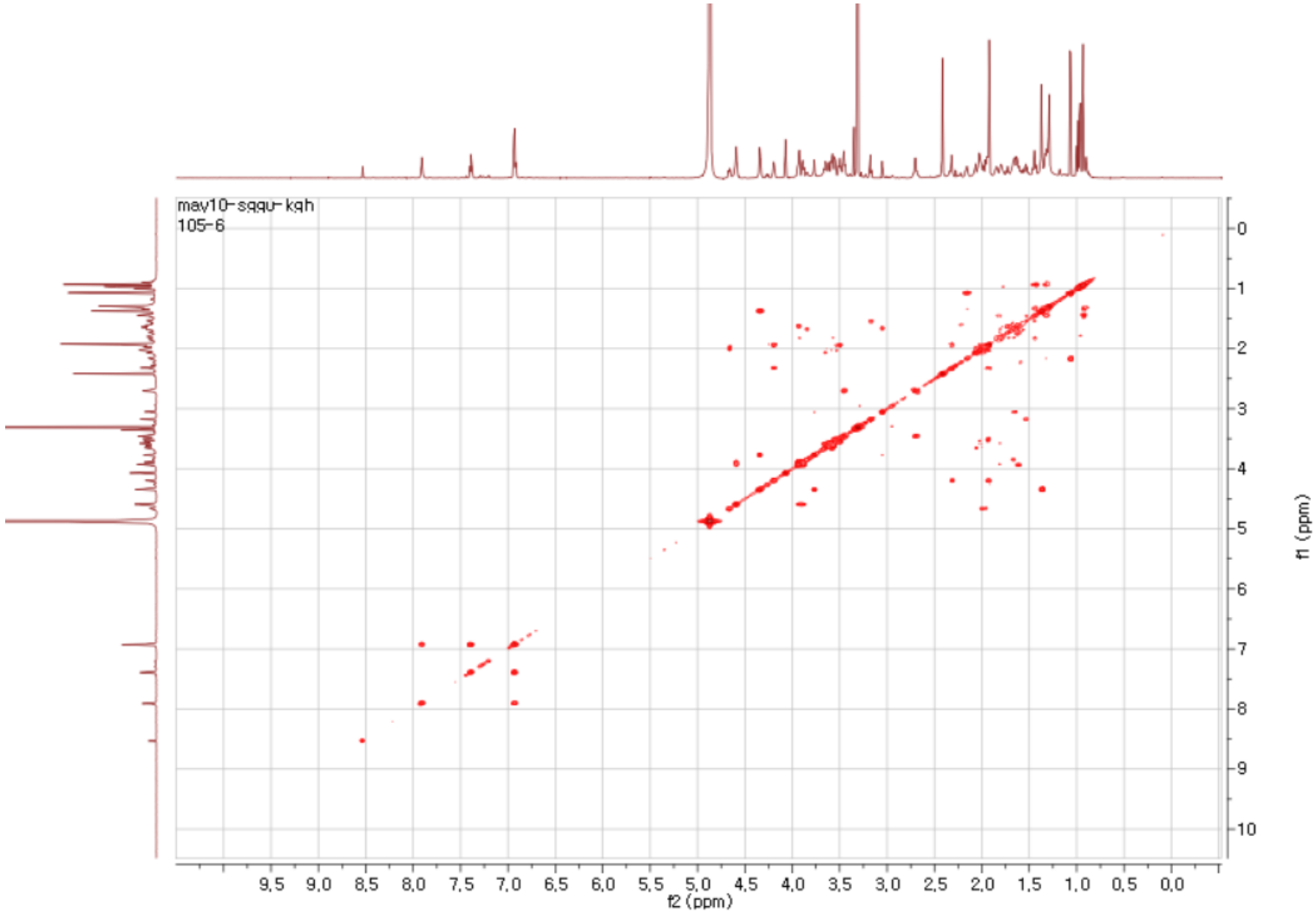

Figure S32. ^{1}H-^{1}H COSY spectrum of madurastatin E1 (**2**) (CD_3OD, 800 MHz)

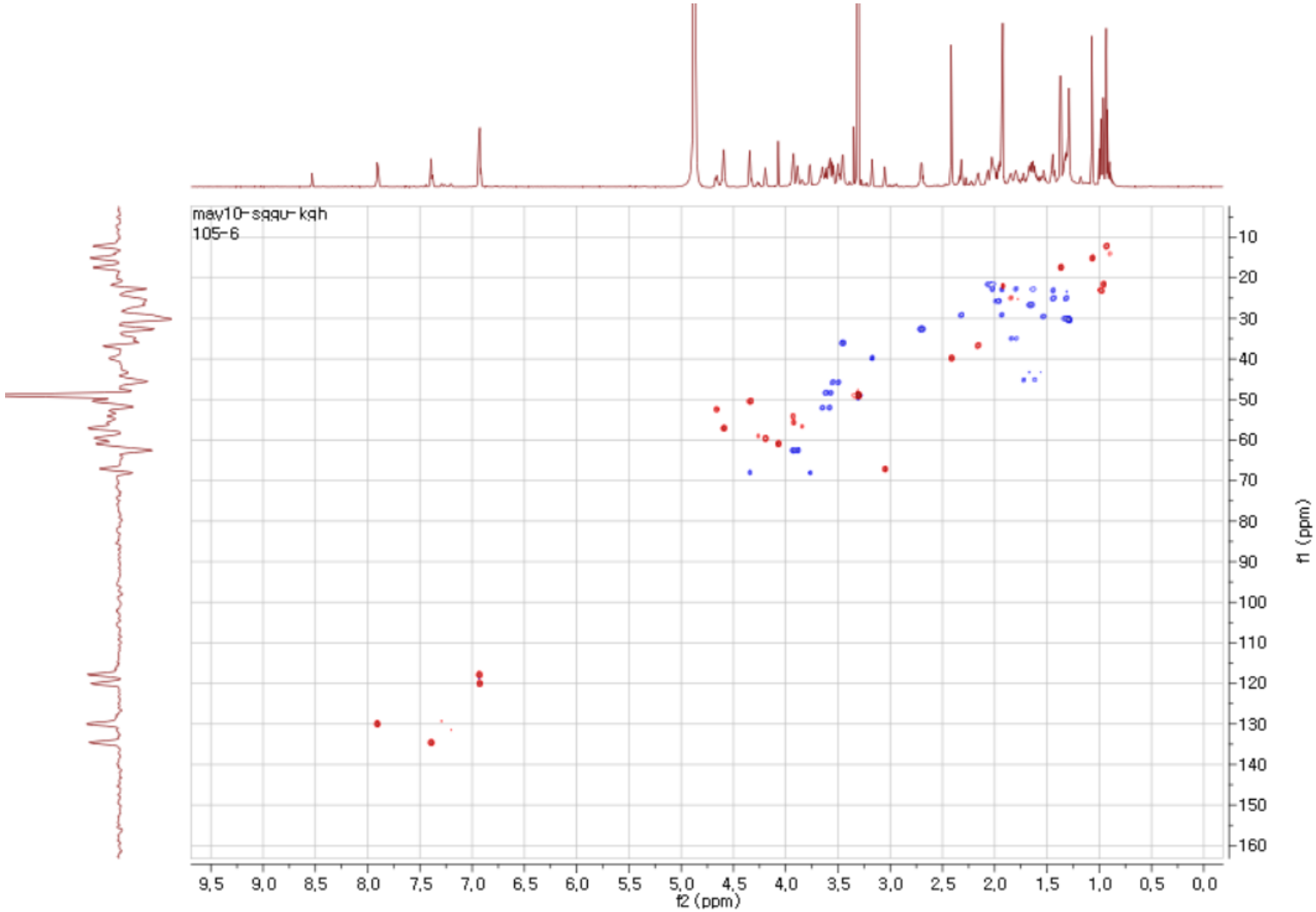

Figure S33. HSQC spectrum of madurastatin E1 (**2**) (CD_3OD, 800 MHz)

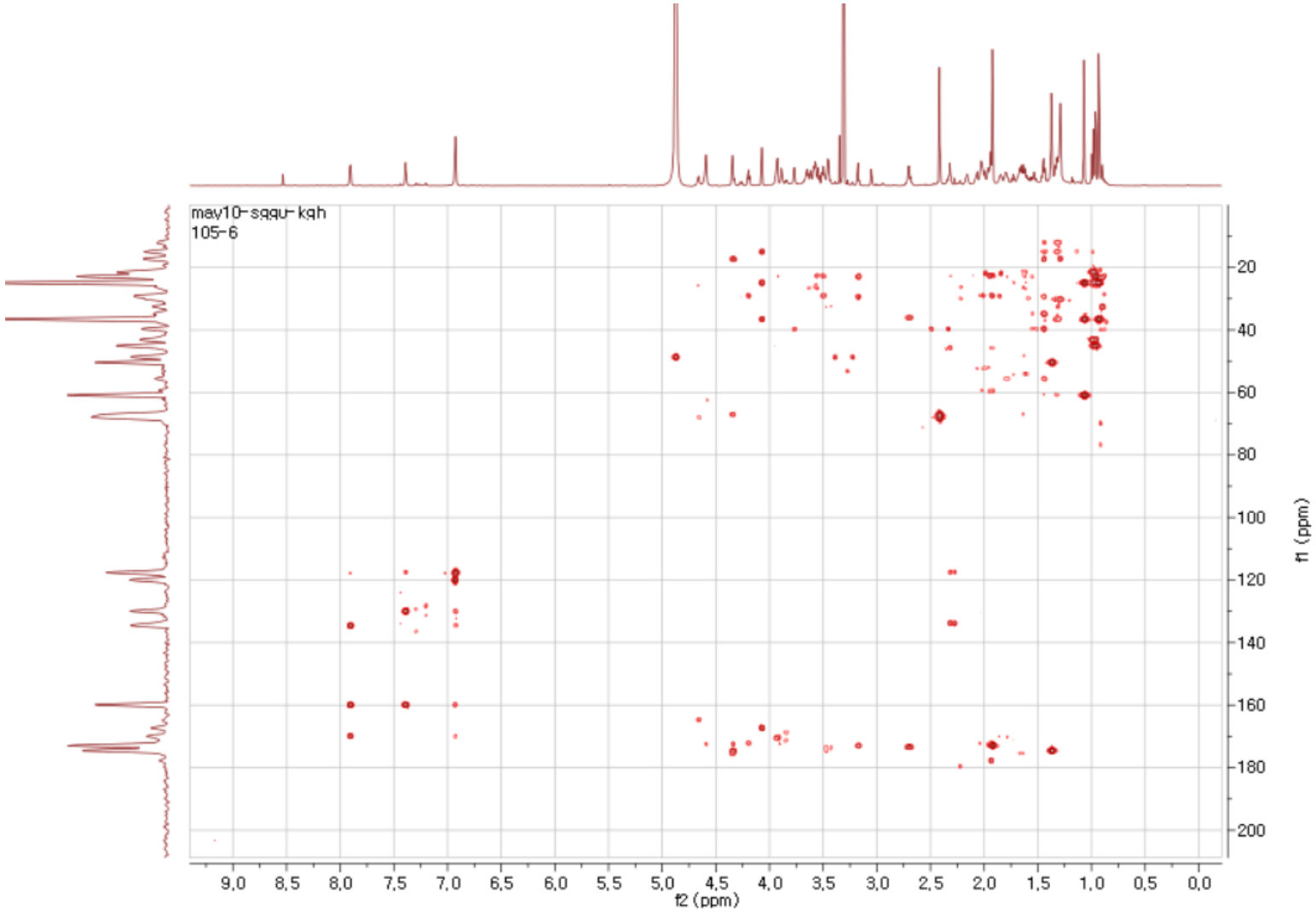

Figure S34. HMBC spectrum of madurastatin E1 (**2**) (CD_3OD, 800 MHz)

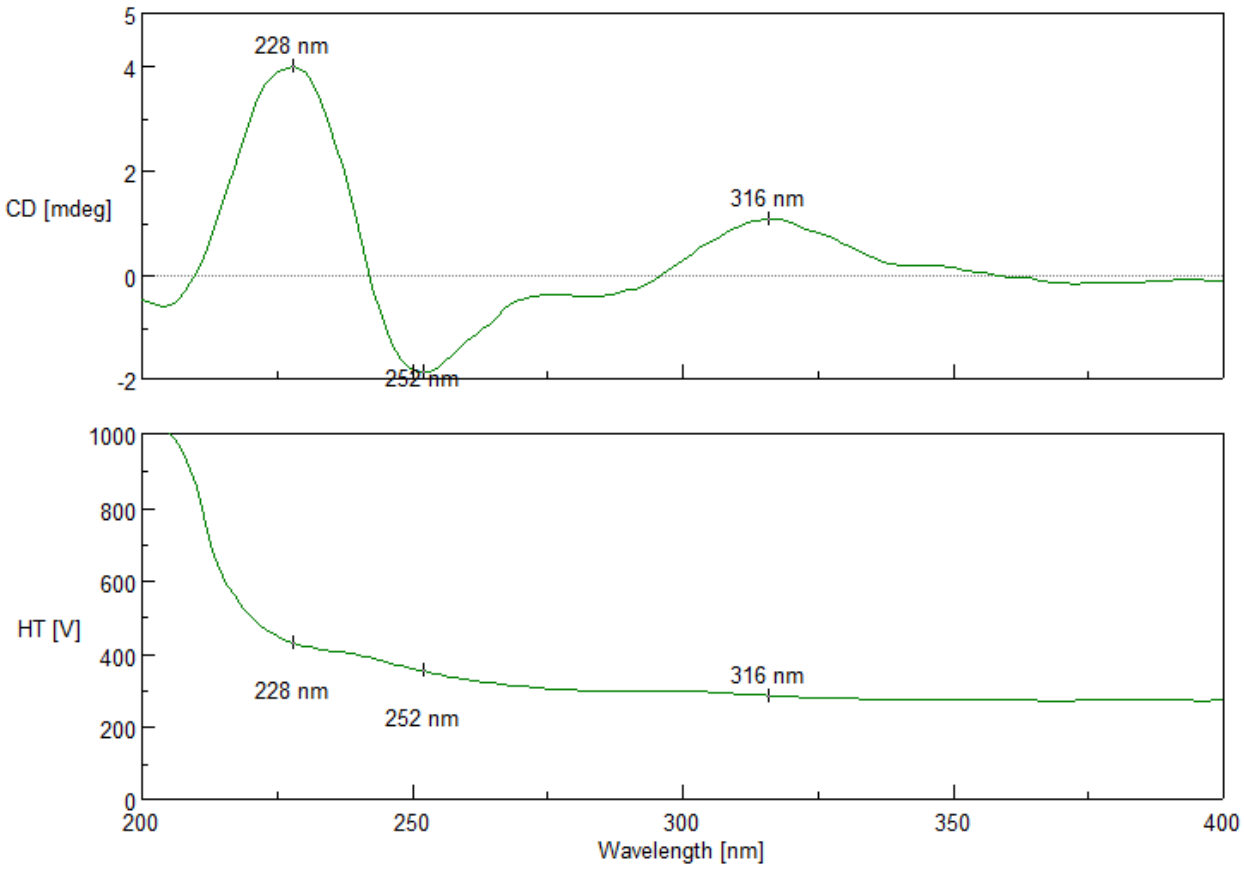

Figure S35. ECD spectrum of madurastatin E1 (**2**) (MeOH)

Single Mass Analysis
Tolerance = 5.0 mDa / DBE: min = -1.5, max = 50.0
Element prediction: Off
Number of isotope peaks used for i-FIT = 3
Monoisotopic Mass, Even Electron Ions
1865 formula(e) evaluated with 9 results within limits (up to 50 closest results for each mass)
Elements Used:

Mass	Calc. Mass	mDa	PPM	DBE	Formula	i-FIT	i-FIT Norm	Fit Conf %	C	H	N	O
636.3017	636.3015	0.2	0.3	28.5	C45 H38 N3 O	708.4	8.053	0.03	45	38	3	1
	636.3020	-0.3	-0.5	10.5	C32 H46 N O12	706.1	5.755	0.32	32	46	1	12
	636.3012	0.5	0.8	-1.5	C16 H46 N9 O17	710.0	9.589	0.01	16	46	9	17
	636.3033	-1.6	-2.5	15.5	C33 H42 N5 O8	704.1	3.784	2.27	33	42	5	8
	636.2993	2.4	3.8	11.5	C28 H42 N7 O10	706.9	6.570	0.14	28	42	7	10
	636.3047	-3.0	-4.7	20.5	C34 H38 N9 O4	700.4	0.031	96.93	34	38	9	4
	636.3052	-3.5	-5.5	2.5	C21 H46 N7 O15	711.0	10.626	0.00	21	46	7	15
	636.2980	3.7	5.8	6.5	C27 H46 N3 O14	709.0	8.644	0.02	27	46	3	14

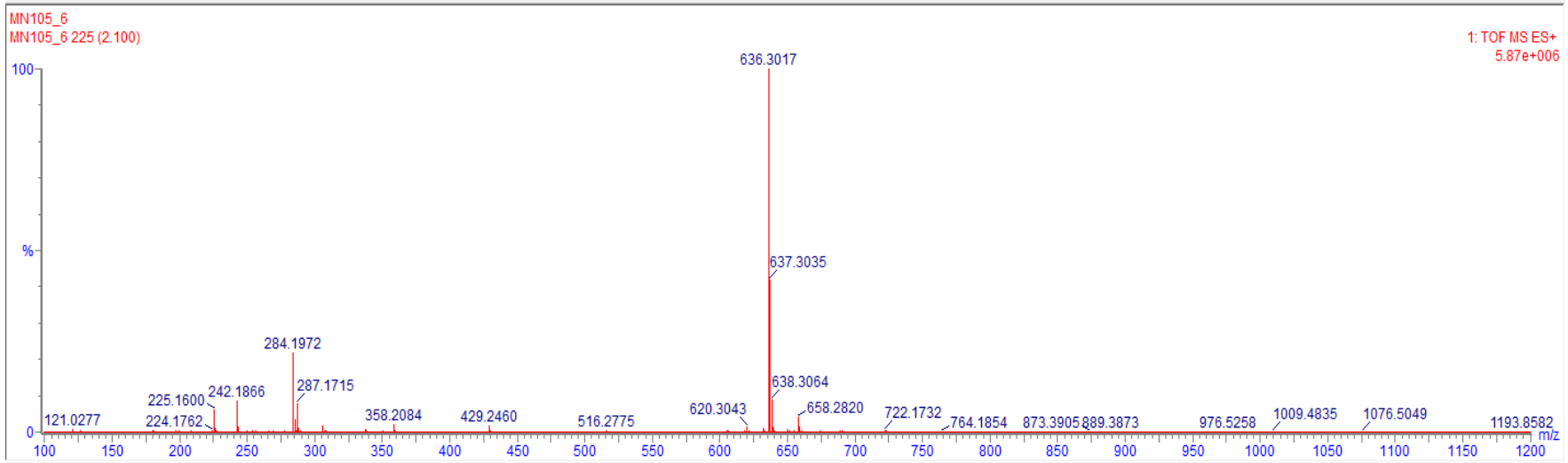

Figure S36. HR-ESIMS spectrum of madurastatin E1 (**2**)

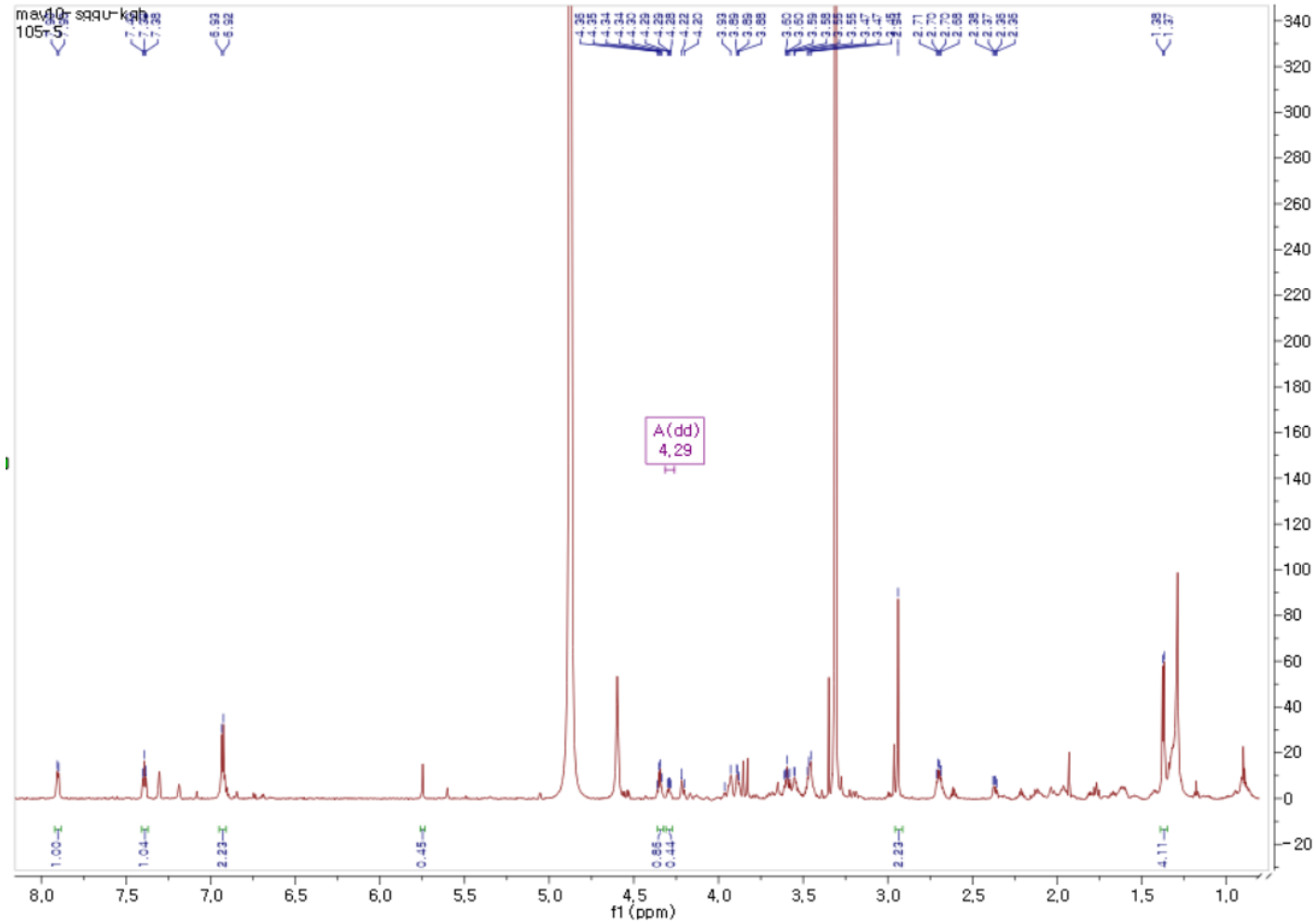

Figure S37. ^{1}H NMR spectrum of madurastatin F1 (**3**) (CD_3OD, 800 MHz)

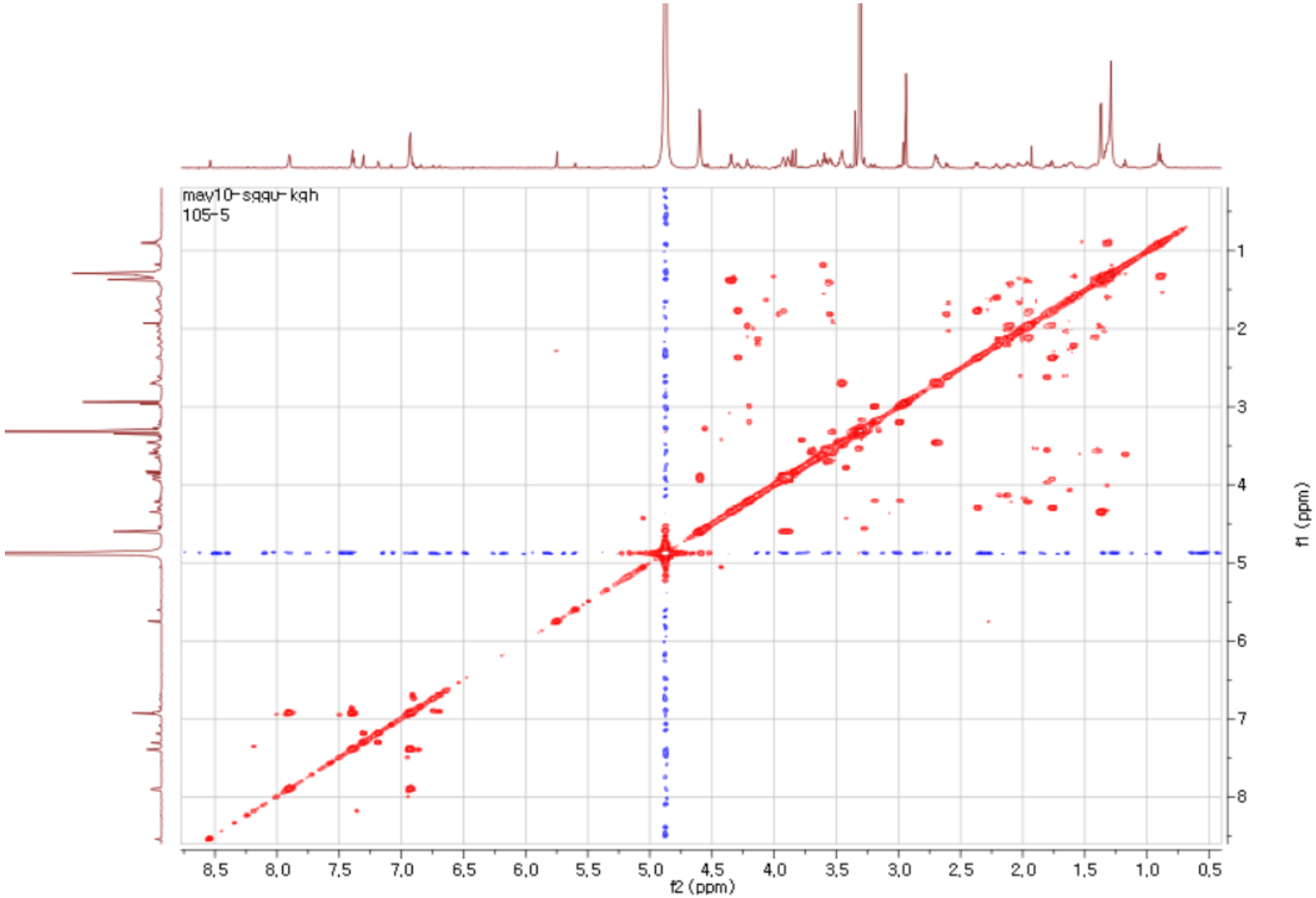

Figure S38. ^{1}H-^{1}H COSY spectrum of madurastatin F1 (**3**) (CD_3OD, 800 MHz)

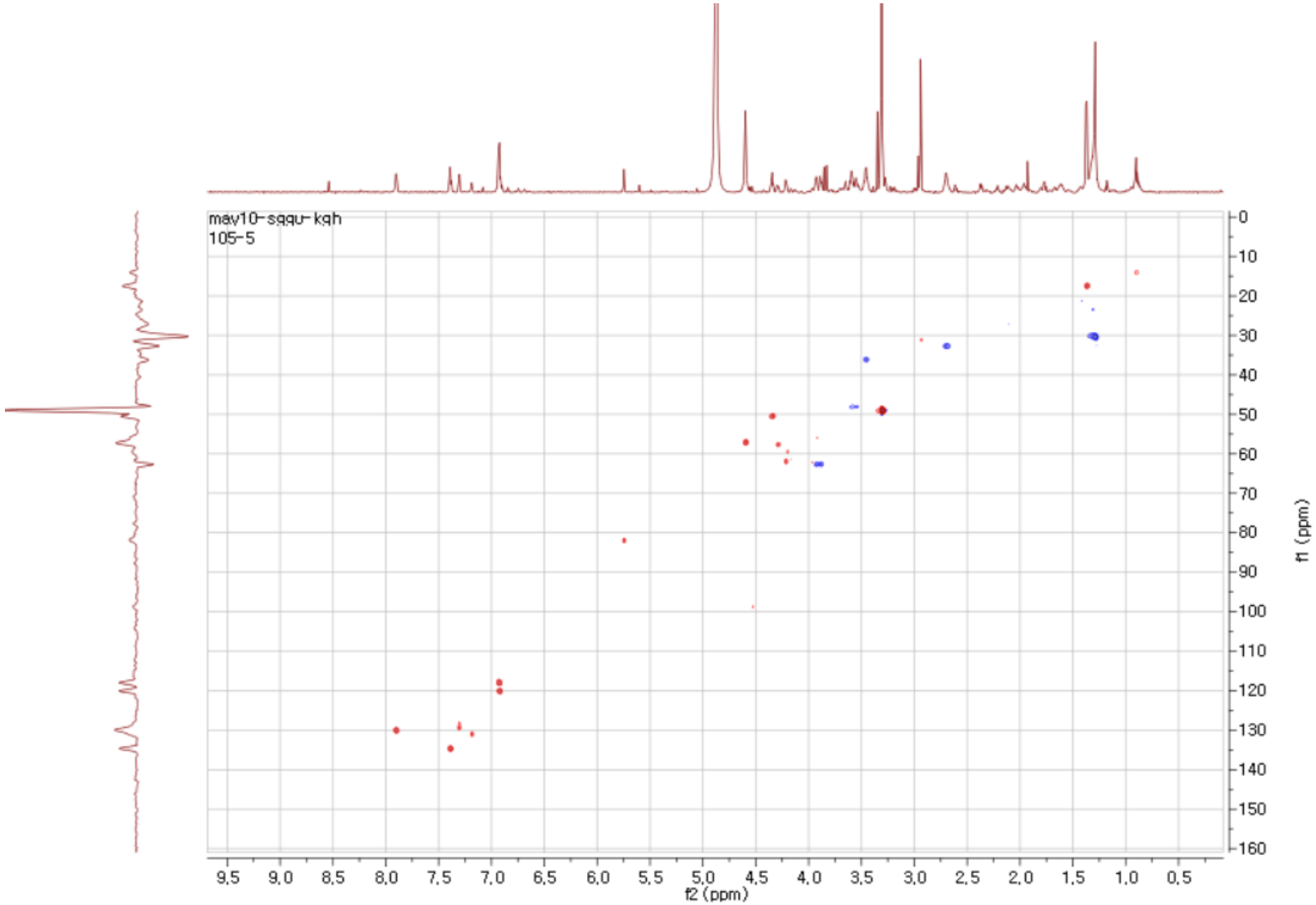

Figure S39. HSQC spectrum of madurastatin F1 (**3**) (CD_3OD, 800 MHz)

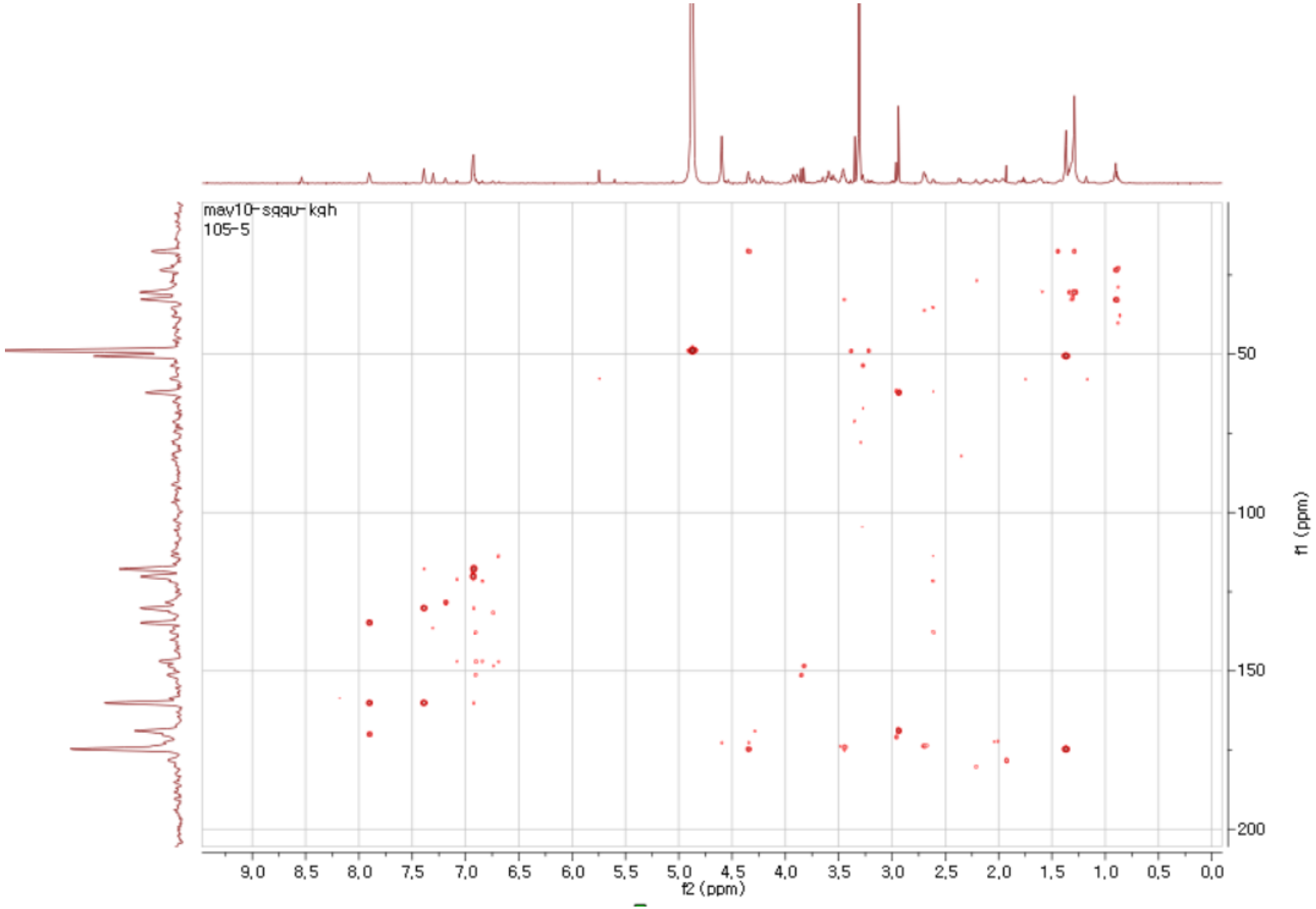

Figure S40. HMBC spectrum of madurastatin F1 (**3**) (CD_3OD, 800 MHz)

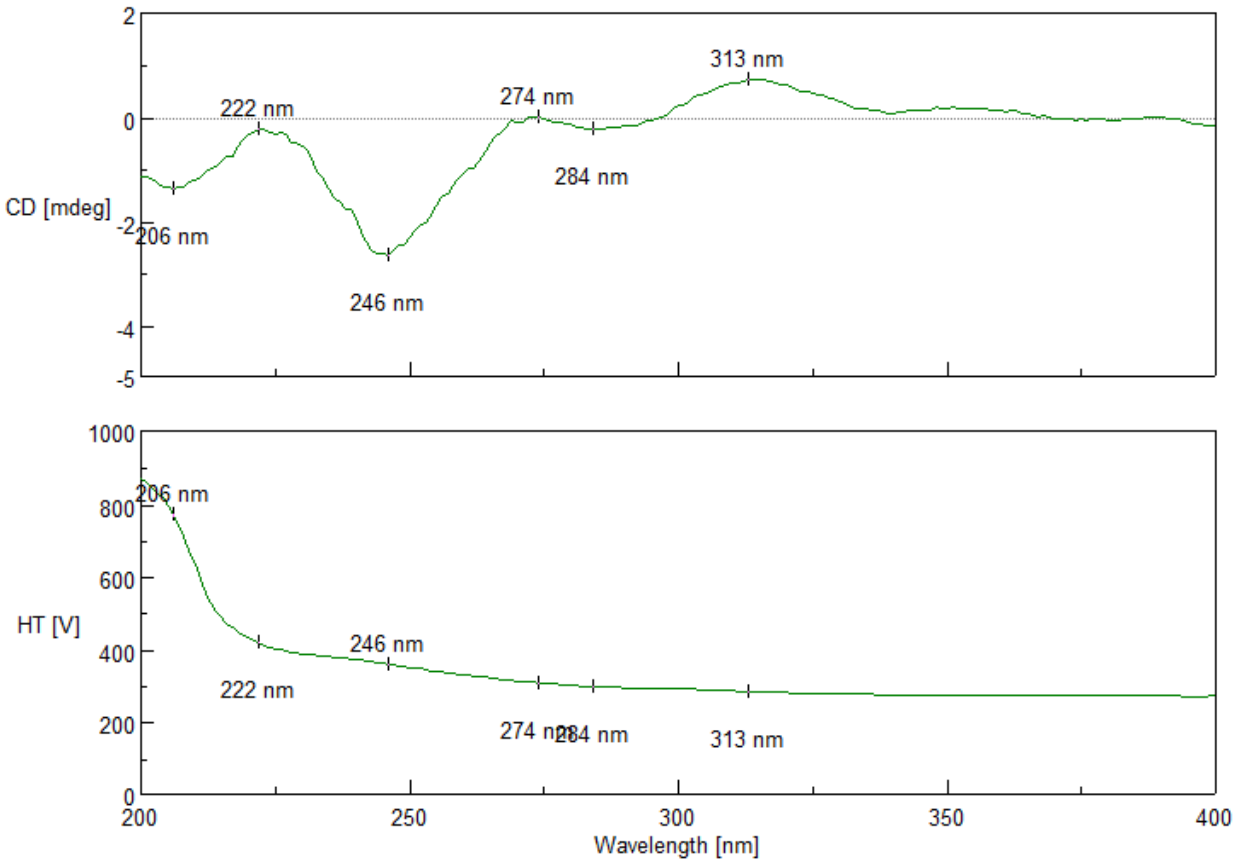

Figure S41. ECD spectrum of madurastatin F1 (**3**) (MeOH).

Single Mass Analysis
Tolerance = 5.0 mDa / DBE: min = -1.5, max = 50.0
Element prediction: Off
Number of isotope peaks used for i-FIT = 3
Monoisotopic Mass, Even Electron Ions
1721 formula(e) evaluated with 12 results within limits (up to 50 closest results for each mass)
Elements Used:

Mass	Calc. Mass	mDa	PPM	DBE	Formula	i-FIT	i-FIT Norm	Fit Conf %	C	H	N	O
605.2568	605.2571	-0.3	-0.5	12.5	C27 H37 N6 O10	477.5	2.431	8.80	27	37	6	10
	605.2558	1.0	1.7	7.5	C26 H41 N2 O14	478.3	3.147	4.30	26	41	2	14
	605.2553	1.5	2.5	25.5	C39 H33 N4 O3	478.7	3.610	2.70	39	33	4	3
	605.2585	-1.7	-2.8	17.5	C28 H33 N10 O6	477.6	2.447	8.66	28	33	10	6
	605.2590	-2.2	-3.6	-0.5	C15 H41 N8 O17	483.2	8.091	0.03	15	41	8	17
	605.2593	-2.5	-4.1	29.5	C44 H33 N2 O	481.4	6.284	0.19	44	33	2	1
	605.2539	2.9	4.8	20.5	C38 H37 O7	478.0	2.853	5.76	38	37		7
	605.2598	-3.0	-5.0	11.5	C31 H41 O12	475.9	0.826	43.78	31	41		12

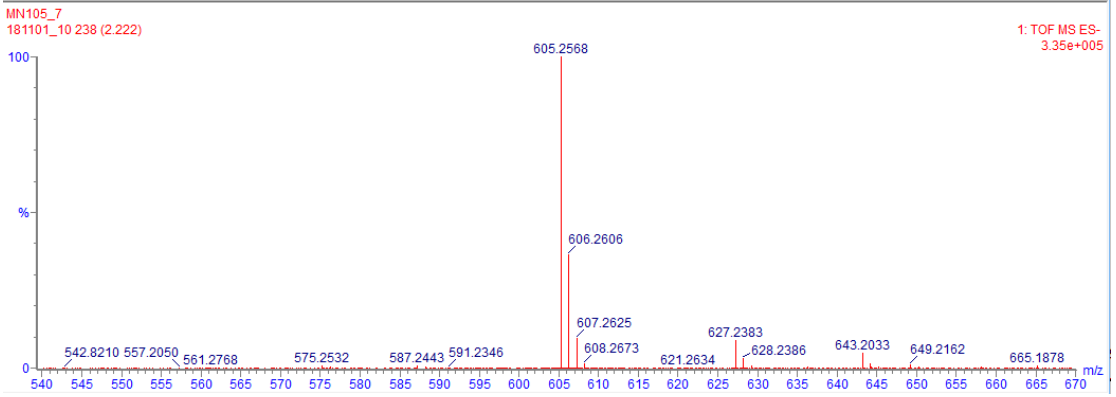

Figure S42. HR-ESIMS spectrum of madurastatin F1 (**3**)

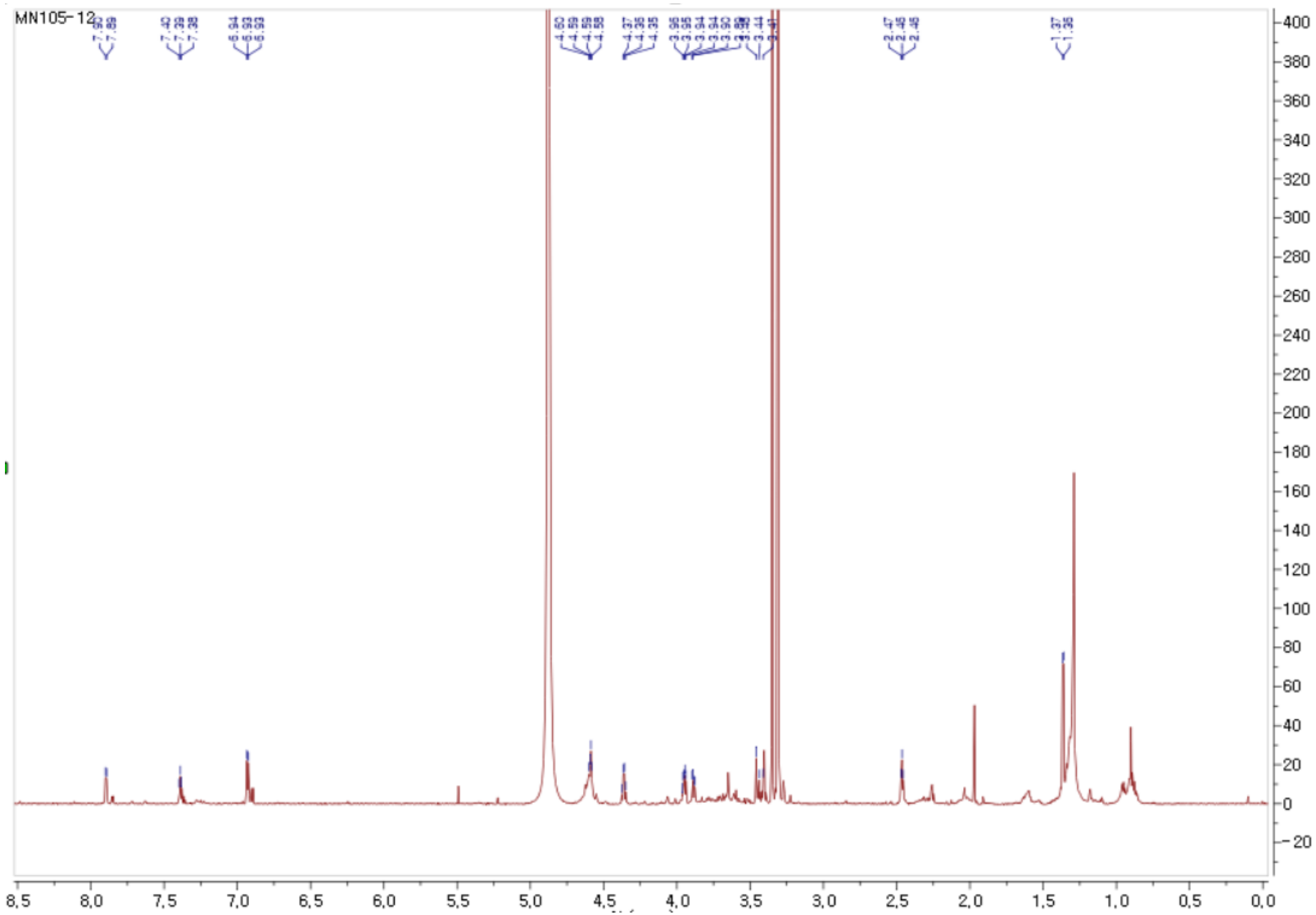

Figure S43. ^{1}H NMR spectrum of madurastatin G1 (**4**) (CD_3OD, 800 MHz)

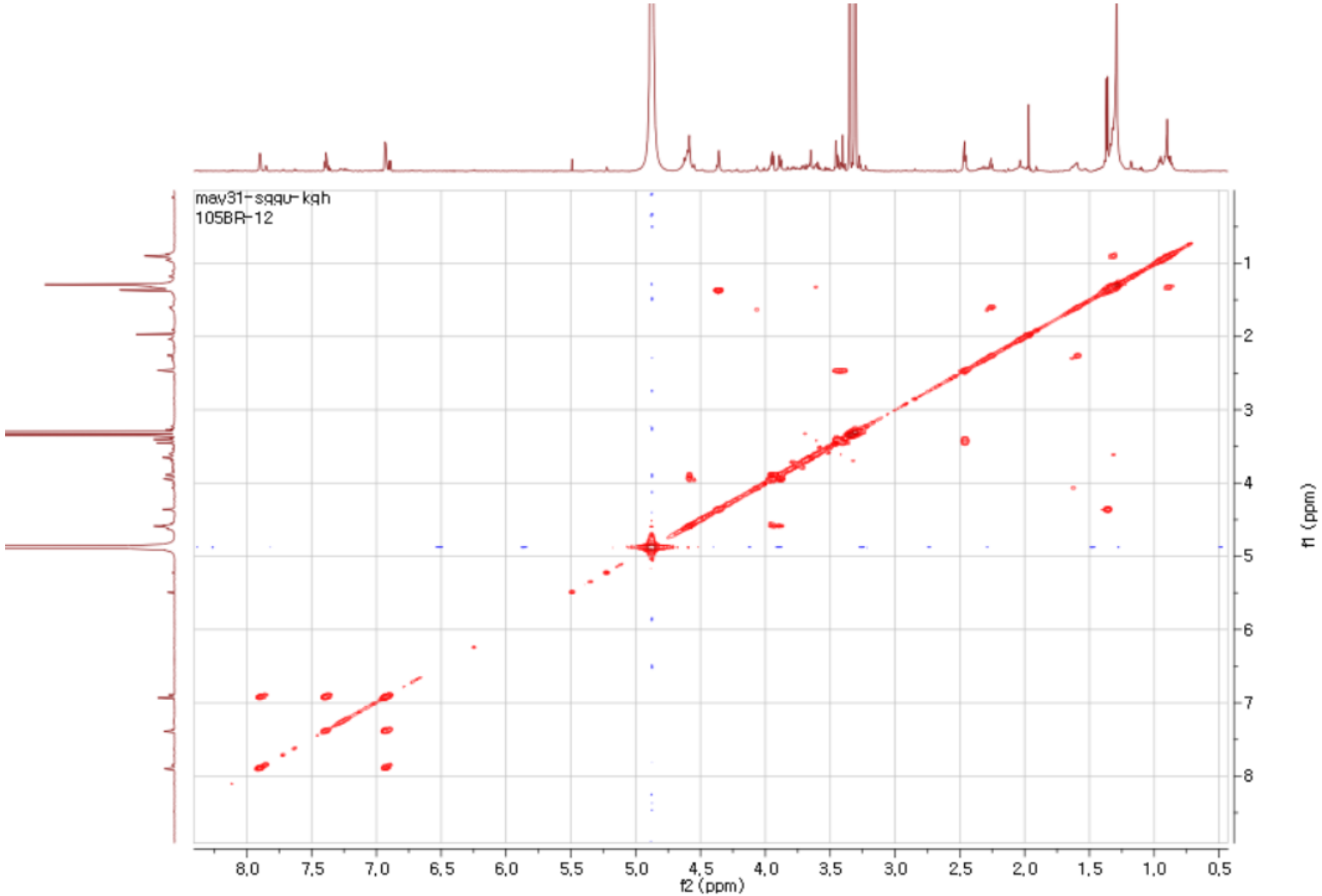

Figure S44. ^{1}H-^{1}H COSY spectrum of madurastatin G1 (**4**) (CD_3OD, 800 MHz)

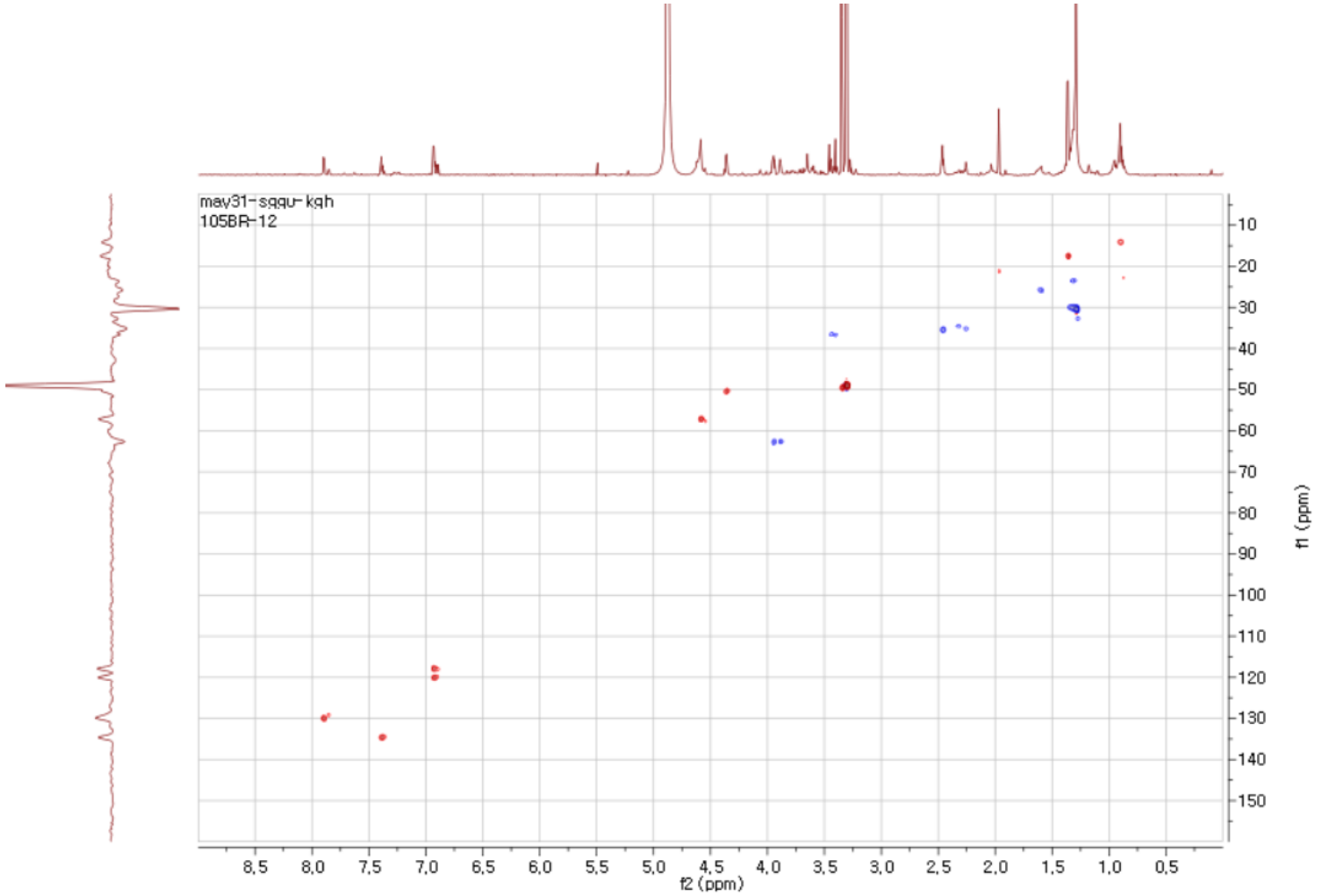

Figure S45. HSQC spectrum of madurastatin G1 (**4**) (CD_3OD, 800 MHz)

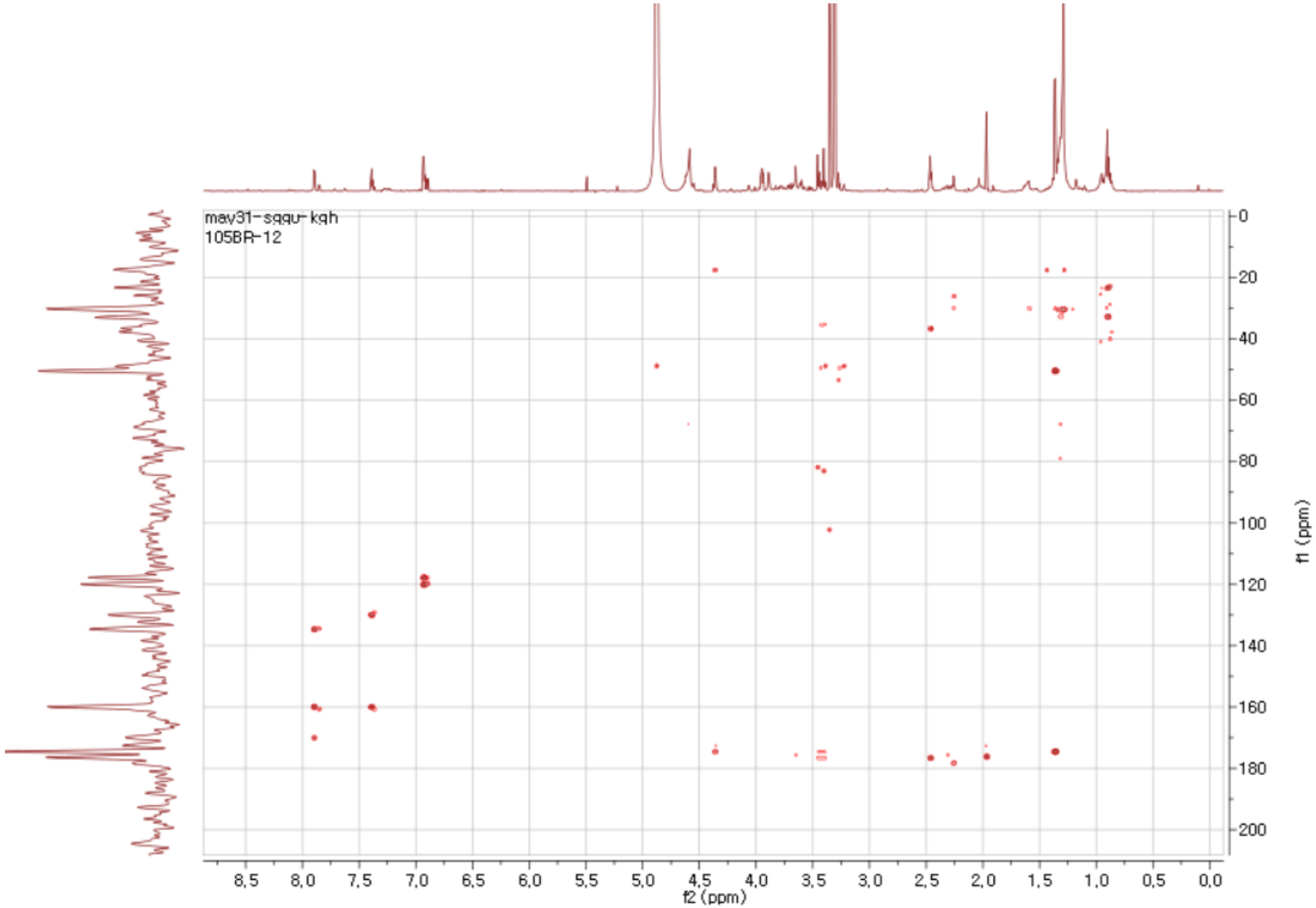

Figure S46. HMBC spectrum of madurastatin G1 (**4**) (CD_3OD, 800 MHz)

Single Mass Analysis
Tolerance = 5.0 mDa / DBE: min = -1.5, max = 50.0
Element prediction: Off
Number of isotope peaks used for i-FIT = 3
Monoisotopic Mass, Even Electron Ions
663 formula(e) evaluated with 8 results within limits (up to 50 closest results for each mass)
Elements Used:

Mass	Calc. Mass	mDa	PPM	DBE	Formula	i-FIT	i-FIT Norm	Fit Conf %	C	H	N	O
368.1451	368.1458	-0.7	-1.9	7.5	C16 H22 N3 O7	583.1	0.543	58.11	16	22	3	7
	368.1439	1.2	3.3	20.5	C28 H18 N	595.1	12.571	0.00	28	18	1	
	368.1471	-2.0	-5.4	12.5	C17 H18 N7 O3	587.1	4.585	1.02	17	18	7	3
	368.1431	2.0	5.4	8.5	C12 H18 N9 O5	583.5	0.942	38.99	12	18	9	5
	368.1418	3.3	9.0	3.5	C11 H22 N5 O9	586.5	4.003	1.83	11	22	5	9
	368.1490	-3.9	-10.6	-0.5	C5 H22 N9 O10	592.0	9.507	0.01	5	22	9	10
	368.1498	-4.7	-12.8	11.5	C21 H22 N O5	591.9	9.344	0.01	21	22	1	5
	368.1404	4.7	12.8	-1.5	C10 H26 N O13	590.2	7.735	0.04	10	26	1	13

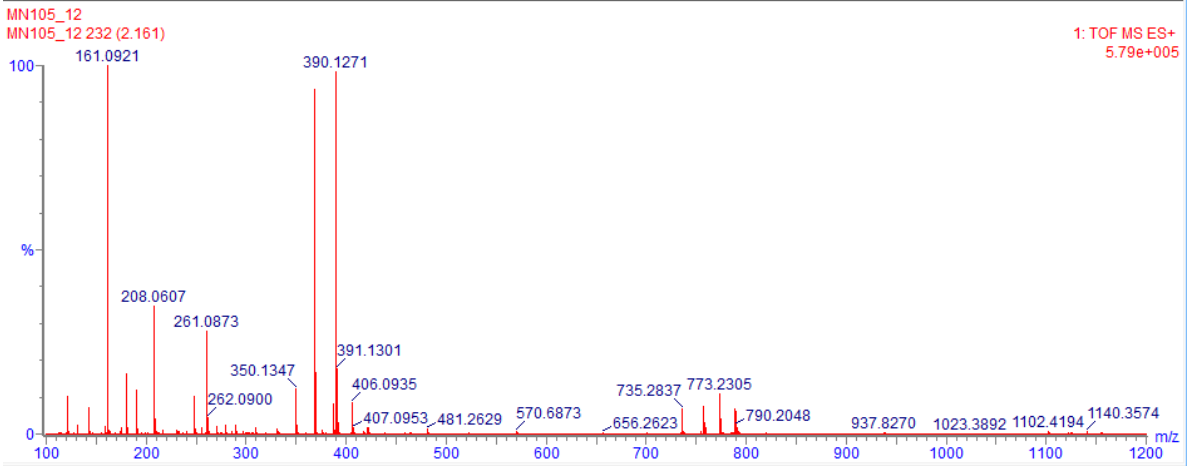

Figure S47. HRESI-MS spectrum of madurastatin G1 (**4**)

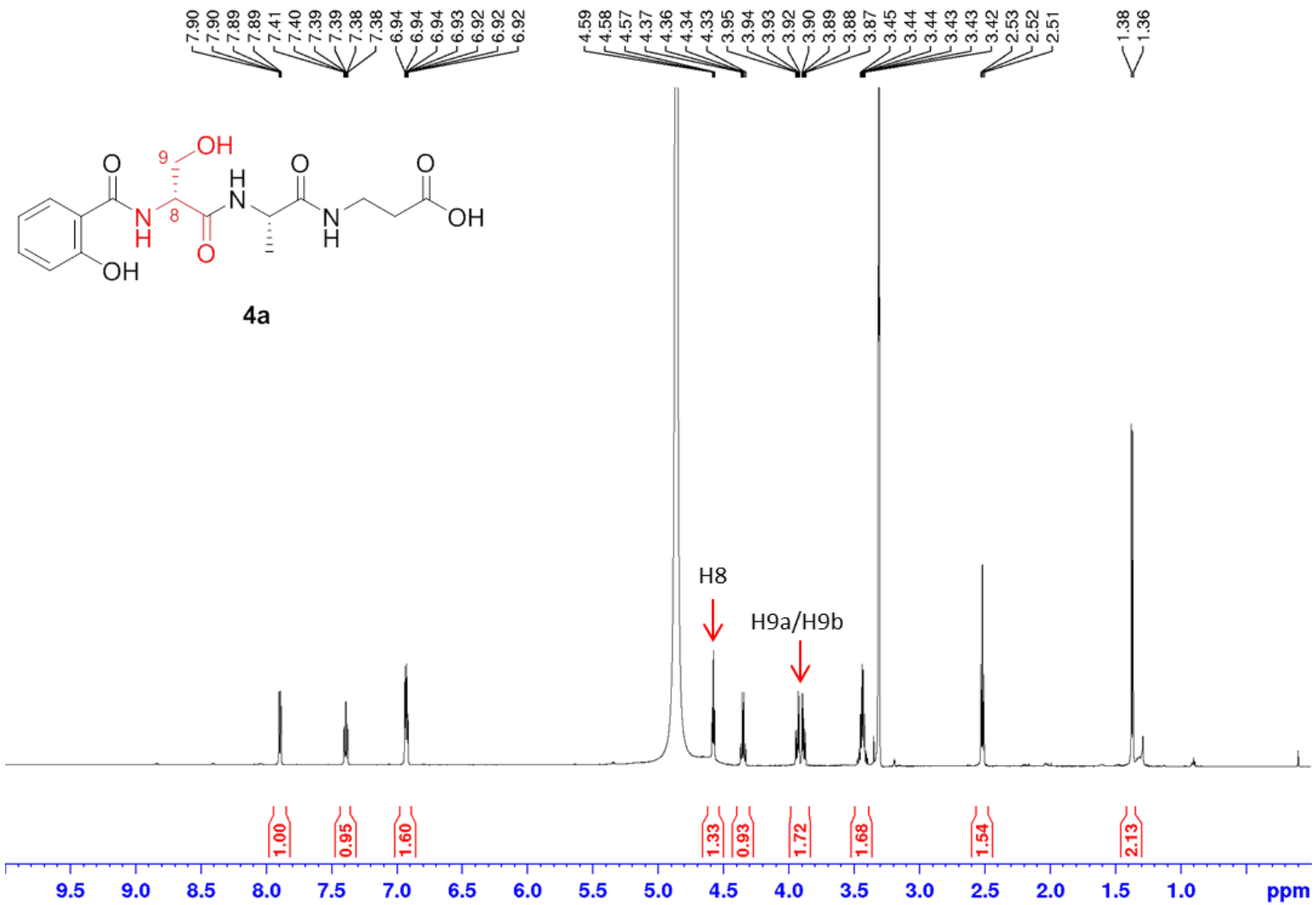

Figure S48. ^{1}H NMR spectrum of synthetic salicyl-D-Ser-Ala-ßAla-OH (**4a**) (CD_3OD, 600 MHz, 300 K)

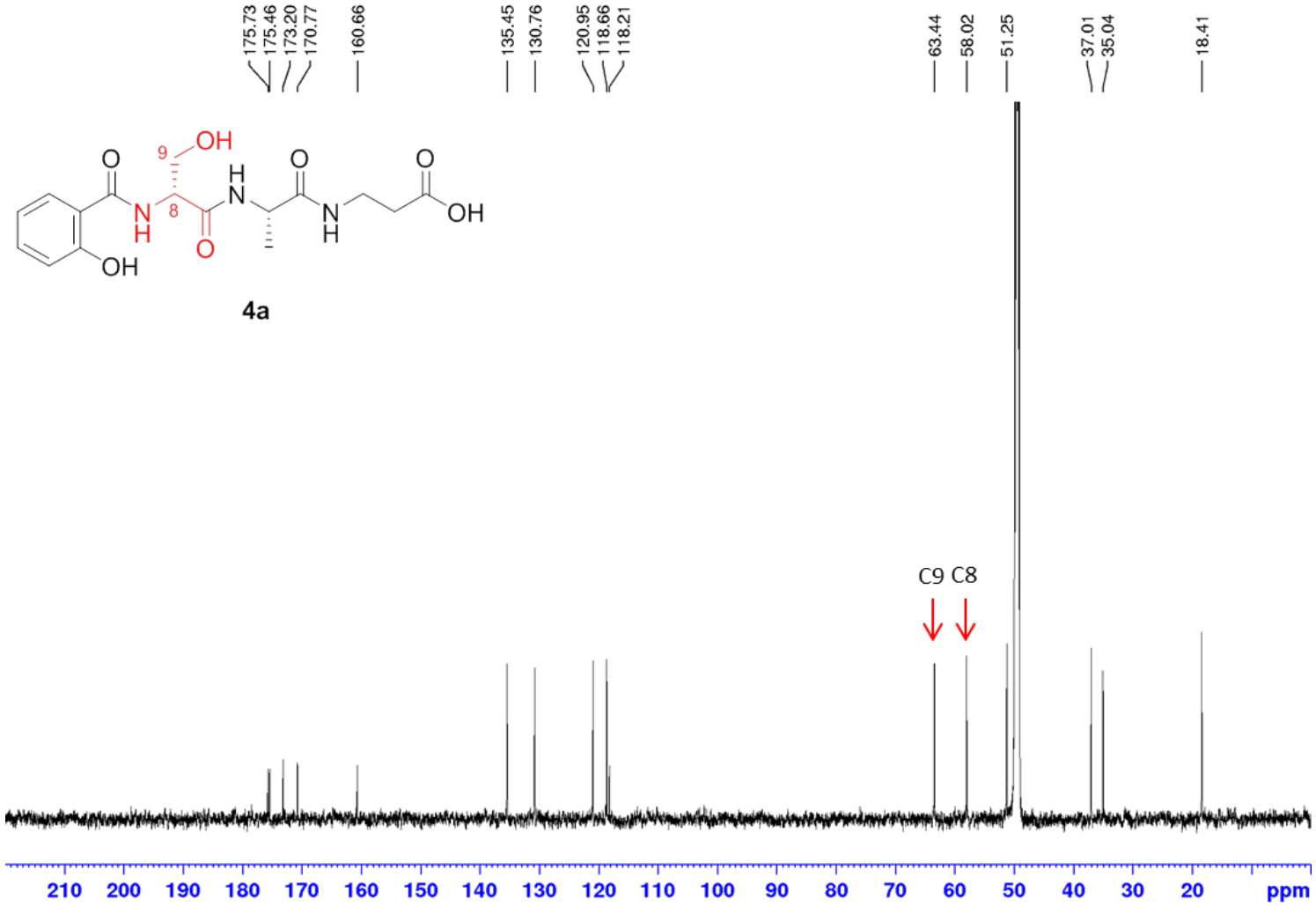

Figure S49. ^{13}C NMR spectrum of synthetic salicyl-D-Ser-Ala-ßAla-OH (**4a**) (CD_3OD, 150 MHz, 300 K)

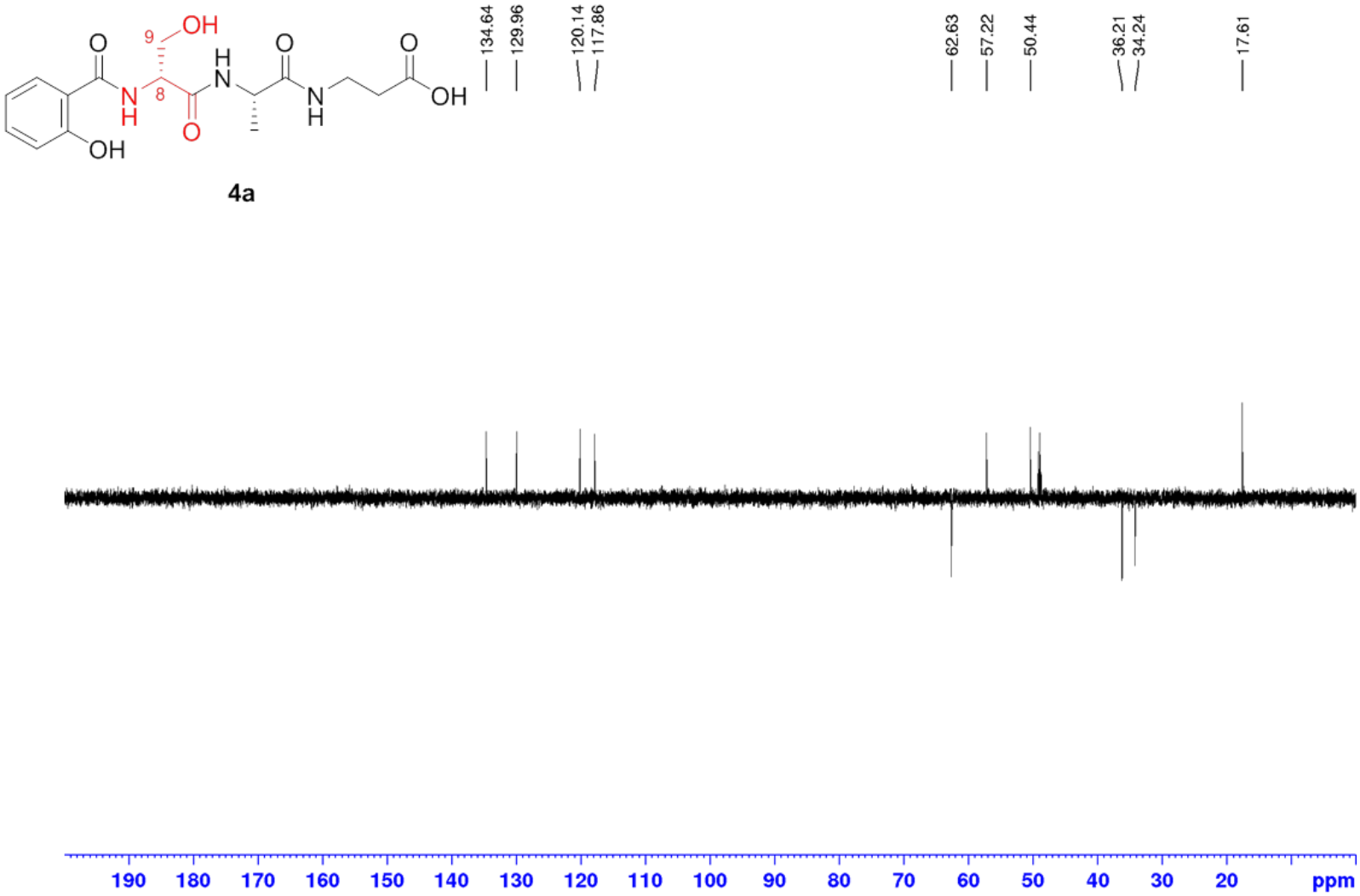

Figure S50. DEPT135 NMR spectrum of synthetic salicyl-D-Ser-Ala-ßAla-OH (**4a**) (CD_3OD, 150 MHz, 300 K)

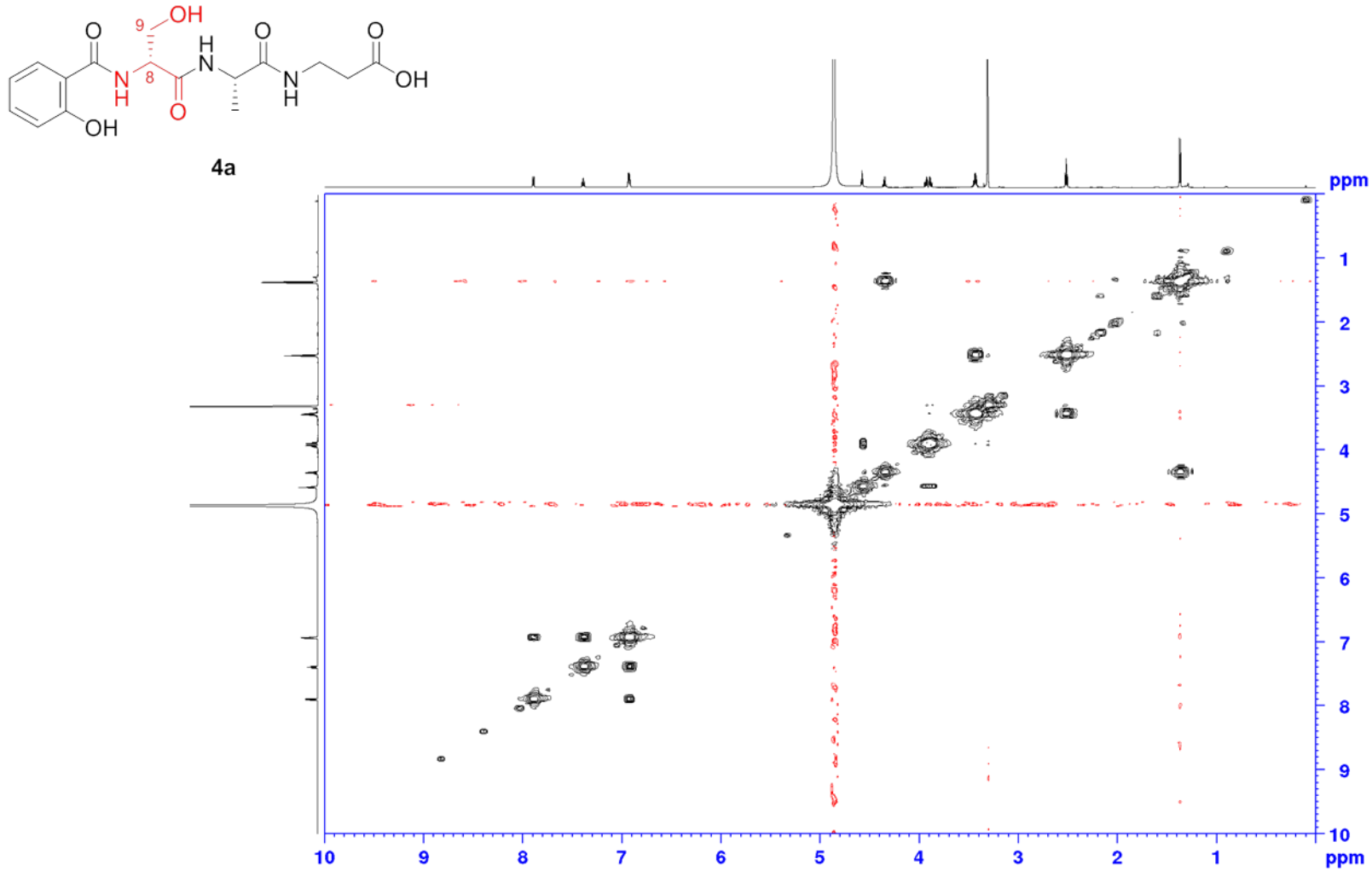

Figure S51. ^{1}H-^{1}H COSY NMR spectrum of synthetic salicyl-D-Ser-Ala-ßAla-OH (**4a**) (CD_3OD, 600 MHz, 300 K)

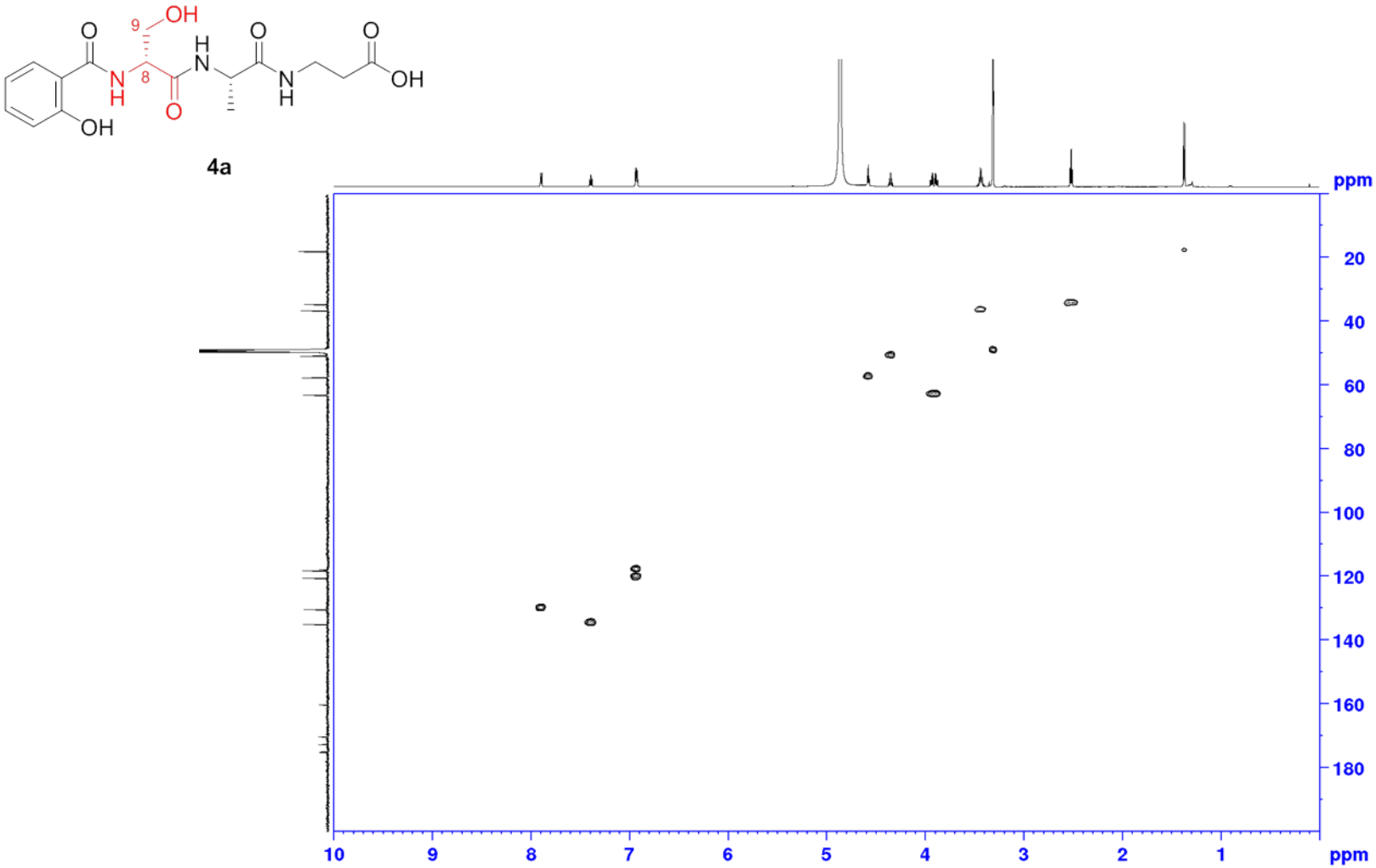

Figure S52. HSQC NMR spectrum of synthetic salicyl-D-Ser-Ala-ßAla-OH (**4a**) (CD_3OD, 600 MHz, 300 K)

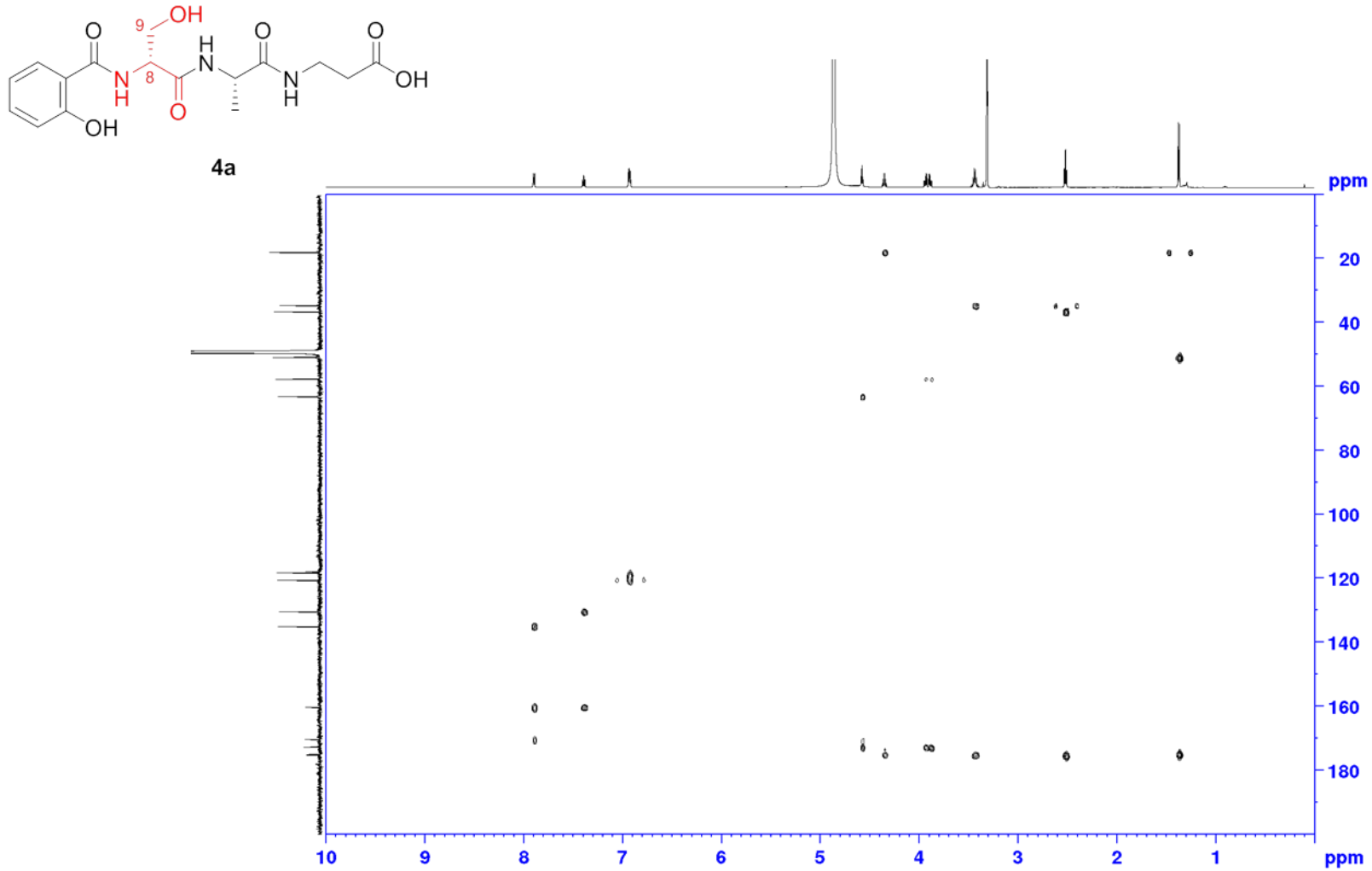

Figure S53. HMBC NMR spectrum of synthetic salicyl-D-Ser-Ala-ßAla-OH (**4a**) (CD_3OD, 600 MHz, 300 K)

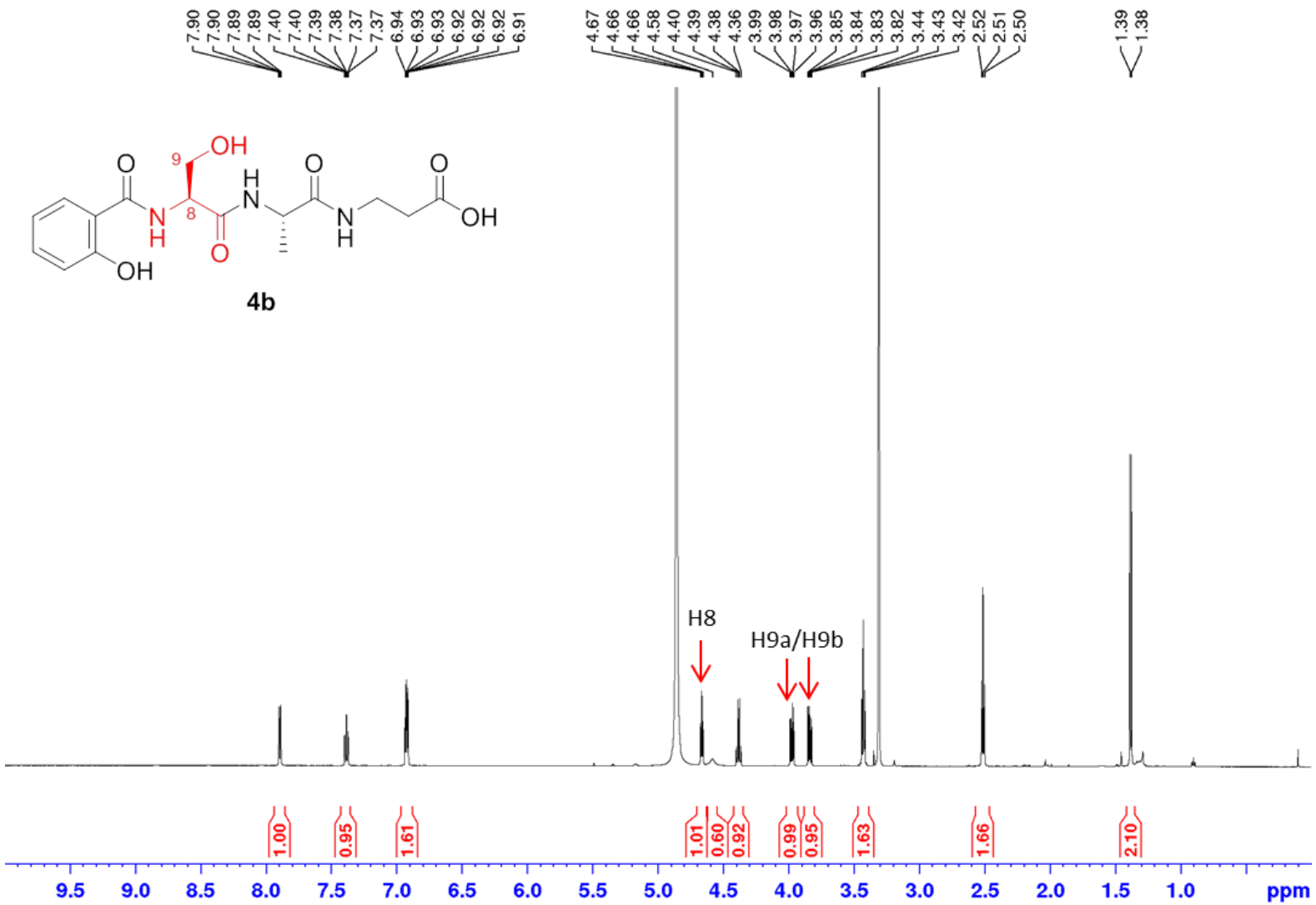

Figure S54. ^{1}H NMR spectrum of synthetic salicyl-L-Ser-Ala-ßAla-OH (**4b**) (CD_3OD, 600 MHz, 300 K)

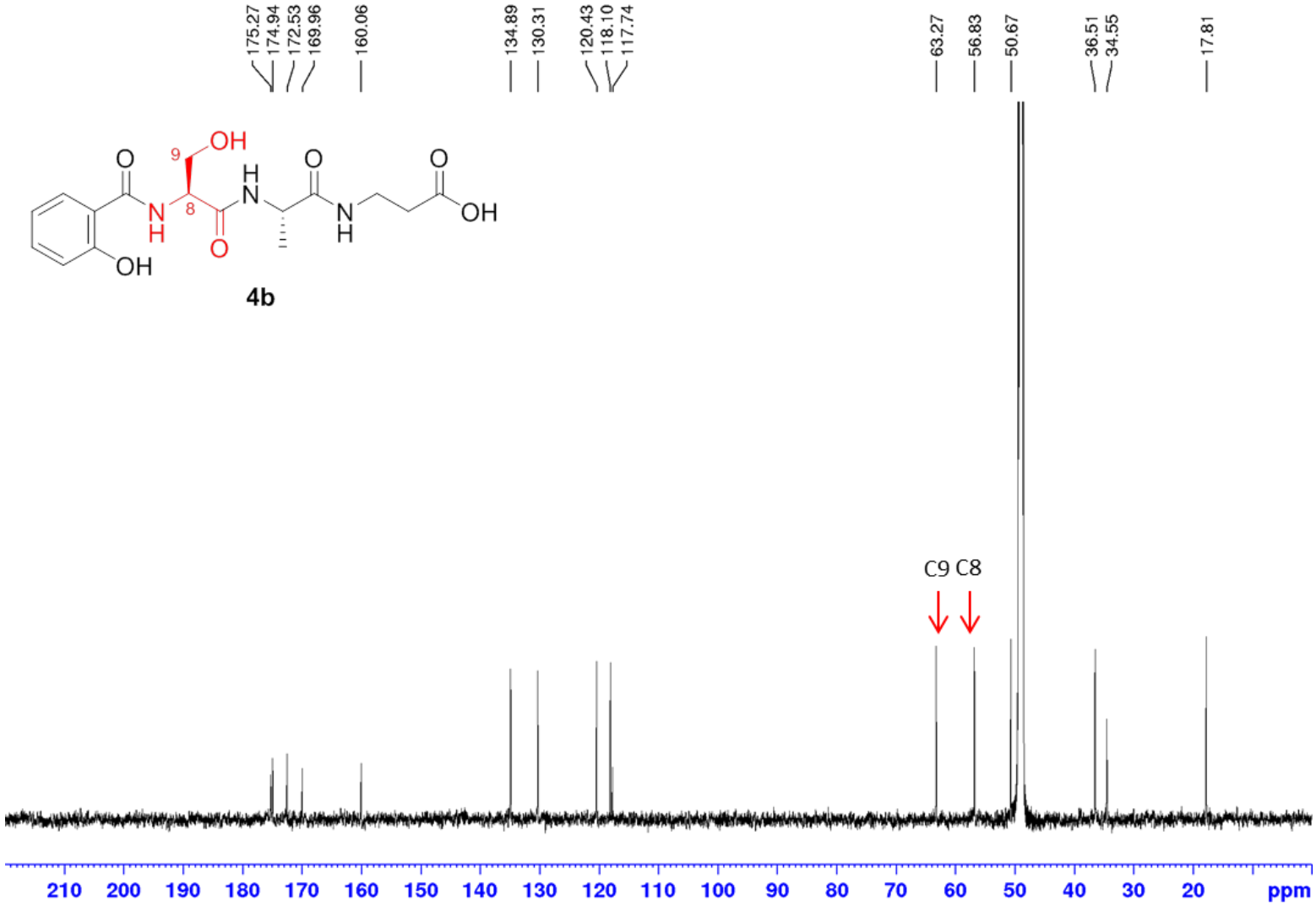

Figure S55. ^{13}C NMR spectrum of synthetic salicyl-L-Ser-Ala-ßAla-OH (**4b**) (CD_3OD, 150 MHz, 300 K)

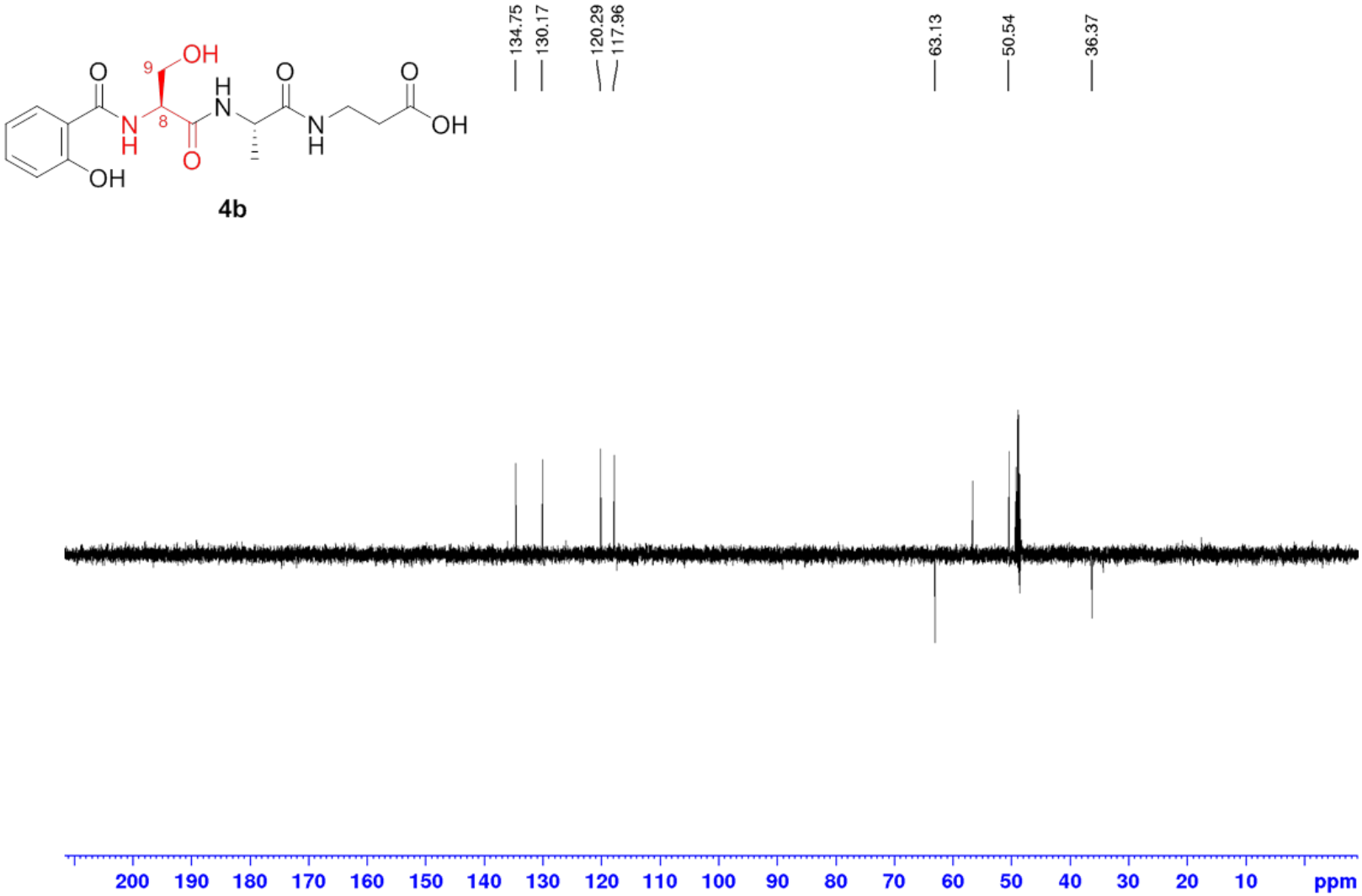

Figure S56. DEPT135 NMR spectrum of synthetic salicyl-L-Ser-Ala-ßAla-OH (**4b**) (CD_3OD, 150 MHz, 300 K)

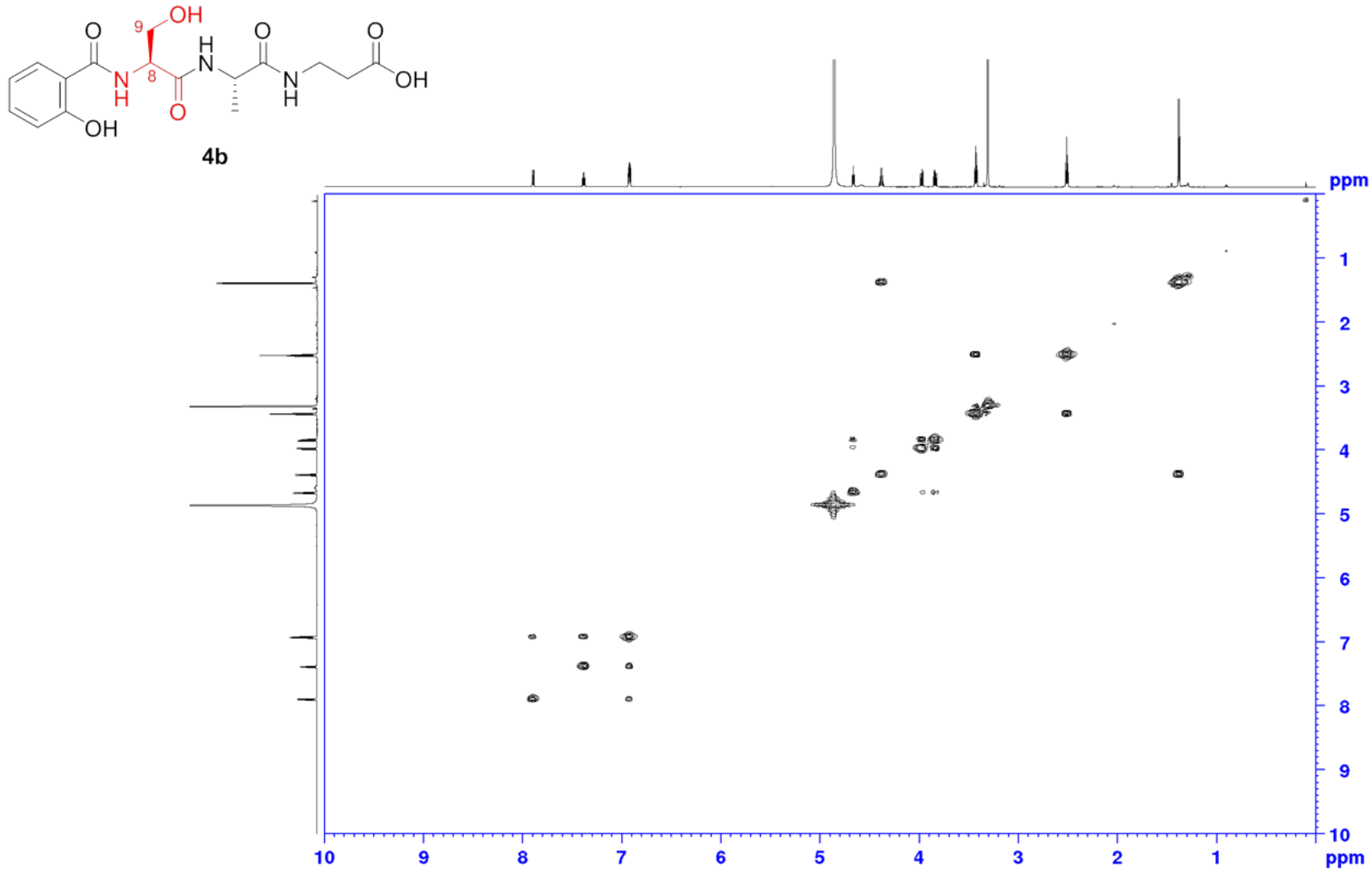

Figure S57. ^{1}H-^{1}H COSY NMR spectrum of synthetic salicyl-L-Ser-Ala-ßAla-OH (**4b**) (CD_3OD, 600 MHz, 300 K)

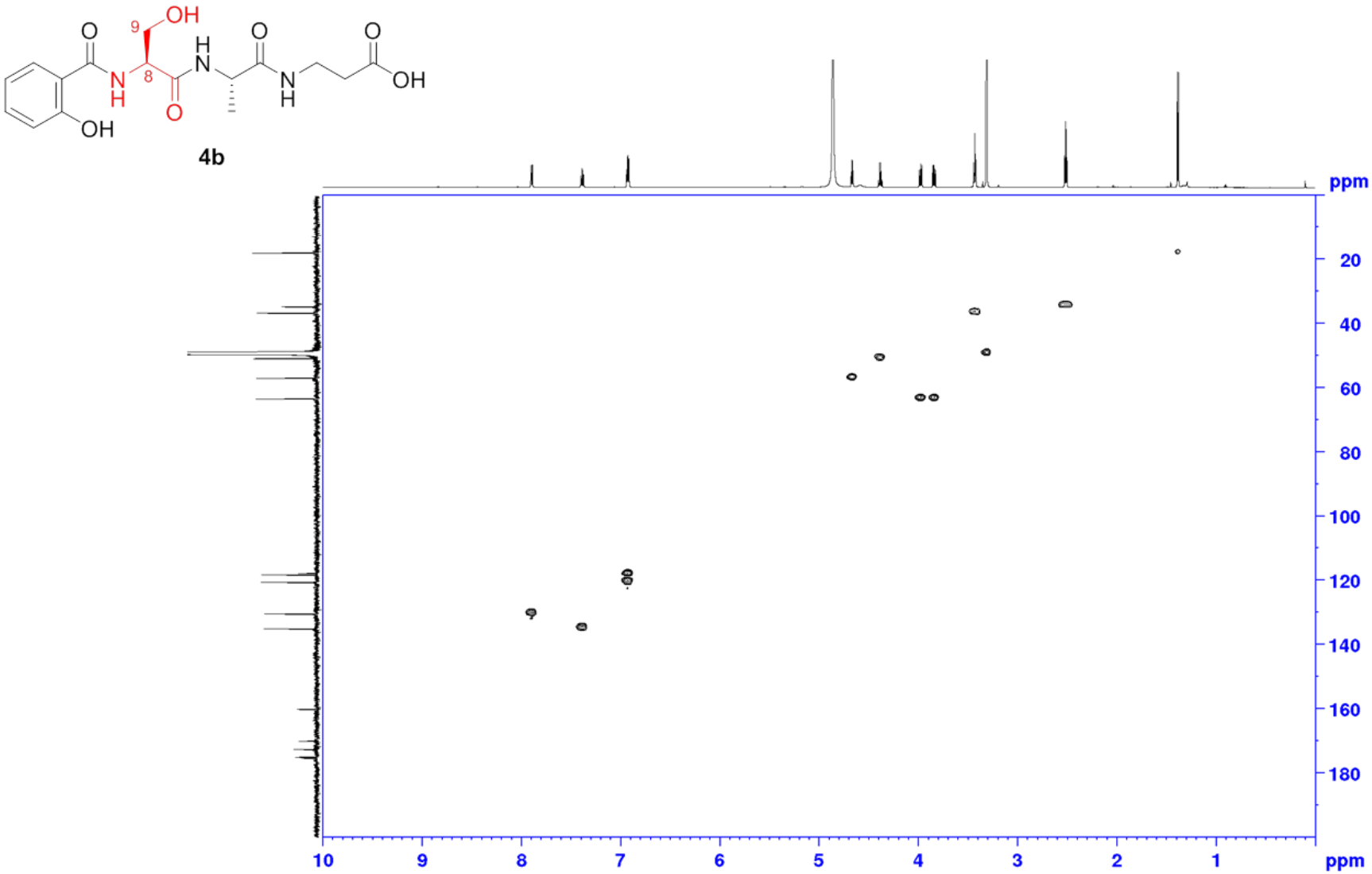

Figure S58. HSQC NMR spectrum of synthetic salicyl-L-Ser-Ala-ßAla-OH (**4b**) (CD_3OD, 600 MHz, 300 K)

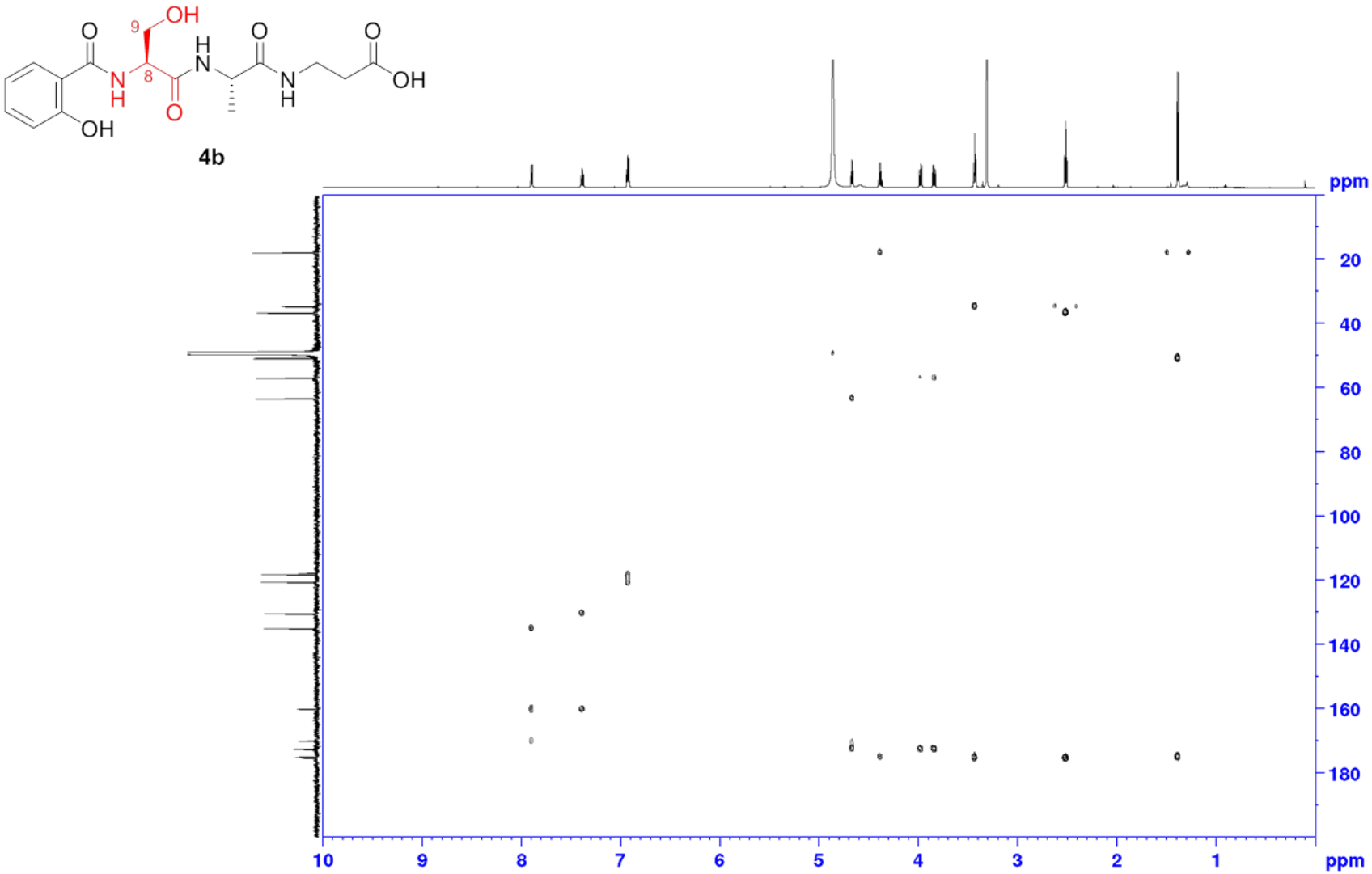

Figure S59. HMBC NMR spectrum of synthetic salicyl-L-Ser-Ala-ßAla-OH (**4b**) (CD_3OD, 600 MHz, 300 K)

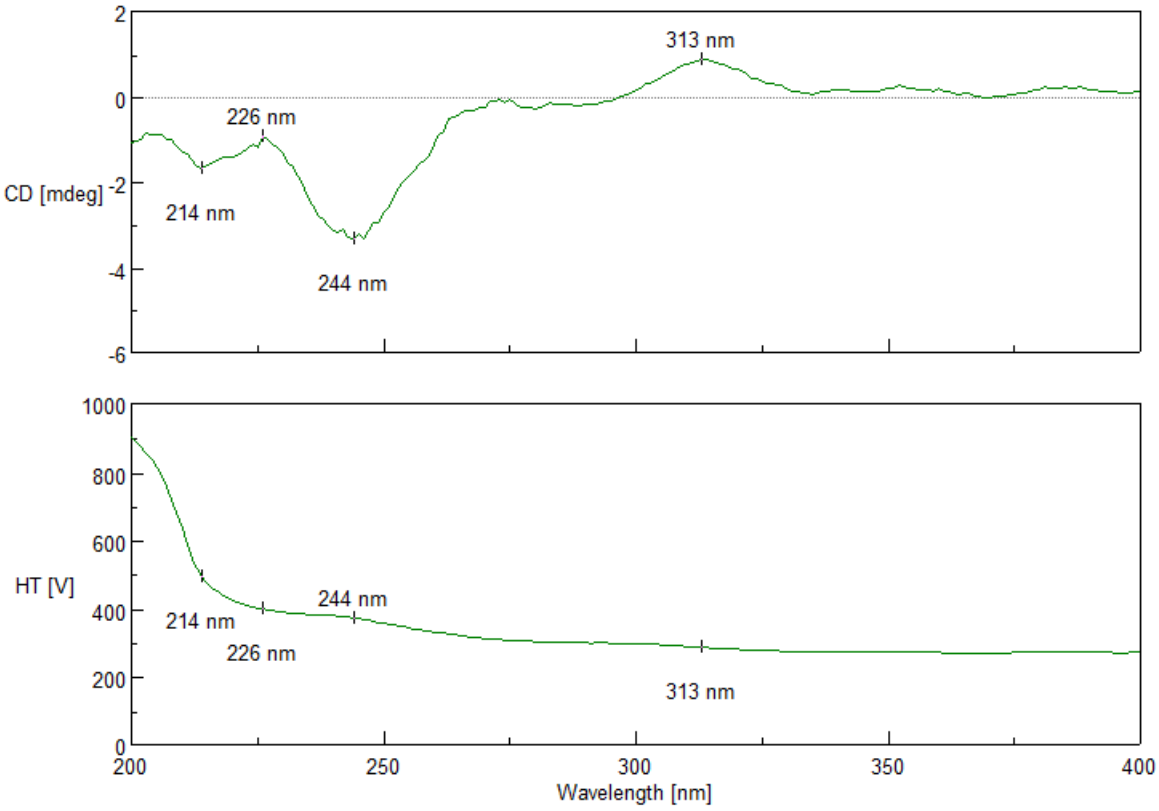

Figure S60. ECD spectrum of madurastatin G1 (**4a**) (MeOH)

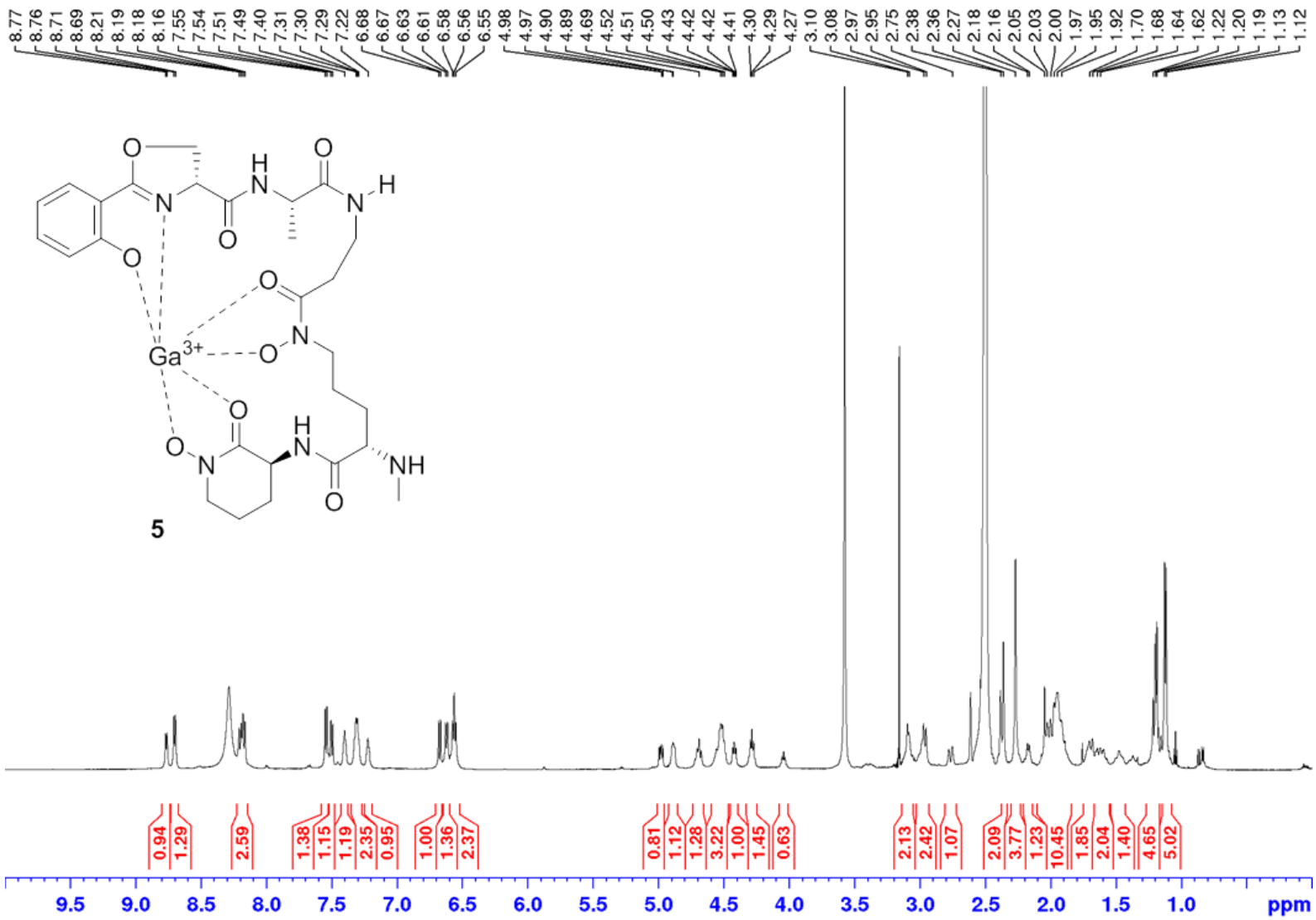

Figure S61. ^{1}H NMR spectrum of Ga^{3+}-madurastatin A1 (**5**) (DMSO-d_6, 600 MHz, 300 K)

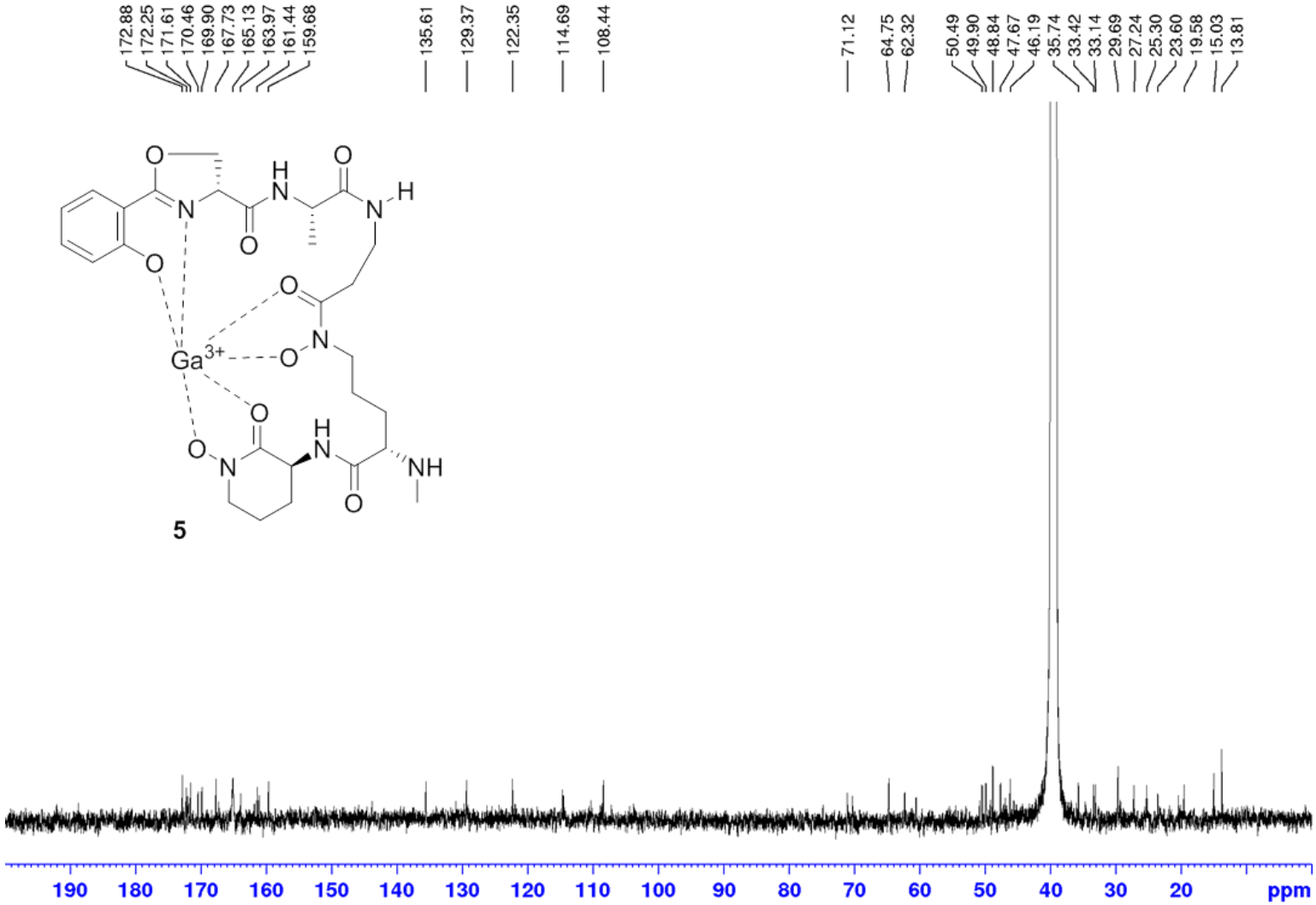

Figure S62. ^{13}C NMR spectrum of Ga^{3+}-madurastatin A1 (**5**) (DMSO-d_6, 150 MHz, 300 K)

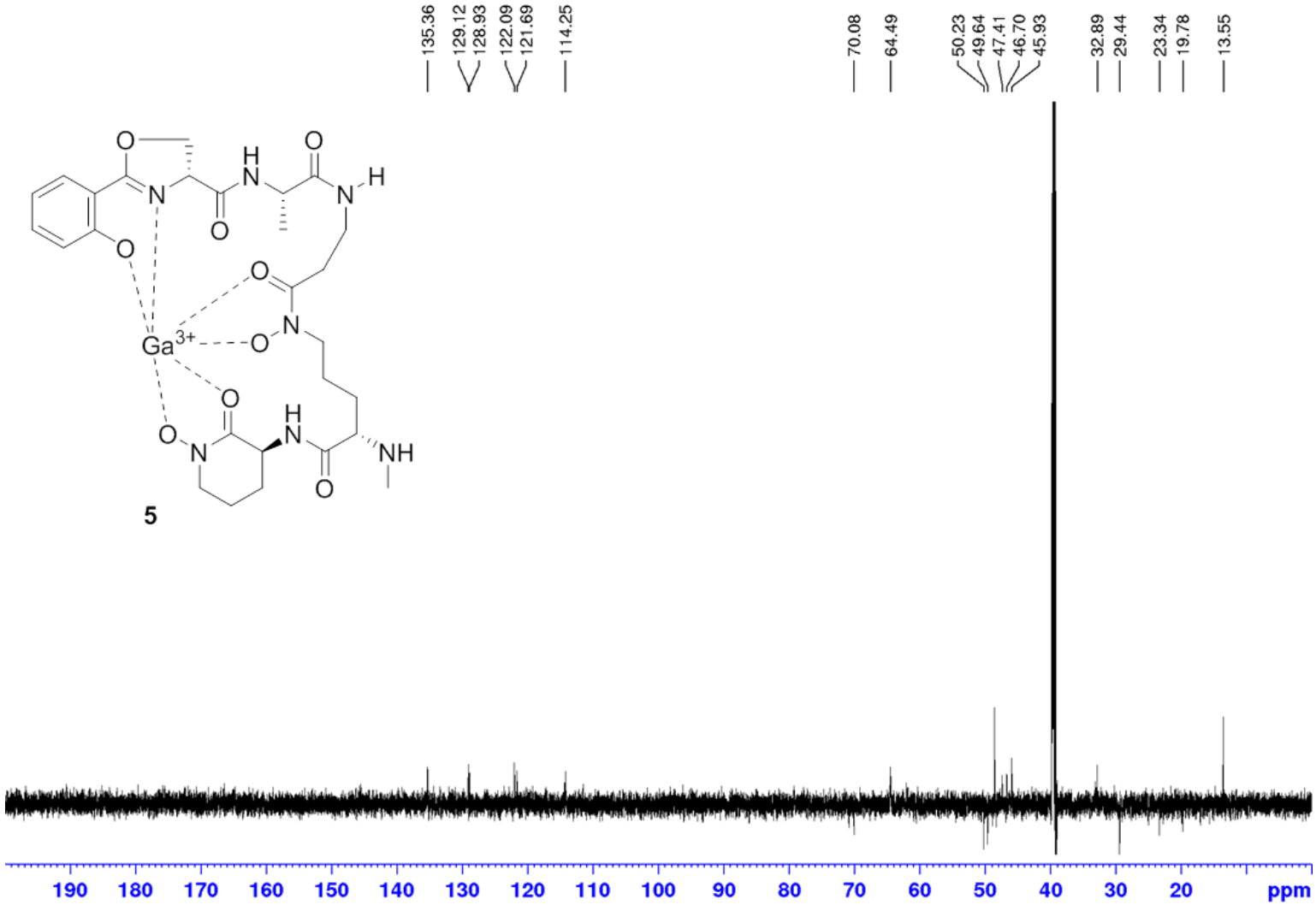

Figure S63. DEPT135 NMR spectrum of Ga^{3+}-madurastatin A1 (**5**) (DMSO-d_6, 150 MHz, 300 K)

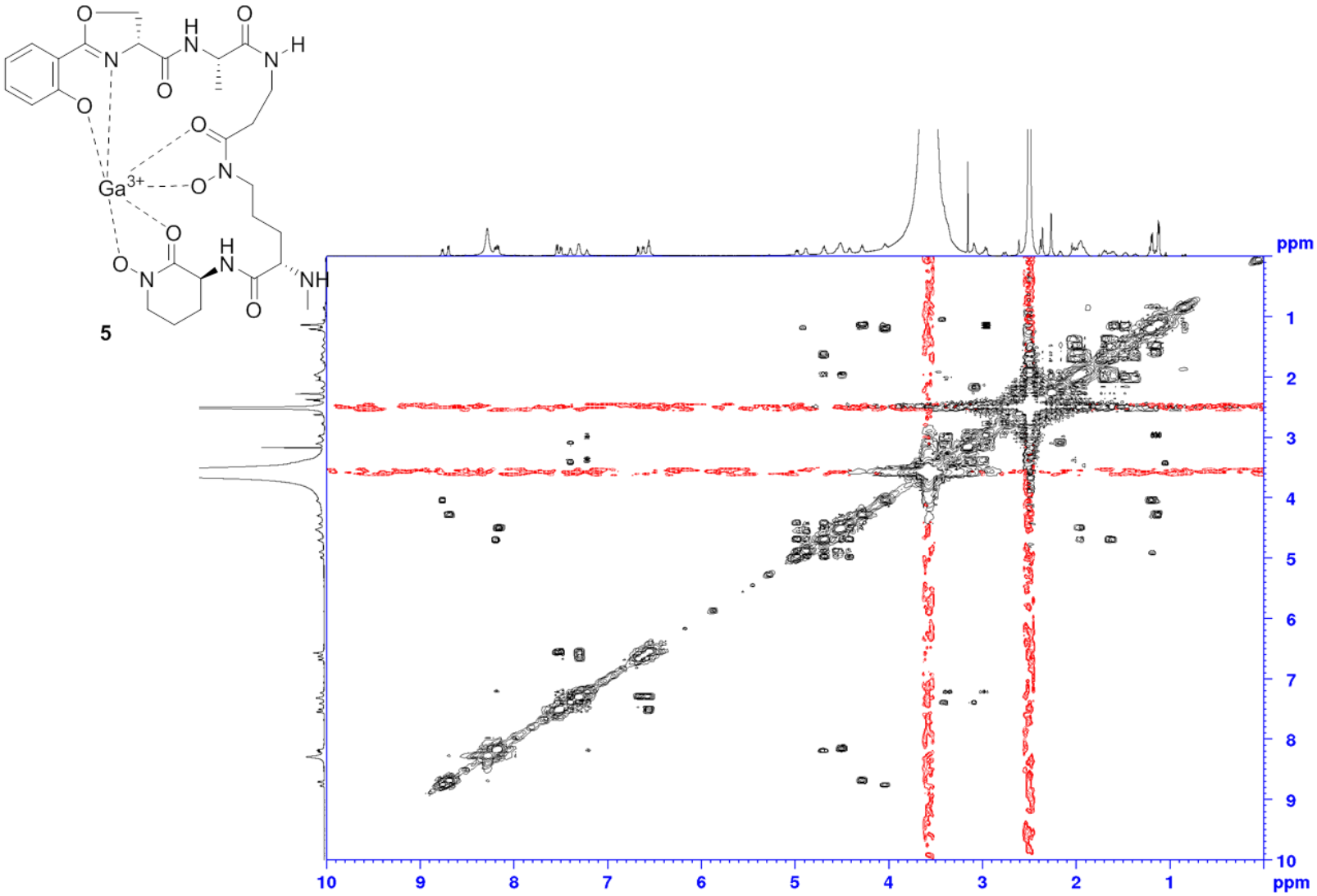

Figure S64. ^{1}H-^{1}H COSY NMR spectrum of Ga^{3+}-madurastatin A1 (**5**) (DMSO-d_6, 600 MHz, 300 K)

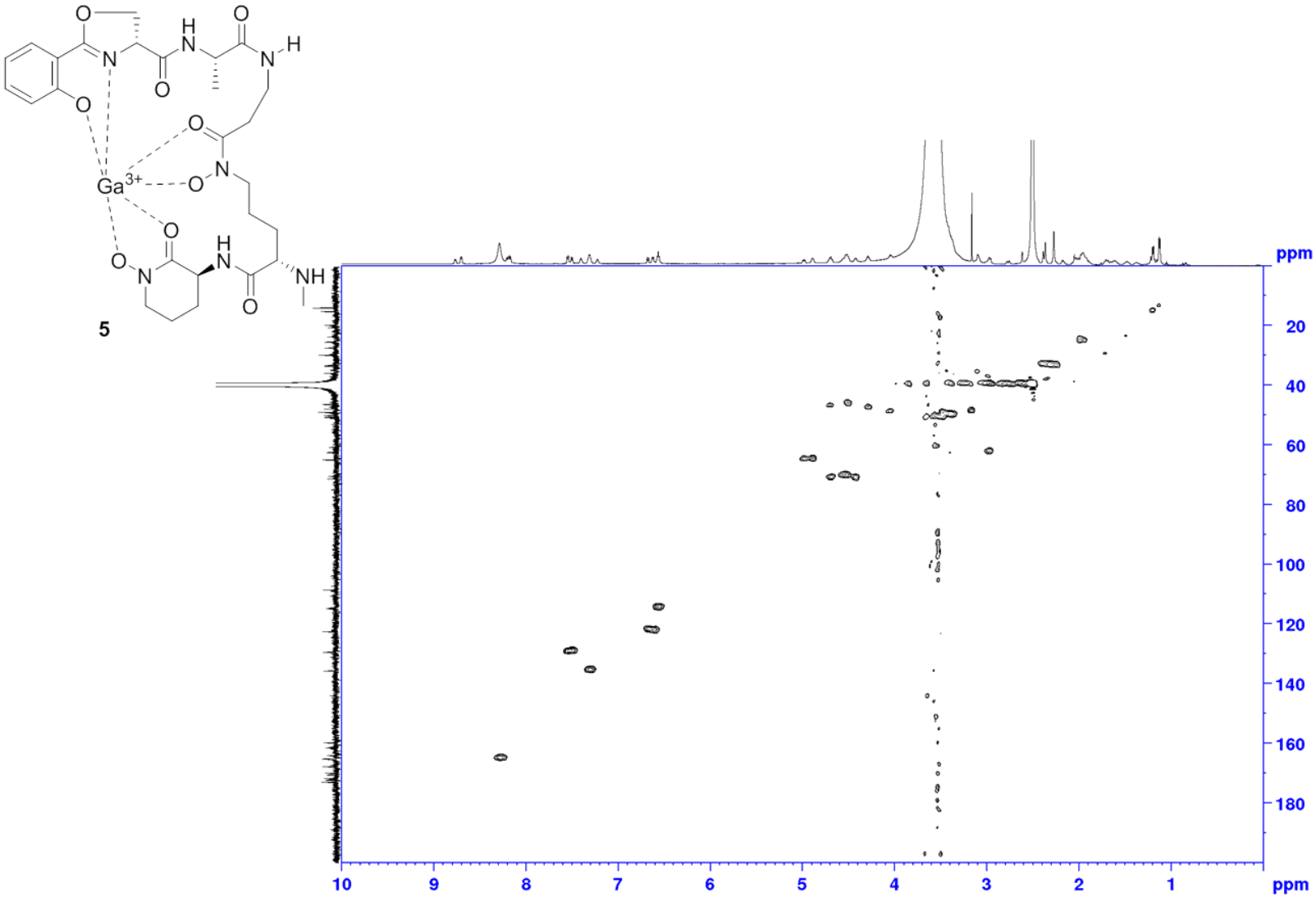

Figure S65. HSQC NMR spectrum of Ga^{3+}-madurastatin A1 (**5**) (DMSO-d_6, 600 MHz, 300 K)

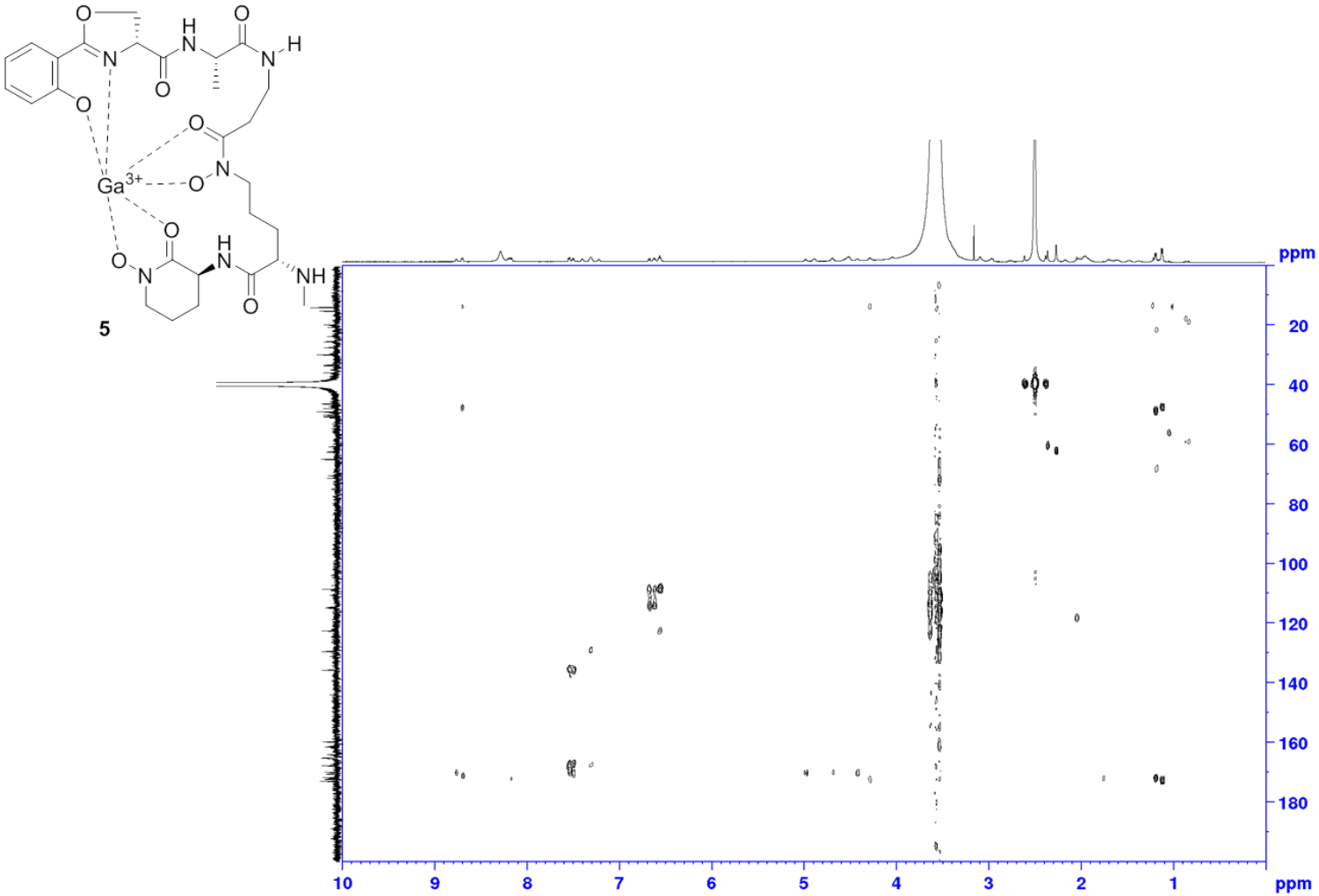

Figure S66. HMBC NMR spectrum of Ga-madurastatin A1 (**5**) (DMSO-d_6, 600 MHz, 300 K).

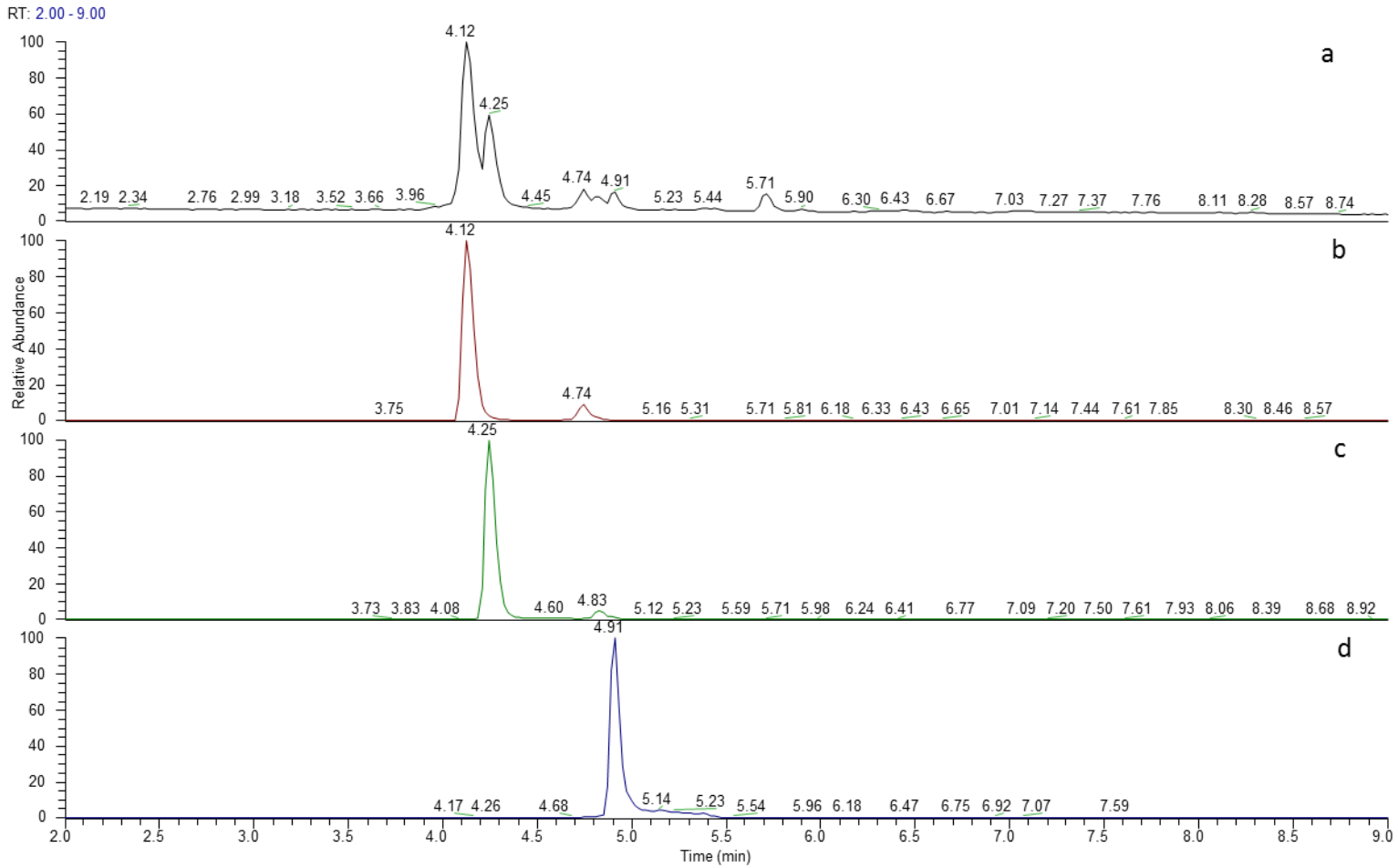

Figure S67. LC-HRESI-MS chromatogram of compound **5** enriched HPLC fraction. A) Total ion chromatogram (TIC); B) Extracted ion chromatogram (EIC) of Ga^{3+} complex of **5** for *m/z* 672.1891; C) Extract ion chromatogram (EIC) of Fe^{3+} complex of **5** for *m/z* 659.1984; D) Extracted ion chromatogram (EIC) of apo-**5** for *m/z* 606.2866.

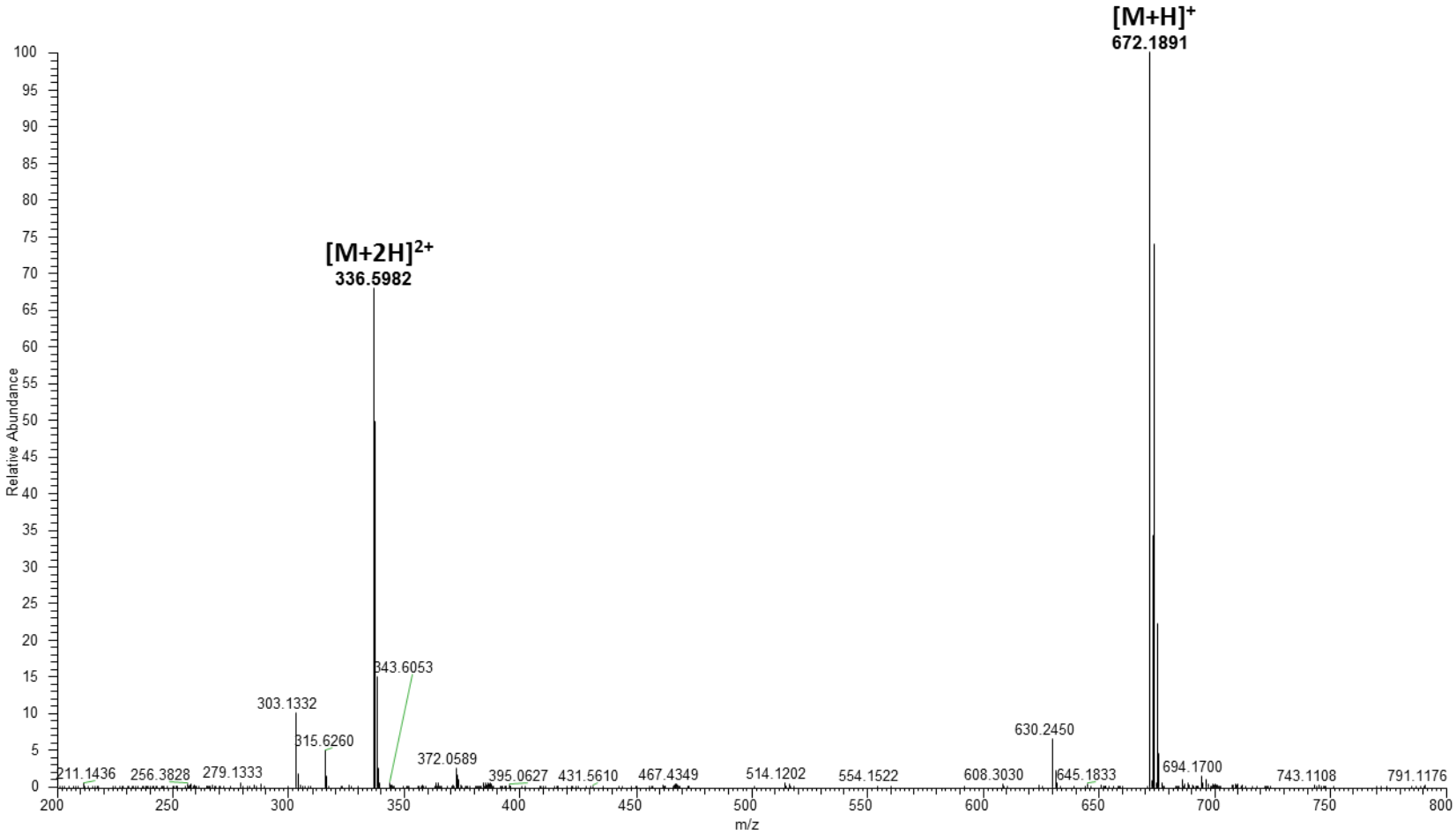

Figure S68. LC-HRESI-MS spectrum of Ga^{3+} complex of **5**, positive mode.

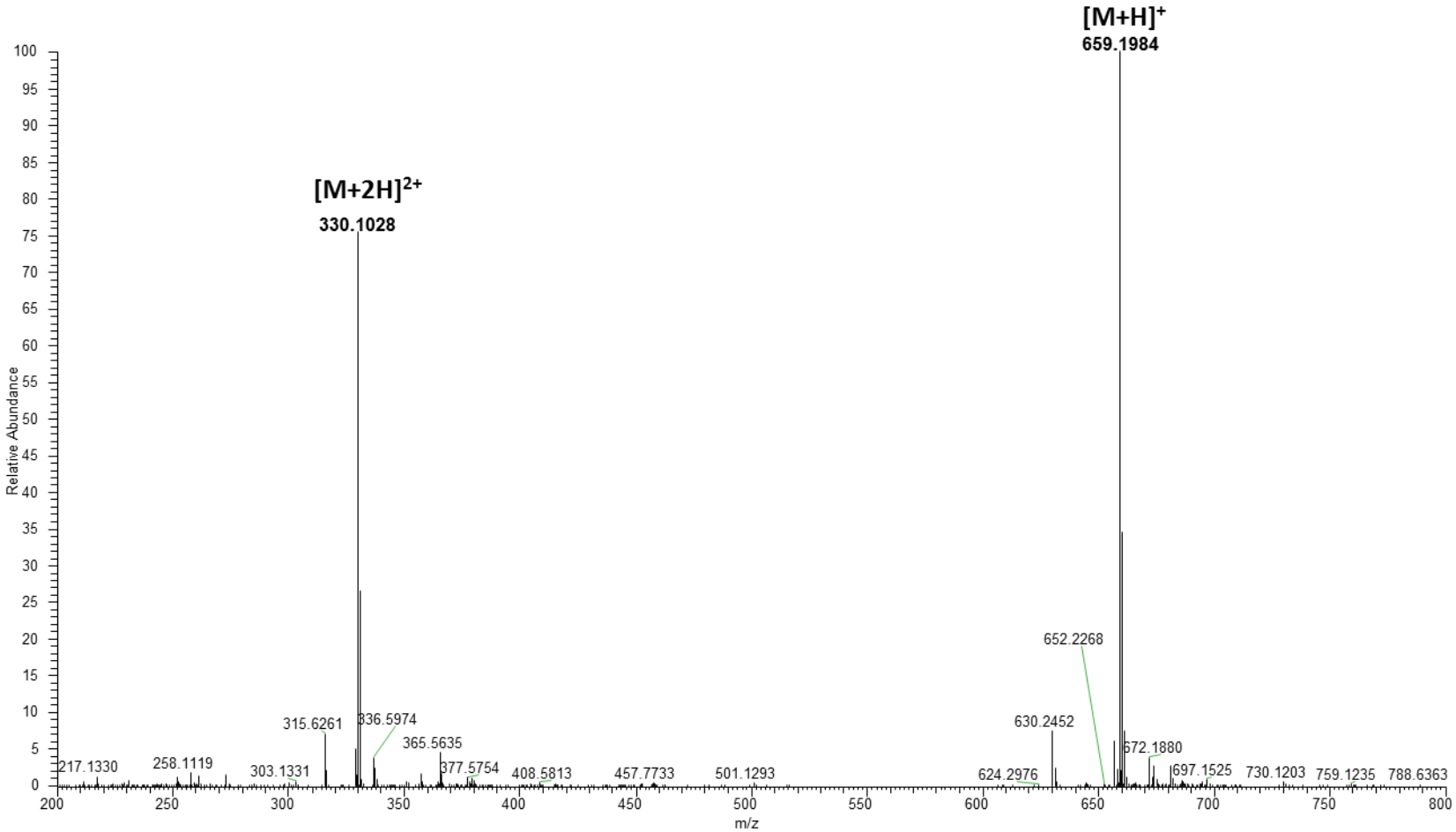

Figure S69. LC-HRESI-MS spectrum of Fe complex of **5**, positive mode.

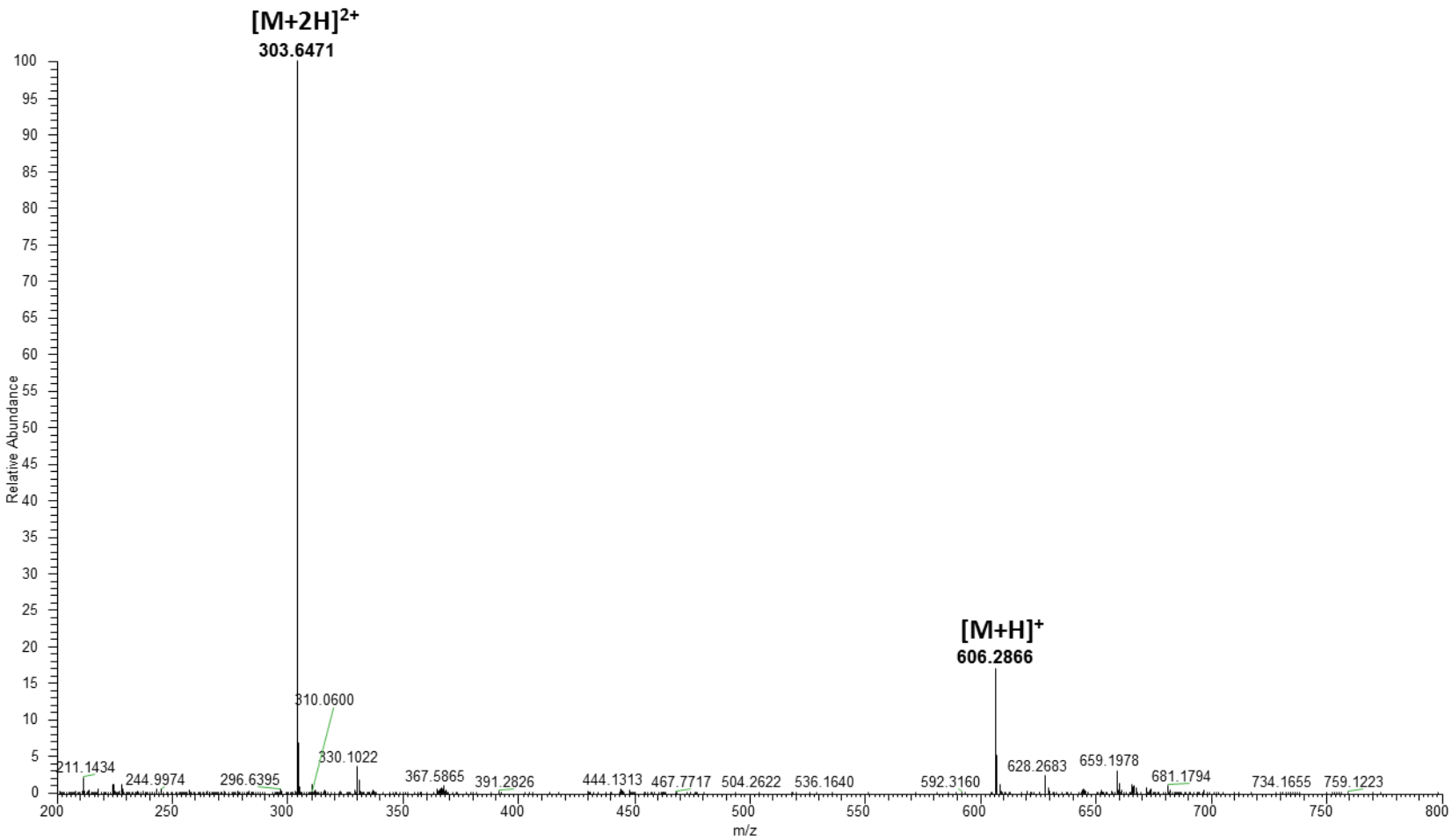

Figure S70. LC-HRESI-MS spectrum of apo form of **5**, positive mode.

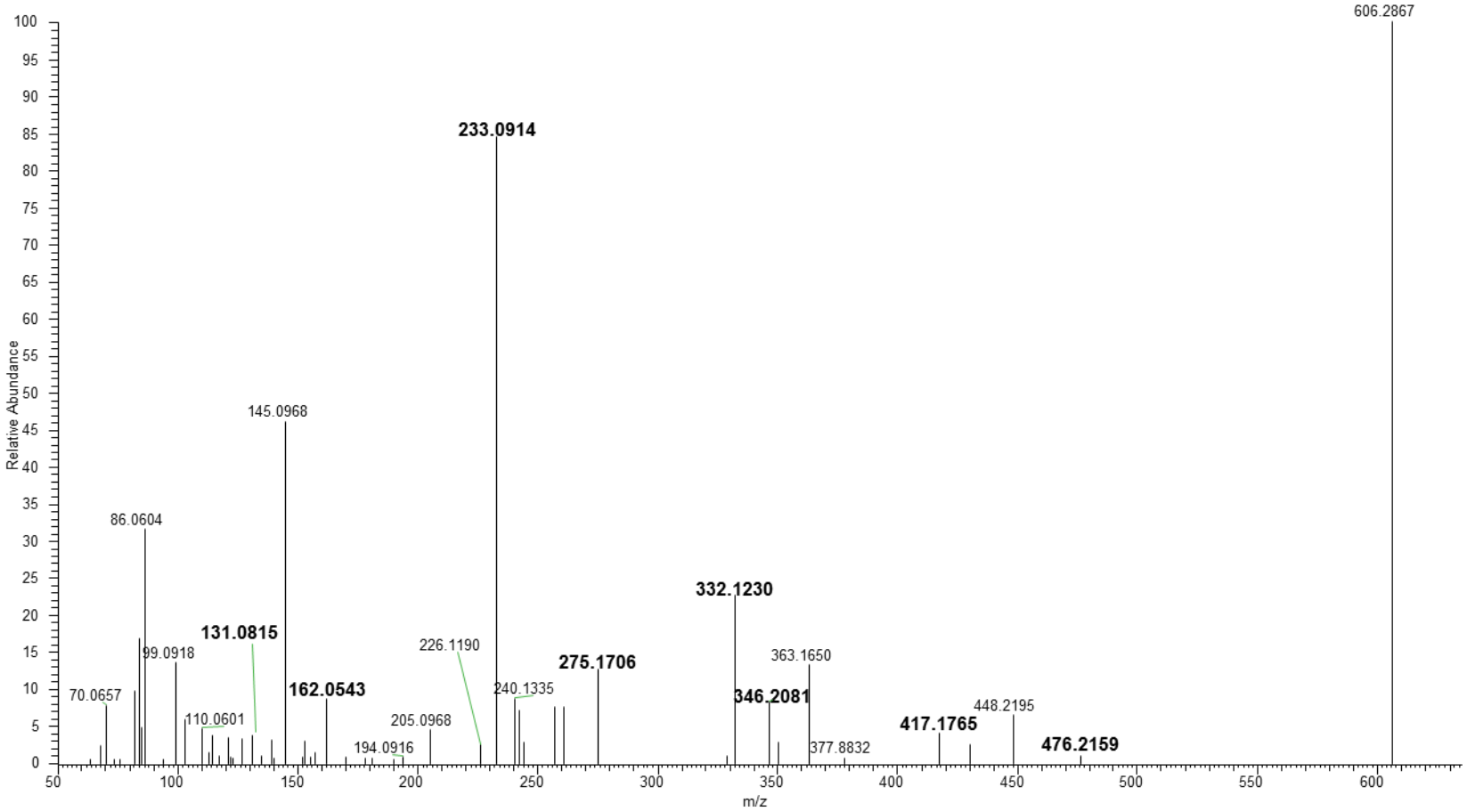

Figure S71. LC-HRESI-MS/MS spectrum of apo form of **5,** positive mode.

1) L-Ser

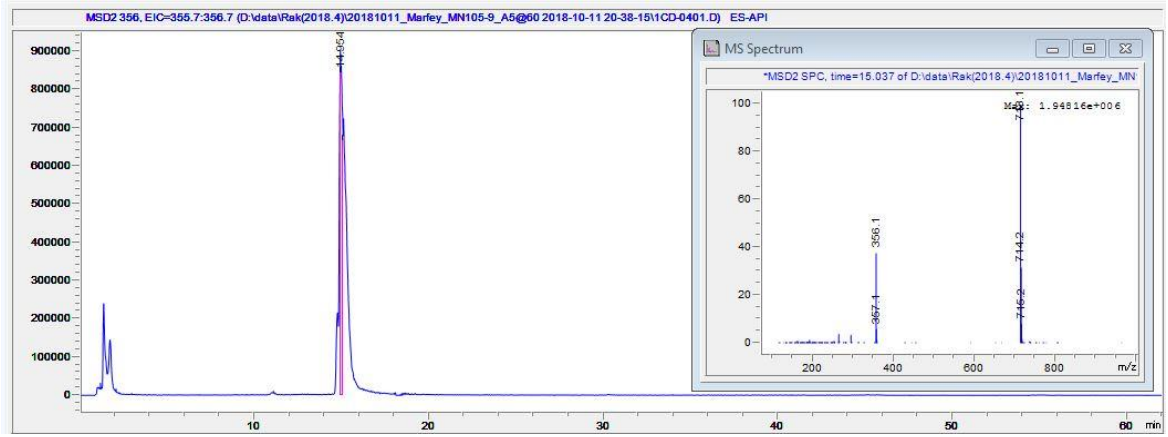
MSD2 356, EIC=355.7:356.7 (D:\data\Rak(2018.4)\20181011_Marfey_MN105-9_A5@60 2018-10-11 20-38-15\1CD-0401.D) ES-API
14.054
MS Spectrum
*MSD2 SPC, time=15.037 of D:\data\Rak(2018.4)\20181011_Marfey_MN
Max: 1.94816e+006
356.1
357.1
714.2
715.2
m/z
min

2) D-Ser

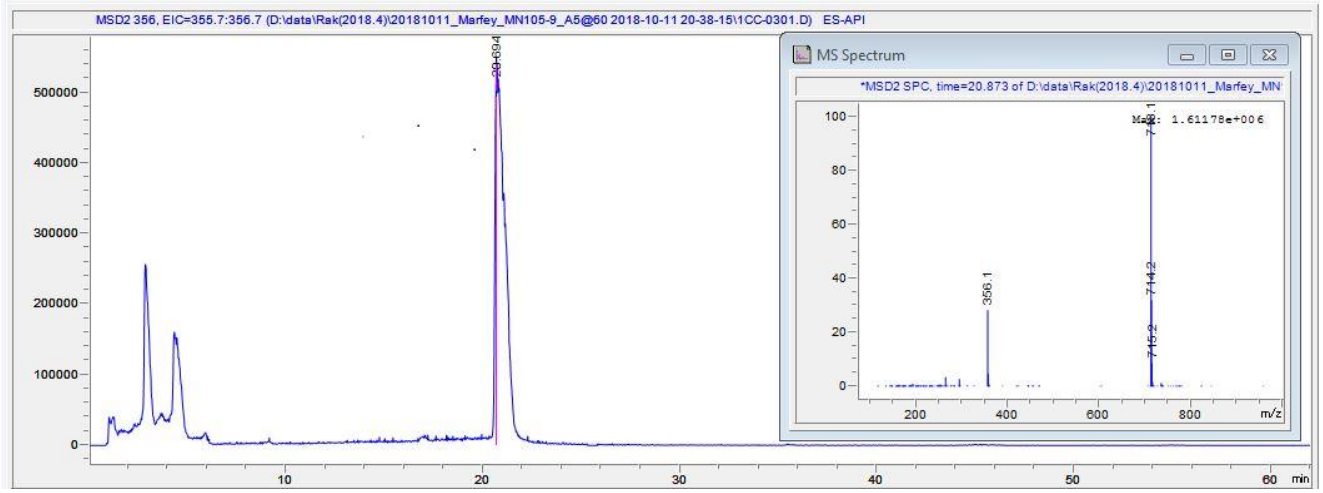
MSD2 356, EIC=355.7:356.7 (D:\data\Rak(2018.4)\20181011_Marfey_MN105-9_A5@60 2018-10-11 20-38-15\1CC-0301.D) ES-API
20.694
MS Spectrum
*MSD2 SPC, time=20.873 of D:\data\Rak(2018.4)\20181011_Marfey_MN
Max: 1.61178e+006
356.1
714.2
715.2
m/z
min

3) L-Ala

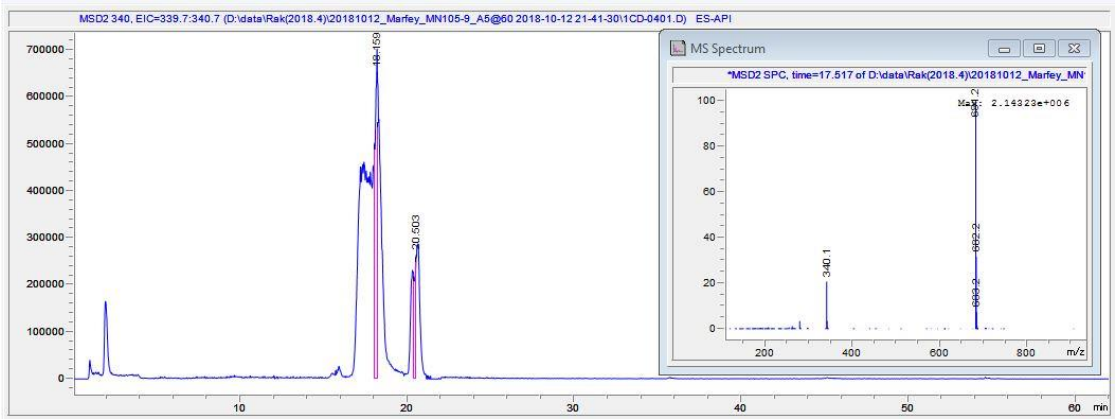
MSD2 340, EIC=339.7:340.7 (D:\data\Rak(2018.4)\20181012_Marfey_MN105-9_A5@60 2018-10-12 21-41-30\1CD-0401.D) ES-API
18.159
20.503
MS Spectrum
*MSD2 SPC, time=17.517 of D:\data\Rak(2018.4)\20181012_Marfey_MN
Max: 2.14323e+006
340.1
662.2
min

4) D-Ala

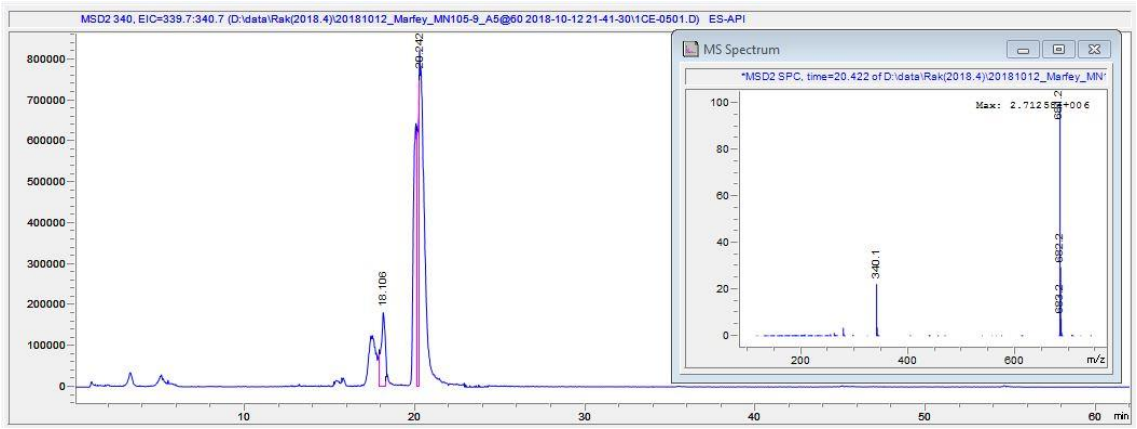
MSD2 340, EIC=339.7:340.7 (D:\data\Rak(2018.4)\20181012_Marfey_MN105-9_A5@60 2018-10-12 21-41-30\1CE-0501.D) ES-API
18.106
20.242
MS Spectrum
*MSD2 SPC, time=20.422 of D:\data\Rak(2018.4)\20181012_Marfey_MN
Max: 2.712554+006
340.1
662.2
min

5) L-Orn

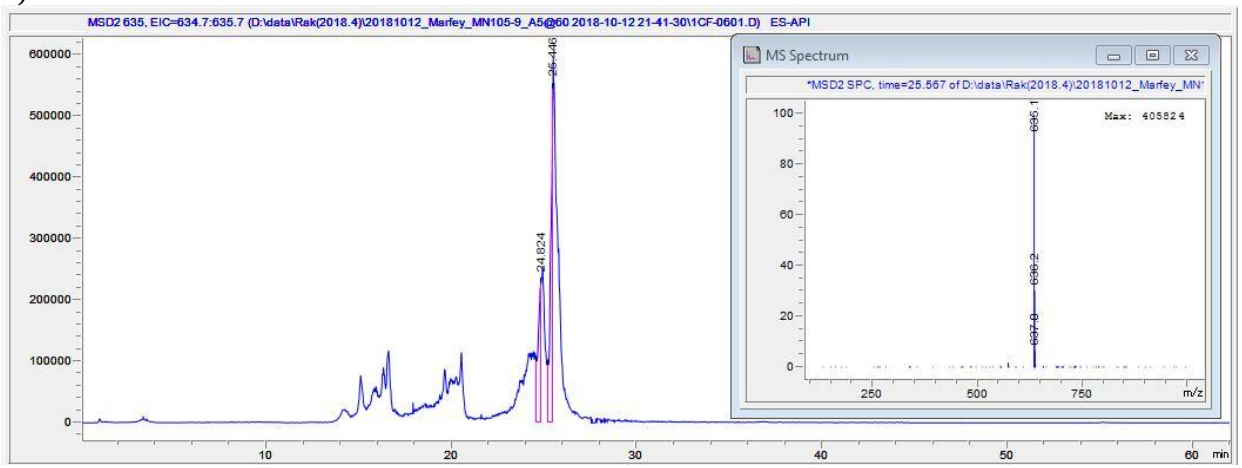
MSD2 635, EIC=634.7:635.7 (D:\data\Rak(2018.4)\20181012_Marfey_MN105-9_A5@60 2018-10-12 21-41-30\1CF-0601.D) ES-API
25.446
24.824
MS Spectrum
*MSD2 SPC, time=25.567 of D:\data\Rak(2018.4)\20181012_Marfey_MN
Max: 405824
635.1
636.2
637.0
m/z
min

6) D-Orn

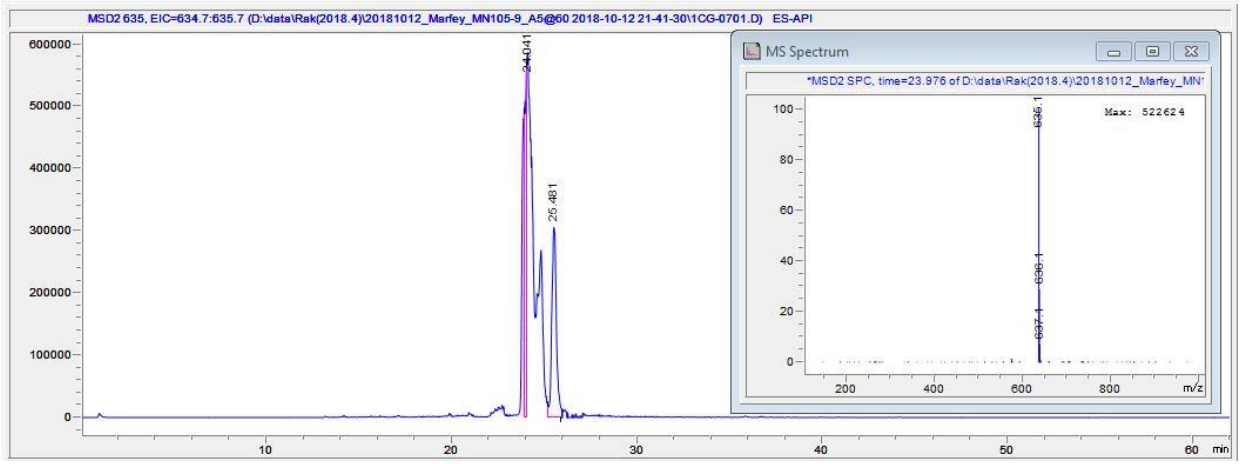
MSD2 635, EIC=634.7:635.7 (D:\data\Rak(2018.4)\20181012_Marfey_MN105-9_A5@60 2018-10-12 21-41-30\1CG-0701.D) ES-API
24.041
25.481
MS Spectrum
*MSD2 SPC, time=23.976 of D:\data\Rak(2018.4)\20181012_Marfey_MN
Max: 522624
636.1
636.1
637.1
m/z
min

7) *N*-methyl-L-Orn

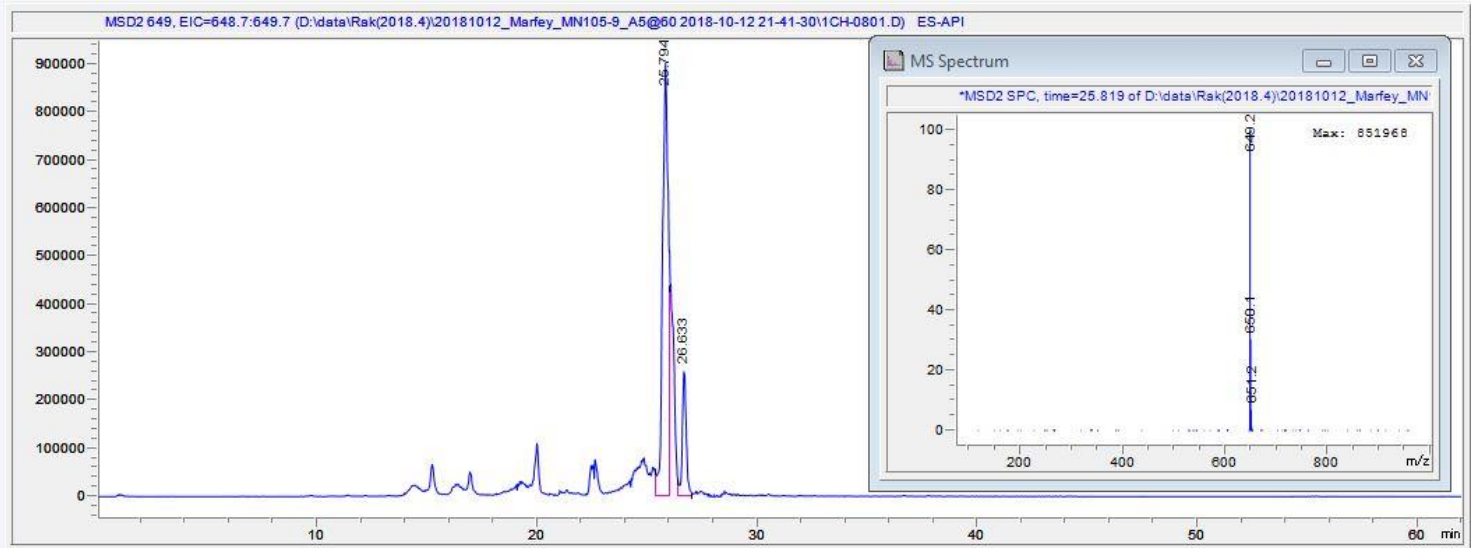

Figure S72. Retention times of the L-FDAA derivatized amino acids of standards

1) D-Ser

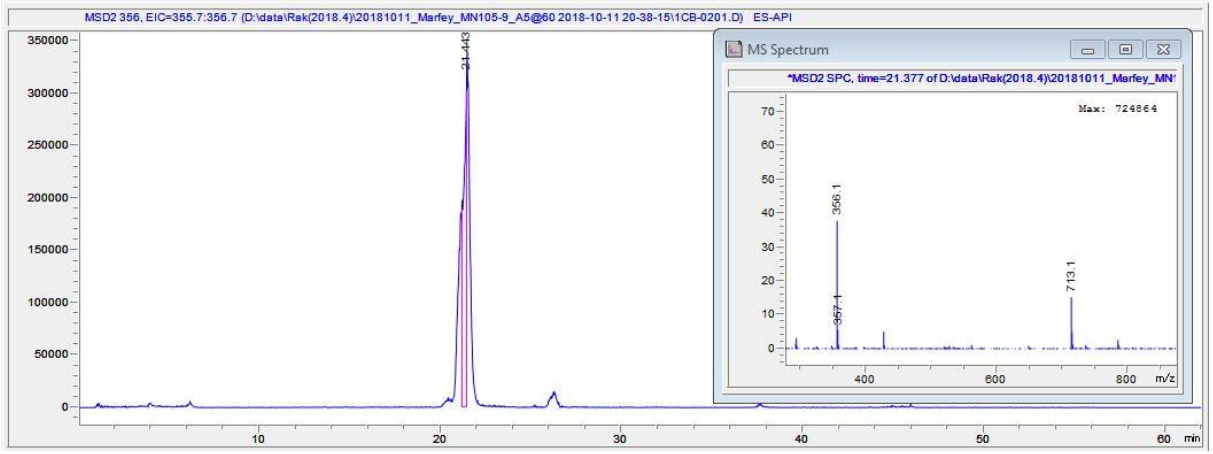
MSD2 356, EIC=355.7:356.7 (D:\data\Rak(2018.4)\20181011_Marfey_MN105-9_A5@60 2018-10-11 20-38-15\1CB-0201.D) ES-API
21.443
MS Spectrum
*MSD2 SPC, time=21.377 of D:\data\Rak(2018.4)\20181011_Marfey_MN
Max: 724864
356.1
357.1
713.1
m/z
min

2) L-Ala

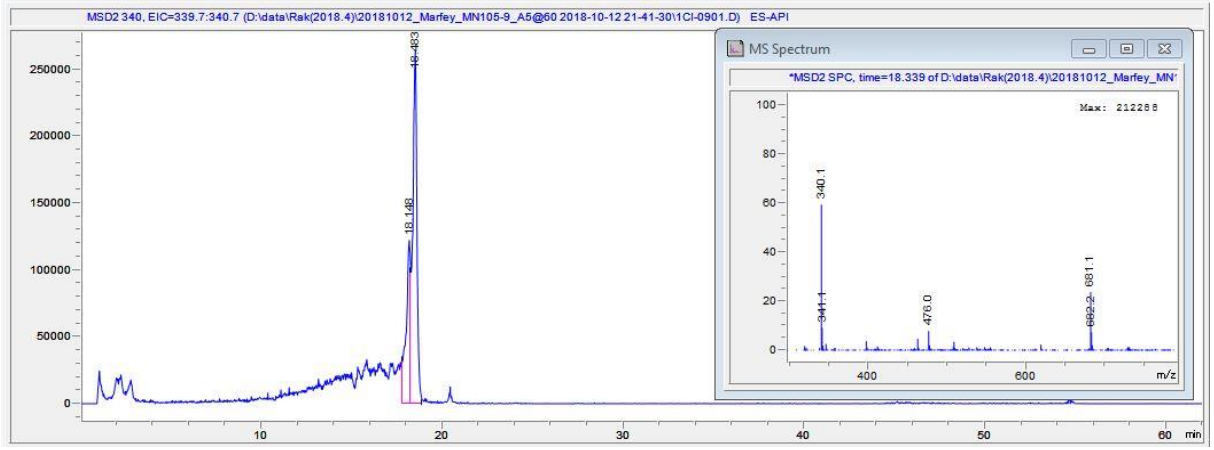
MSD2 340, EIC=339.7:340.7 (D:\data\Rak(2018.4)\20181012_Marfey_MN105-9_A5@60 2018-10-12 21-41-30\1CI-0901.D) ES-API
18.483
18.148
MS Spectrum
*MSD2 SPC, time=18.339 of D:\data\Rak(2018.4)\20181012_Marfey_MN
Max: 212288
340.1
341.1
476.0
681.1
682.2
m/z
min

3) L-Orn

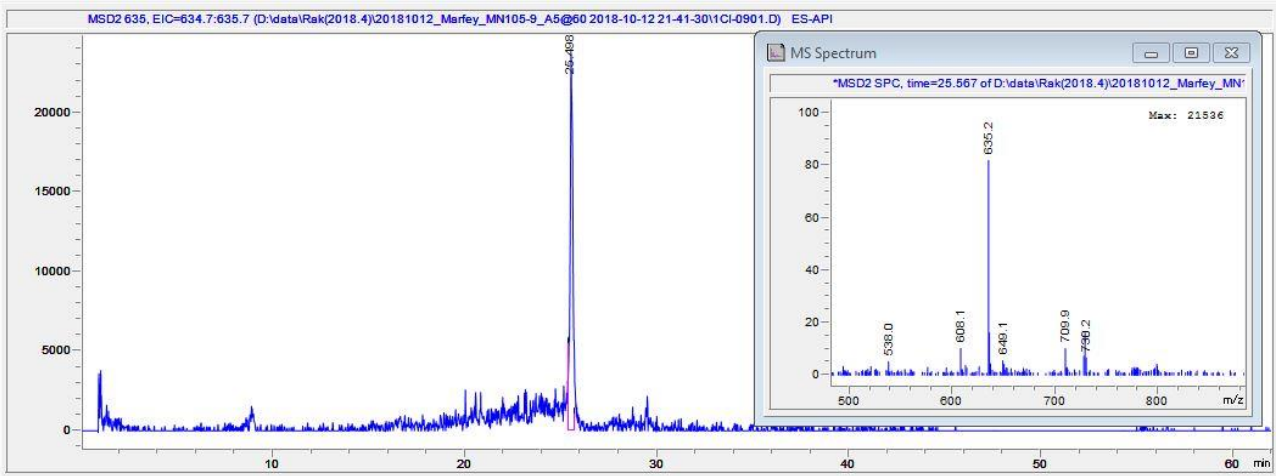

4) *N*-methyl-L-Orn

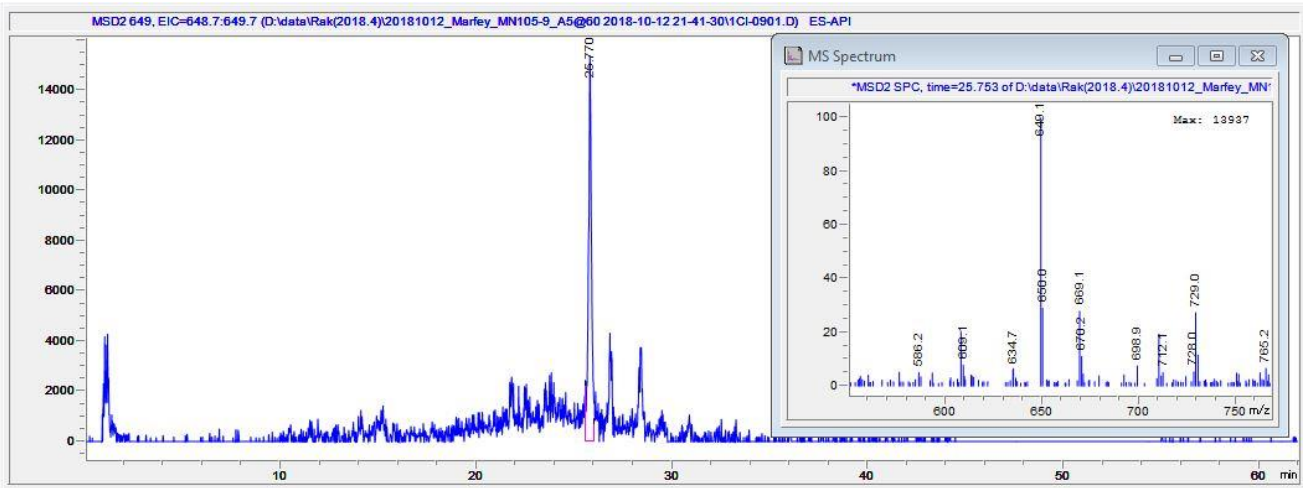

Figure S73. The retention times of the L-FDAA derivatized amino acids from compound **1**

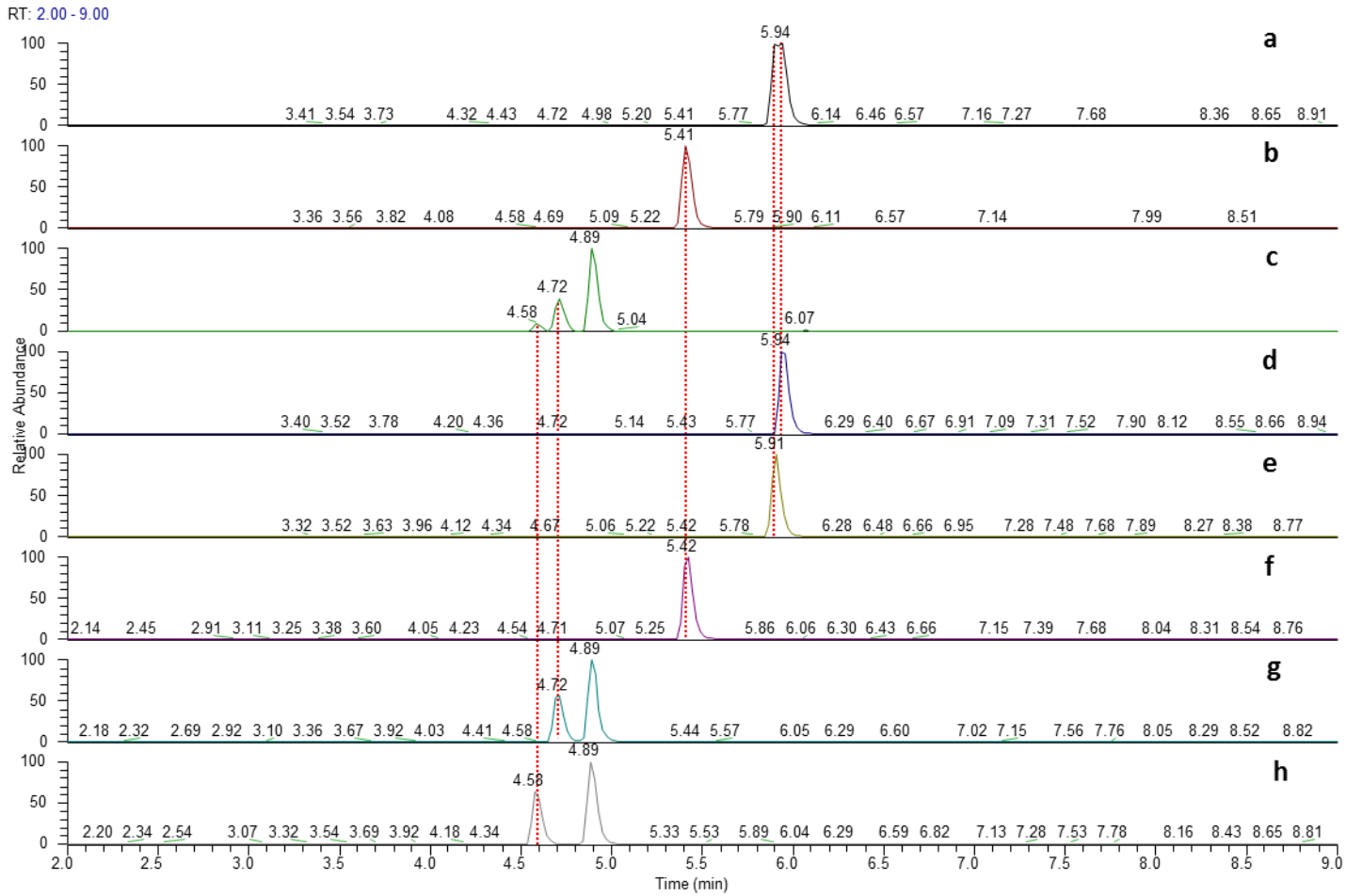

Figure S74. LC-HRESI(+)-MS chromatogram of **5** from Marfey's reaction. A) Extract ion count (EIC) mode of **5** under *m/z* 342.1038; B) EIC of **5** for *m/z* 358.0958; C) EIC of **5** for *m/z* 385.1461; D) EIC of L-alanine for *m/z* 342.1038; e) EIC of ß-alanine for *m/z* 342.1038; F) EIC of D-serine for *m/z* 358.0987; G) EIC of L-ornithine for *m/z* 385.1461; H) EIC of D-ornithine for *m/z* 385.1461.

12. Computational analysis

Determination of the absolute configuration of 2, 3, and 4 utilizing DP4+ probability analysis

All conformers proposed in this study were acquired through the MacroModel (version 2019-3, Schrödinger LLC) module with 'mixed torsional/low mode sampling' implemented with the MMFF94 force field. All searches were set initially in the gas phase with a 10 kJ/mol energy window limit and 10,000 maximum numbers of steps to thoroughly explore all potential conformers. The Polak-Ribiere conjugate gradient (PRCG) protocol was established with 10,000 maximum iterations and a 0.001 kJ (mol Å)-1 convergence threshold on the rms gradient to minimize conformers. Conformers proposed in this study within 5 kJ/mol found in the MMFF force field were selected for geometry optimization by Tmolex 4.3.1 at B3LYP/6-31+G(d,p) level for DP4+ analysis. Geometrically optimized conformers for possible diastereomers were used for calculation of gauge-invariant atomic orbital (GIAO) magnetic shielding tensors at the B3-LYP/6-31+G(d,p) level. Chemical shift values were calculated from the magnetic shielding tensors using the equation where δ is the calculated NMR chemical shift for nucleus x, and σ^o is the shielding tensor for the proton and carbon nuclei in tetramethylsilane calculated with the B3-LYP/6-31+G(d,p) basis set. DP4+ probability analysis was processed upon using an Excel sheet from Grimblat et al.

$$\delta_{calc}^{x} = \sigma^{o} - \sigma^{x}$$

Reference - Grimblat N, Zanardi MM, Sarotti AM. Beyond DP4: An Improved Probability for the Stereochemical Assignment of Isomeric Compounds using Quantum Chemical Calculations of NMR Shifts. J. Org. Chem. 2015, 80, 12526–12534. DOI: 10.1021/acs.joc.5b02396

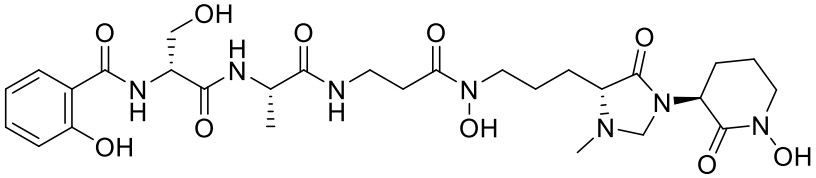

2a (isomer 1)

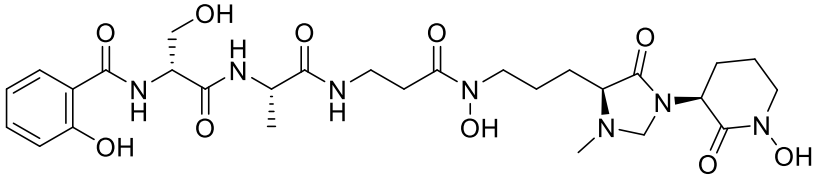

2b (isomer 2)

	A	B	C	D	E	F	G	H
1	Functional		Solvent?		Basis Set		Type of Data	
2	B3LYP		PCM		6-31+G(d,p)		Unscaled Shifts	
3								
4			Isomer 1	Isomer 2	Isomer 3	Isomer 4	Isomer 5	Isomer 6
5	sDP4+ (H data)		99.81%	0.19%	-	-	-	-
6	sDP4+ (C data)		94.86%	5.14%	-	-	-	-
7	sDP4+ (all data)		99.99%	0.01%	-	-	-	-
8	uDP4+ (H data)		100.00%	0.00%	-	-	-	-
9	uDP4+ (C data)		99.99%	0.01%	-	-	-	-
10	uDP4+ (all data)		100.00%	0.00%	-	-	-	-
11	DP4+ (H data)		100.00%	0.00%	-	-	-	-
12	DP4+ (C data)		100.00%	0.00%	-	-	-	-
13	DP4+ (all data)		100.00%	0.00%	-	-	-	-

Figure S77. DP4+ probability analysis for the determination of the absolute configuration of **2**.

Table S8. Computationally calculated ^{1}H and ^{13}C chemical shifts of **2a** and **2b** by utilizing computational analysis.

^{13}C					^{1}H				
Number	**Carbon Position**	**Exp.**	**Cal. (2a)**	**Cal. (2b)**	**Number**	**Carbon Position**	**Exp.**	**Cal. (2a)**	**Cal. (2b)**
2	7	169.9	165.2728	163.4656	46	8	4.59	5.074306	5.345409
4	8	57.1	55.20058	59.42911	47	11	4.33	4.800245	4.74795
5	9	62.6	63.97466	65.75498	48	20	3.05	2.974075	3.36041
7	10	172.5	161.1361	163.3842	49	23	4.66	4.610292	5.468065
9	11	50.5	48.68818	49.37156	51	9	3.89	3.752492	4.469758
10	12	17.4	13.99346	13.50855	52	9	3.94	5.202133	4.543015
11	13	174.5	163.7526	167.197	55	12	1.37	1.294229	1.544476
13	14	36.1	37.25645	37.43815	56	12	1.37	2.063354	2.013605
14	15	32.6	29.64457	35.283	57	12	1.37	1.454928	1.364429
15	16	173.3	161.9423	163.3026	59	14	3.45	3.910041	4.32409
17	17	48.4	50.80929	49.96521	60	14	3.45	3.464107	3.369902
18	18	22.8	25.60947	22.22457	61	15	2.7	3.920363	2.675825
19	19	25.8	30.43759	29.36288	62	15	2.7	2.114761	3.646223
20	20	67.1	67.11923	64.57762	63	17	3.57	3.798672	4.49381
21	21	175.6	167.5696	166.7402	64	17	3.61	3.884172	3.122189
23	23	52.4	51.76685	49.71993	65	18	1.78	2.870353	1.834152
24	22	164.7	158.526	154.929	66	18	1.78	1.517401	2.36329
27	26	52	50.31306	46.96174	67	19	1.96	1.911056	2.036638
28	25	21.7	21.68292	20.26947	68	19	1.96	2.977445	1.402546
29	24	29.1	24.84744	24.58044	70	26	3.58	3.799027	3.933583
33	2'	68	65.81639	65.06898	71	26	3.65	3.98868	4.096239
34	1'	39.8	41.81052	35.8639	72	25	2.02	2.561105	3.118378
39	6	110.8	110.9555	112.3856	73	25	2.06	2.141459	2.355353
40	5	159.9	155.1464	153.6029	74	24	1.93	2.033508	2.866865
42	4	117.9	111.9297	111.5217	75	24	2.32	2.024047	1.950064
43	3	134.6	128.6401	126.2888	76	2'	3.77	3.922784	4.334645
44	2	120.1	113.2392	111.6818	77	2'	4.34	5.209335	4.383168
45	1	130	122.8229	124.5964	78	1'	2.41	2.959558	2.525204
					79	1'	2.41	2.696261	2.335418
					80	1'	2.41	2.681286	2.778556
					83	4	6.93	7.458973	7.40061
					84	3	7.39	7.987773	7.817887
					85	2	6.92	7.464603	7.287848
					86	1	7.91	8.51591	9.054206

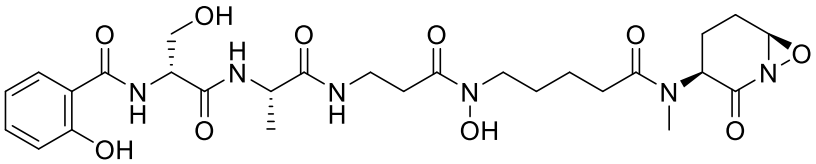

3a (isomer 1)

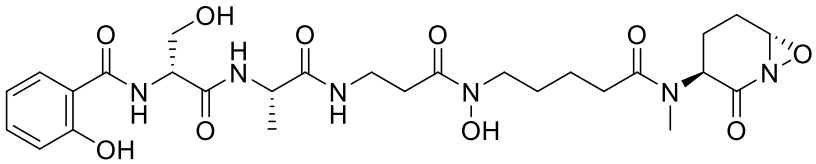

3b (isomer 2)

Functional	Solvent?	Basis Set	Type of Data
B3LYP	PCM	6-31+G(d,p)	Unscaled Shifts

	Isomer 1	Isomer 2	Isomer 3	Isomer 4	Isomer 5	Isomer 6
sDP4+ (H data)	99.81%	0.19%	-	-	-	-
sDP4+ (C data)	94.86%	5.14%	-	-	-	-
sDP4+ (all data)	99.99%	0.01%	-	-	-	-
uDP4+ (H data)	100.00%	0.00%	-	-	-	-
uDP4+ (C data)	99.99%	0.01%	-	-	-	-
uDP4+ (all data)	100.00%	0.00%	-	-	-	-
DP4+ (H data)	100.00%	0.00%	-	-	-	-
DP4+ (C data)	100.00%	0.00%	-	-	-	-
DP4+ (all data)	100.00%	0.00%	-	-	-	-

Figure S78. DP4+ probability analysis for the determination of the absolute configuration of **3**.

Table S9. Computationally calculated ^{1}H and ^{13}C chemical shifts of **3a** and **3b**.

^{13}C					^{1}H				
Number	Carbon Position	Exp.	Cal. (3a)	Cal. (3b)	Number	Carbon Position	Exp.	Cal. (3a)	Cal. (3b)
2	7	170	160.5903	160.5234	44	8	4.59	4.631003	4.820117
4	8	57.1	62.86777	53.03642	45	11	4.34	4.833402	4.596502
5	9	62.7	65.91441	61.59993	46	23	4.21	5.975929	3.868249
7	10	172.7	164.5502	168.001	47	26	5.75	4.851111	4.913251
9	11	50.5	49.03761	49.81175	49	9	3.88	4.550162	4.735255
10	12	17.5	13.76205	13.88643	50	9	3.92	4.153045	3.957464
11	13	174.7	167.78313	160.0837	53	12	1.37	1.503121	1.338947
13	14	36.2	37.437905	34.19106	54	12	1.37	1.662706	2.094933
14	15	32.7	38.06332	32.98501	55	12	1.37	2.187544	1.400099
15	16	173.7	164.5221	159.5322	57	14	3.45	3.346108	3.347411
17	17	48.1	46.21344	47.30333	58	14	3.45	4.758935	4.465732
18	18	21.3	26.34591	26.96609	59	15	2.69	3.187704	2.384879
19	19	26.6	22.825104	21.32364	60	15	2.69	3.074812	3.076843
20	20	36.7	32.74787	32.47453	61	17	3.54	3.390861	4.257409
21	21	168.9	167.011	169.5919	62	17	3.59	4.681018	3.907527
23	1'	31.2	30.88223	35.93094	63	18	1.37	2.452509	2.539811
24	23	62.2	55.56439	63.08499	64	18	1.42	1.54178	2.054973
25	22	165.1	180.4103	184.4774	65	19	1.59	2.006431	2.071863
28	26	82	75.167104	83.79448	66	19	1.59	1.904742	2.74923
29	25	29.5	23.92746	22.4573	67	20	2.21	2.834107	2.852999
30	24	27.3	19.53747	25.70477	68	20	2.21	2.406359	3.543028
37	6	110.8	118.5147	114.9216	69	1'	2.94	2.878543	3.536832
38	5	160.1	149.5373	148.8029	70	1'	2.94	3.765719	3.361618
40	4	118	116.2586	111.5684	71	1'	2.94	2.901278	2.900082
41	3	134.7	125.7791	126.9738	72	25	1.76	3.655556	3.172215
42	2	120.1	115.0363	113.3307	73	25	2.37	2.758331	2.856274
43	1	130.1	126.2527	126.9063	74	24	1.96	2.095066	2.25103
					75	24	2.11	2.650822	2.778286
					78	4	6.93	7.467884	7.229921
					79	3	7.39	7.8578	7.956974
					80	2	6.92	7.551378	7.491198
					81	1	7.9	8.798749	8.717146

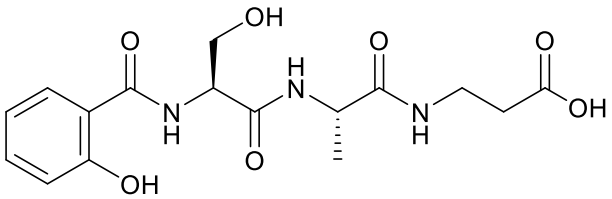

4a (isomer 1)

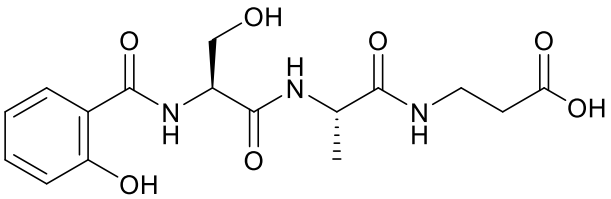

4b (isomer 2)

	A	B	C	D	E	F	G	H
1	Functional		Solvent?		Basis Set		Type of Data	
2	B3LYP		PCM		6-31G(d,p)		Unscaled Shifts	
3								
4			Isomer 1	Isomer 2	Isomer 3	Isomer 4	Isomer 5	Isomer 6
5	sDP4+ (H data)		0.00%	100.00%	-	-	-	-
6	sDP4+ (C data)		3.96%	96.04%	-	-	-	-
7	sDP4+ (all data)		0.00%	100.00%	-	-	-	-
8	uDP4+ (H data)		0.11%	99.89%	-	-	-	-
9	uDP4+ (C data)		95.49%	4.51%	-	-	-	-
10	uDP4+ (all data)		2.34%	97.66%	-	-	-	-
11	DP4+ (H data)		0.00%	100.00%	-	-	-	-
12	DP4+ (C data)		46.56%	53.44%	-	-	-	-
13	DP4+ (all data)		0.00%	100.00%	-	-	-	-

Figure S79. DP4+ probability analysis for the determination of the absolute configuration of **4**.

Table S10. Computationally calculated ^{1}H and ^{13}C chemical shifts of **4a** and **4b**.

		^{13}C					^{1}H		
Number	**Carbon Position**	**Exp.**	**Cal. (4a)**	**Cal. (4b)**	**Number**	**Carbon Position**	**Exp.**	**Cal. (4a)**	**Cal. (4b)**
2	7	170.1	165.0521229	164.6196408	27	8	4.58	4.794934191	5.111637643
4	8	57.2	50.79478112	51.40460449	28	11	4.36	3.672143863	4.796459595
5	9	62.7	63.5122637	64.00086012	30	9	3.95	4.900170362	4.181258205
7	10	172.4	166.9900025	166.2295643	31	9	3.9	4.197322552	4.956484969
9	11	50.4	53.44984272	48.53496608	34	12	1.36	2.400512666	1.904480416
10	12	17.6	14.40003394	13.68094842	35	12	1.36	2.081014771	1.41775361
11	13	174.6	159.8779278	160.7404168	36	12	1.36	1.373678608	1.585012052
13	14	36.6	34.95607177	36.35813935	38	14	3.4	4.139687081	3.402398351
14	15	35.5	32.74167797	33.38552828	39	14	3.43	3.263340774	4.166260892
15	16	176.6	168.9366612	166.6856974	40	15	2.46	2.606371402	2.587448452
20	6	110.9	107.23349	107.2987511	41	15	2.46	3.162121711	3.165058852
21	5	160	157.8409407	157.8379895	44	4	6.93	7.420027649	7.396021335
23	4	117.9	112.2566452	112.2877593	45	3	7.39	7.917815776	7.873104799
24	3	134.7	128.2718912	128.0896635	46	2	6.92	7.285074126	7.246656355
25	2	120.1	110.7142363	110.7422293	47	1	7.9	7.285074126	8.342464317
26	1	130	121.9311209	121.2402818					

13. Bioactivities

C. neoformans strains used in the current study were described in the previous studies.[3,4] All strains were cultured in yeast extract, bacto peptone with glucose (YPD; Biopure) or low-iron medium (LIM). For siderophore assay, *C. neoformans* cells were inoculated in 3 ml YPD broth and incubated for overnight at 30 C. Cells were pelleted and washed twice with iron-chelated phosphate buffered saline (PBS) and resuspended in LIM. Cells were incubated at 30 °C for overnight, pelleted, and washed twice using chelated PBS. Cells were resuspended in PBS. Total 2.0×10^5 cells were inoculated either in 200 μl of LIM, or in 200 μl of media containing iron-free or iron-loaded compound. Cells were grown for 36 hours at 30 °C, 5 μl of them were spotted on YPD agar medium, incubated for 24 hours at 30°, and photographs were taken. Each compound was mixed with $FeCl_3$ in a 1:0.9 molar ratio to prepare the iron-loaded form,[5,6] and added to LIM at a final concentration of 10 μM. Ferroxamine was used as a siderophore reference (positive control).

Antifungal activity of each compound was evaluated by determination of minimum inhibitory concentration (MIC) following Clinical and Laboratory Standards Institute (CLSI) guideline.[7] Cell viability was measured by spreading cultured from the 96 well-plate containing different concentrations of the compound and counting colony-forming unit (CFU).

14. Biosynthetic Pathway Analysis and Construction of phylogenetic trees

Amino Acid sequences were aligned using ClustalW[8] and the phylogenetic tree was built with Fasttree[9] 2 via the bioinformatics platform Galaxy.[10] The amino acid sequences of the A and the C Domains of Actinobacteria were retrieved from the antiSMASH database.[11] We used the sequences for A-Domains with a specificity for all proteinogenic amino acids as well as the unnatural amino acids ornithine, D-ornithine, n-methyl ornithine, and beta alanine. For the C-domains we used C-Domains to every currently known class of C-Domain. The phylogenetic trees were visualized using iTOL.[12]

Table S11. Comparison of adenylation domain active side residues extracted by NRPSPredictor 2[13]based on Amino acid sequences from known NRPS's.

A domain	Active side residues[a]	Substrate	Accession number
ReneL_A2	DILQIGMVYK		
Swb16 (SW-163C)	DILQI**TL**VYK	Gly/Ala	BAI63288
Ecm6 (echinomycin)	DILQI**TL**VYK		BAE98155
Mad31_A1 (madurastatin D)	DILQ*L*GM*I***W**K	Gly	WP_141576257
ReneL_A3	IDTTISLGDK		
Mad31_A2_(madurastatin D)	IDTTISLGDK	β-ala	WP_141576257
CahD_A1 (Cahuitamycin)	ID*V*TISL*A*DK		AMK48228.1
BlmIV (Bleomycin)	*V*D**WV**ISL*A*DK		AAG02364
ReneL_A3	DMENLGLINK		
Mad31_A3_(madurastatin D)	DMENLGLINK	Orn	WP_141576257
AMYAL_RS0130210 (Albachelin)	DMENLGLINK		WP_084702182
ReneQ_A1	DLFNLGLIHK		
Mad63 (madurastatin D)	DLFNLGLIHK	Cys/Ser	WP_141576286
GobJ (Gobichelin)	DLFNLGLIHK		AGE11891

[a]Major variation in Bold, minor variation in italics

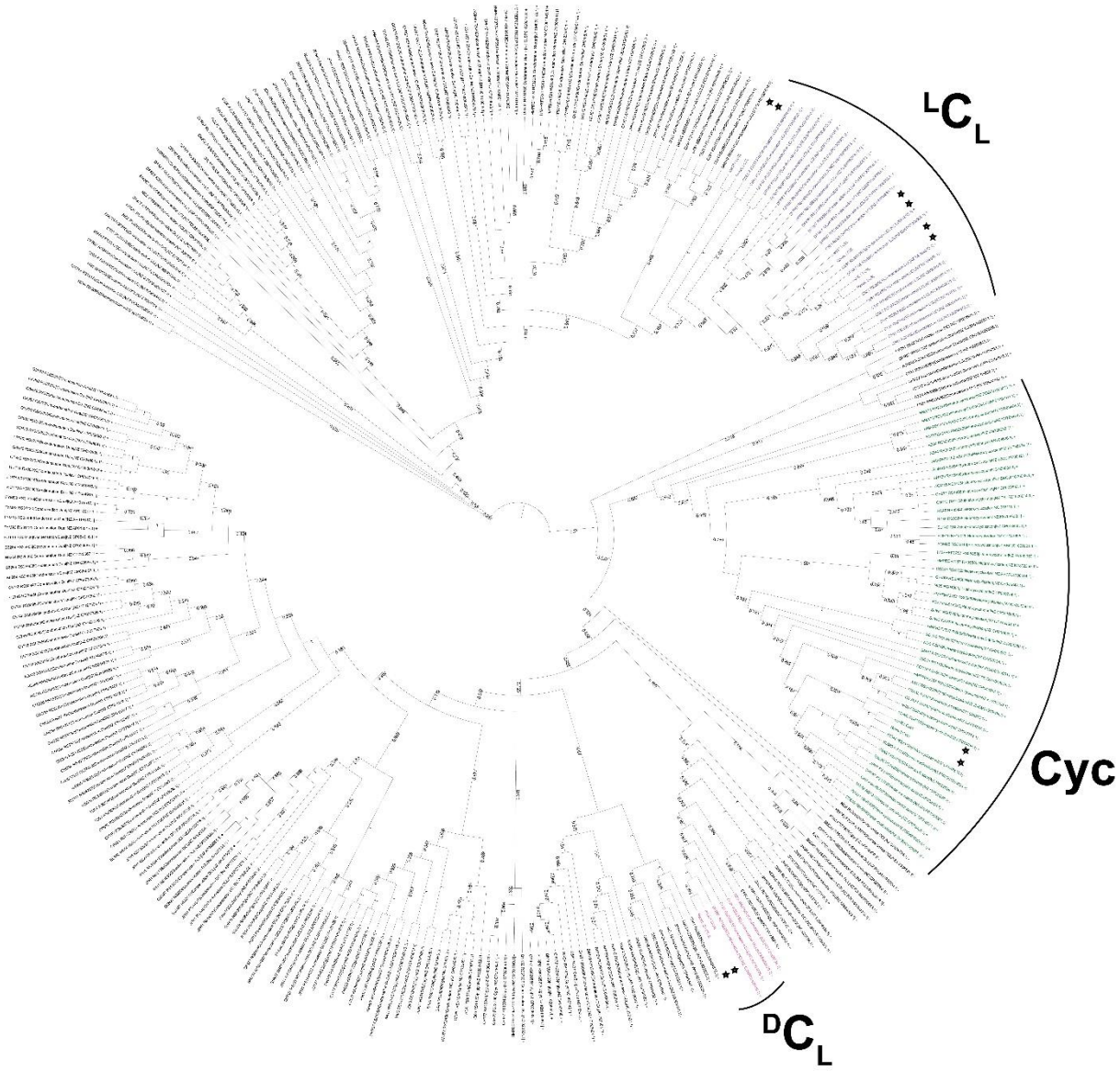

Figure S75. Phylogenetic analysis of Condensation Domains (C-domains of the *rene* cluster and the *mad* cluster are marked with a star).C-domains were aligned using ClustalW. The tree was created with fastree 2 (green: heterocyclization domains marked with Cyc; pink: condensation domains for the condensation of a D- and an L-amino acid ($^{D}C_{L}$), blue: Condensation domains for the condensation of two L-amino acids ($^{L}C_{L}$).

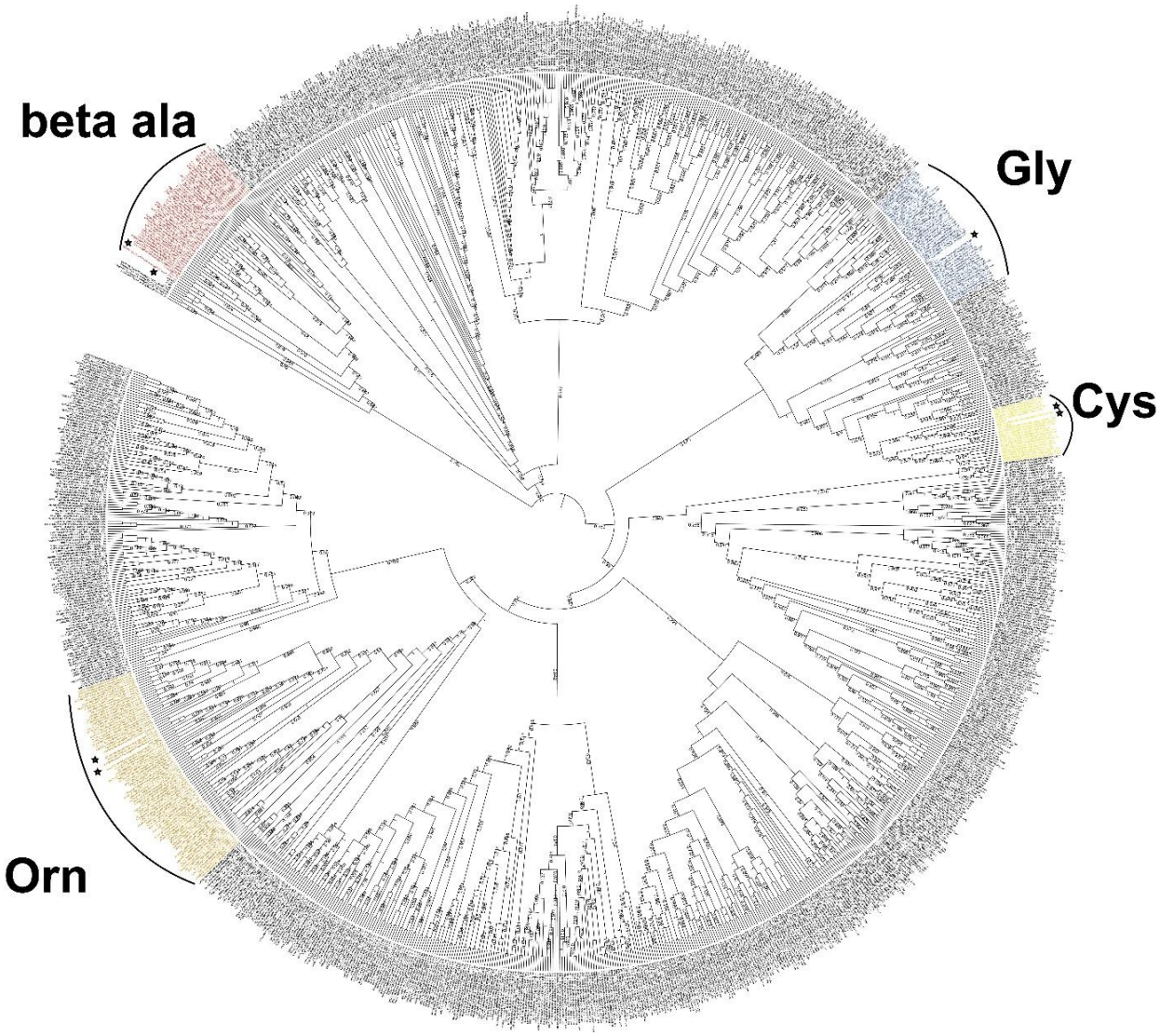

Figure S76. Phylogenetic analysis of Adenylation Domains (A-domains of the *rene* cluster and the *mad* cluster are marked with a star). A-domains were aligned using ClustalW. The tree was created with fastree 2 (yellow: A-domains with a specificity of Cys, blue: A-domains for glycine, orange: ornithine and derivatives thereof, red: beta-alanine)

Table S12. Top BLAST hits of genes in genomic region of putative madurastatin cluster in *Actinomadura* sp. RB99

Protein Name	size (AA)	Closest Homolog(s)[a]	Annotation	Identity (%)/ Alignment length (%)[b]	Accession number
RB99_01611 hypothetical protein	437	F9B16_25520 F8568_RS34155 ACTIVE_0127	acyltransferase family protein *Actinomadura montaniterrae* acyltransferase family protein *Actinomadura* sp. LD22 acyltransferase family protein *Actinomadura verrucosospora*	94.39/93 93.51/95 95.85/93.1	KAB2376107 WP_151597828 WP_173091757.1
RB99_01612 hypothetical protein	402	F8568_RS34160 F9B16_RS25530 ACTIVE_0126	helix-turn-helix domain-containing protein *Actinomadura* sp. LD22 helix-turn-helix domain-containing protein *Actinomadura montaniterrae* putative PucR family transcriptional regulator *Actinomadura verrucosospora*	96.12/96 96.12/100 95.02/100	WP_151597838 WP_151542657 QKG18492
RB99_01613 hypothetical protein	299	F9B16_RS25535 ACTIVE_0125 ERS075342_07230	esterase *Actinomadura montaniterrae* esterase *Actinomadura verrucosospora* esterase *Mycobacterium tuberculosis*	89.85/88 89.26/99 79.19/99	WP_151542664 QKG18491 CNG48089
RB99_01614 hypothetical protein	293	F9B16_RS25540 ACTIVE_0124 F8568_RS34170	DMT family transporter *Actinomadura montaniterrae* DMT family transporter *Actinomadura verrucosospora* DMT family transporter *Actinomadura* sp. LD22	96.92/99 95.56/100 94.18/99	WP_151542658 WP_173091753 WP_151597829
RB99_01615 putative diacylglycerol O-acyltransferase tgs3	640	F8568_RS34175 ACTIVE_0123 DTB52_RS20895	phosphatase PAP2 family protein *Actinomadura* sp. LD22 phosphatase PAP2 family protein *Actinomadura verrucosospora* phosphatase PAP2 family protein *Actinomadura madurae*	74.49/100 59.71/99 59.71/99	WP_151597830 WP_173091751 WP_111831501
RB99_01616 hypothetical protein	291	F9B16_RS40675 ACTIVE_0122 C4U03_RS16735 orf-4 RdmB Orf15	SAM-dependent methyltransferase *Actinomadura montaniterrae* SAM-dependent methyltransferase*Actinomadura verrucosospora* SAM-dependent methyltransferase *Actinomadura echinospora* s-adenosyl methyltransferase *Actinomadura* sp. ATCC 39365 S-adenosyl methyltransferase *Streptomyces* sp. methyltransferase *Actinoplanes garbadinensis*	92.99/93 86.96/93 60.44/93 54.47/87 48.45/88 46.03/86	WP_151545595 WP_173091749 WP_103938709 AKQ99279 AWW87417 ACR33048
RB99_01617 hypothetical protein	103	ACTIVE_0121 F9B16_RS40670 AA75_RS35610	hypothetical protein ACTIVE_0121 *Actinomadura verrucosospora* hypothetical protein *Actinomadura montaniterrae* hypothetical protein Kitasatospora sp. MBT63	86.73/95 94.52/70 72.53/86	QKG18487 WP_151545600 WP_033824513
RB99_01618 Benzoate 1,2-dioxygenase electron transfer component	234	F9B16_40660 F8568_034235 ACTIVE_0120	Oxidoreductase *Actinomadura montaniterrae* oxidoreductase *Actinomadura* sp. LD22 oxidoreductase FAD/NAD(P)-binding domain-containing protein *Actinomadura verrucosospora*	94.02/100 92.31/100 91.45/100	WP_151545594 WP_151597213.1 QKG18486
RB99_01619 Putative protein-methionine-sulfoxide reductase subunit YedZ1	199	F9B16_RS40660 F8568_RS34190 ACTIVE_0119 yuiH	molybdopterin-dependent oxidoreductase *Actinomadura montaniterrae* sulfite oxidase-like oxidoreductase *Actinomadura* sp. LD22 molybdopterin-dependent oxidoreductase *Actinomadura verrucosospora* putative molybdopterin containing enzyme subunit *Bacillus subtilis* subsp. *subtilis* str. 168	93.47/100 91.96/100 91.46/100 42.64/96	WP_151545593 WP_151597212 WP_173091745.1 CAB15192
RB99_01620 Ribonuclease BN	357	F9B16_40650 A2W34_02445 GEU28_04040	MBL fold metallo-hydrolase *Actinomadura montaniterrae* MBL fold metallo-hydrolase Chloroflexi bacterium RBG_16_64_32 MBL fold metallo-hydrolase *Dehalococcoidia* bacterium	95.52/100 63.19/91 59.63/91	WP_151545592.1 OGO46291.1 MPZ22713.1
RB99_01622 hypothetical protein	575	F9B16_RS40645 F8568_RS34200 ACTIVE_0118	ankyrin repeat domain-containing protein *Actinomadura montaniterrae* ankyrin repeat domain-containing protein *Actinomadura* sp. LD22 ankyrin repeat domain-containing protein *Actinomadura verrucosospora*	88.68/99 88.3/99 83.77/99	WP_151545599.1 WP_151597226.1 WP_173091743
RB99_01623 HTH-type transcriptional repressor KstR2 (kstR2_2)	201	F9B16_RS40615 F8568_RS34230 ACTIVE_0117	TetR family transcriptional regulator *Actinomadura montaniterrae* TetR family transcriptional regulator *ctinomadura* sp. LD22 TetR family transcriptional regulator *Actinomadura verrucosospora*	97.5//97 95.5/99 92.42/98	WP_151545597 WP_151597206.1 QKG18483
RB99_01624 3-methylmercaptopropionyl-CoA	548	F8568_030915 ACTIVE_0116	long-chain-fatty-acid--CoA ligase *Actinomadura* sp. LD22 atty-acid--CoA ligase FadD14 *Actinomadura verrucosospora*	97.45/100 97.45/100	WP_151597205 QKG18482

ligase **(*rene*A)**		F9B16_RS40610 norE aurE	long-chain-fatty-acid--CoA ligase *Actinomadura montaniterrae* aryl-coA ligase *Streptomyces orinoci* putative acyl-coA ligase *Streptomyces thioluteus*	97.63/100 32.7/97 32.34/89	WP_151545587 CAO85890 CAE02600
RB99_01625 putative enoyl-CoA hydratase 1 **(*rene*B)**	150	F9B16_RS40605 ACTIVE_0115 F8568_RS34240 htdZ iga16 salS Strop_1034	MaoC family dehydratase N-terminal domain-containing protein *Actinomadura montaniterrae* MaoC family dehydratase N-terminal domain-containing protein *Actinomadura verrucosospora* MaoC family dehydratase N-terminal domain-containing protein *Actinomadura* sp. LD22 3-hydroxyacyl-thioester dehydratase Z *Mycobacterium tuberculosis* (strain CDC 1551 / Oshkosh) MaoC dehydratase *Streptomyces* sp. MSC090213JE08 SalS *Salinispora tropica* MaoC domain protein dehydratase *Salinispora tropica* CNB-440	94/100 94/100 90.6/99 59.7/74.3 56.29/99 55.38/86 55.38/86	WP_151545586 WP_173091741 WP_151597204 P9WNP2 BAX64257 ABP73636 ABP53508
RB99_01626 rebeB Putative aminoglycoside phosphotransferase **(*rene*C)**	346	F8568_RS34245 F9B16_RS40600 ACTIVE_0114 UMAG_06422 MF437311.1:15219..16346 rslP	phosphotransferase *Actinomadura* sp. LD22 phosphotransferase *Actinomadura montaniterrae* aminoglycoside phosphotransferase *Actinomadura verrucosospora* hypothetical protein UMAG_06422 *Ustilago maydis* 521 phosphotransferase *Streptomyces olivaceus* putative phosphotransferase *Streptomyces bottropensis*	93.06/100 93.06/100 91.1/100 34.13/83 34.5/71 32.72/80	WP_151597203 WP_151545596 QKG18480 XP_011392706 AWM72912 AHL46718
RB99_01627 hypothetical protein **(*rene*D)**	113	H7233_02665 H7323_08775 IEZ08_RS11290	aldehyde dehydrogenase family protein *Pseudorhodobacter* sp. aldehyde dehydrogenase family protein *Frankiales* bacterium aldehyde dehydrogenase family protein *Planobispora rosea*	48.45/85 50/88 49/88	MBC7677880 MBC7374068 WP_068922388
RB99_01628 Multidrug resistance protein MdtG´**(*rene*E)**	560	F9B16_RS23765 F8568_RS34255 ACTIVE_0112	MFS transporter *Actinomadura montaniterrae* MFS transporter *Actinomadura* sp. LD22 MFS transporter *Actinomadura verrucosospora*	96.61/100 95/100 93.39/100	WP_151542327 WP_151597201 WP_173091735
RB99_01629 Transcriptional regulator SlyA **(*rene*F)**	155	F9B16_RS23770 F8568_RS34260 ACTIVE_0111 pntR	MarR family transcriptional regulator *Actinomadura montaniterrae* MarR family transcriptional regulator *Actinomadura* sp. LD22 MarR family transcriptional regulator *Actinomadura verrucosospora* PntR *Streptomyces arenae*	94.84/100 91.61/100 84.52/100 43.8/88	WP_151542328 WP_151597200 WP_173091733 ADO85569
RB99_01630 Multidrug efflux protein YfmO (***rene*G**)	422	F9B16_RS23775 ACTIVE_0110 F8568_RS34265 yfmO mem2 rkH gilJ	MFS transporter *Actinomadura montaniterrae* MFS transporter *Actinomadura verrucosospora* MFS transporter *Actinomadura* sp. LD22 Multidrug efflux protein YfmO *Bacillus subtilis* strain 168) Mem2 *Actinoplanes friuliensis* antibiotic efflux protein *Streptomyces* sp. 88-682 putative transmembrane efflux protein *Streptomyces griseoflavus*	97.16/100 96/98 95.97/100 55.2/73.6 33.97/68 32.73/65 29.15/62	WP_151542329 WP_173091731 WP_151597199 O06473 CAM56779 ACZ65473 AAP69589
RB99_01631 hypothetical protein ***(rene*H*)***	290	F8568_RS34270 F9B16_RS23780 ACTIVE_0109	hypothetical protein *Actinomadura* sp. LD22 hypothetical protein *Actinomadura montaniterrae* hypothetical protein *Actinomadura verrucosospora*	96.54/99 95.5/99 92.67/100	WP_151597198 WP_151542330 WP_173091729
RB99_01632 Protein MbtH ***(rene*I*)***	65	F9B16_RS23785 ACTIVE_0108 ETD83_RS12230 SSMG_02539 gobL mbtH tcp17	MbtH family NRPS accessory protein *Actinomadura montaniterrae* MbtH-like protein *Actinomadura verrucosospora* MbtH family protein *Actinomadura* sp. 14C53 mbtH protein *Streptomyces* sp. AA4 amychelin cluster MbtH *Streptomyces* sp. NRRL F-4415 Putative conserved protein MbtH *Mycobacterium tuberculosis H37Rv* MbtH-like short polypeptide *Actinoplanes teichomyceticus*	90.77/100 89 /92 89/90 62.5/98 66.15/100 69.35/87 76.56/98	WP_151542331 QKG18474 WP_138645214 EFL06868 AGE11893.1 CCP45165.1 CAE53358
RB99_01633 L-ornithine N(5)-monooxygenase ***(rene*J*)***	433	F9B16_RS23790 F8568_RS34280 E1291_RS35040 SSMG_02546 gobT SCO0498	lysine N(6)-hydroxylase/L-ornithine N(5)-oxygenase family protein *Actinomadura montaniterrae* lysine N(6)-hydroxylase/L-ornithine N(5)-oxygenase family protein *Actinomadura* sp. LD22 SidA/IucD/PvdA family monooxygenase *Actinomadura verrucosospora* peptide monooxygenase *Streptomyces* sp. AA4 (amychelin cluster) L-ornithine 5-monooxygenase *Streptomyces* sp. NRRL F-4415 putative peptide monooxygenase *Streptomyces coelicolor* A3(2)	95.15/100 94.92/100 93.3/100 59/94 57.55/94 61.41/95	WP_151542332 WP_151597196 WP_173091725 EFL06875 AGE11900 CAB53328

		AMYAL_RS0130205	SidA/IucD/PvdA family monooxygenase *Amycolatopsis alba*	59.77/97	WP_039794392
RB99_01634 Putative ABC transporter substrate-binding lipoprotein YhfQ ***(rene*K)**	338	ACTIVE_0106 F8568_RS34285 F9B16_RS23795 E1291_RS35045 RHA1_ro02320 AMYAL_RS0130225 SCAB_85451	ABC transporter substrate-binding protein *Actinomadura verrucosospora* ABC transporter substrate-binding protein *Actinomadura* sp. LD22 ABC transporter substrate-binding protein *Actinomadura montaniterrae* iron-siderophore ABC transporter substrate-binding protein *Actinomadura roseirufa* ABC Fe(3+) transporter, substrate binding component *Rhodococcus jostii* RHA1 iron-siderophore ABC transporter substrate-binding protein *Amycolatopsis alba* putative secreted siderophore-binding lipoprotein (transport system associated) *Streptomyces scabiei* 87.22	95.73/97 95.12/97 94.21/97 79.64/97 34.64/100 37.17/96 35.76/93	WP_173091723 WP_151597195 WP_151542333 WP_131742362 ABG94126 WP_020635022 CBG75490
RB99_01635 Tyrocidine synthase 3 ***(rene*L)**	4036	F9B16_RS23800 ACTIVE_0105 F8568_RS34290 E1300_RS26465 SCAB_85471 AMYAL_RS0130210 amcE gobR ilaS	amino acid adenylation domain-containing protein *Actinomadura montaniterrae* cyclic nucleotide binding protein *Actinomadura verrucosospora* amino acid adenylation domain-containing protein *Actinomadura* sp. LD22 amino acid adenylation domain-containing protein *Actinomadura fibrosa* putative NRPS/siderophore biosynthesis protein *Streptomyces scabiei* 87.22 non-ribosomal peptide synthetase *Amycolatopsis alba* nonribosomal peptide synthetase (amychelin cluster) nonribosomal peptide synthetase IlaS *Streptomyces atratus*	92.56/99 92.06/99 91.94/99 81.52/99 45.38/99 46.62/99 43.41/89 43.41/89 40.19/99	WP_151542334 QKG18471 WP_151597194 WP_131759779 CBG75492 WP_084702182 EFL06866.1 AGE11898.1 ASX95241
RB99_01636 Salicylate synthase ***(rene*M)**	436	F9B16_RS23805 F8568_RS34295 ACTIVE_0104 SSMG_02545 DT87_RS23310 mbtI	salicylate synthase *Actinomadura montaniterrae* salicylate synthase *Actinomadura* sp. LD22 Chorismate binding-like protein [*Actinomadura verrucosospora*] salicylate synthase *Streptomyces* sp. AA4 (amychelin cluster) MULTISPECIES: salicylate synthase unclassified *Streptomyces* Isochorismate synthase MbtI *Mycobacterium tuberculosis* H37Rv	93.66/94 92.7/94 91.53/100 56.24/99 52.59/95 48.53/51	WP_151542346 WP_151597225 QKG18470.1 EFL06874 WP_037880184 CCP45174.1
RB99_01637 2,3-dihydroxybenzoate-AMP ligase ***(rene*N)**	537	ACTIVE_0103 F9B16_RS23810 F8568_RS34300 SSMG_02542 gobK mxcE mbtA	AMP-binding protein [*Actinomadura verrucosospora*] AMP-binding protein *Actinomadura montaniterrae* AMP-binding protein *Actinomadura* sp. LD22 2,3-dihydroxybenzoate-AMP ligase *Streptomyces* sp. AA4 (amychelin cluster) 2,3-dihydroxybenzoate-AMP ligase *Streptomyces* sp. NRRL F-4415 MxcE *Stigmatella aurantiaca* Sg a15 Bifunctional enzyme MbtA: salicyl-AMP ligase (SAL-AMP ligase) + salicyl-S-ArCP synthetase *Mycobacterium tuberculosis* H37Rv	96.18/97 94.66/97 94.47/97 61.93/97 58.47/98 58.32/97 51.11/97	WP_173100878 WP_151542347 WP_151597224 EFL06871.1 AGE11892.1 AAG31128 CCP45172
RB99_01638 Aspartate 1-decarboxylase ***(rene*O)**	135	F8568_RS34305 ACTIVE_0102 F9B16_RS23815 kirD RSAG_RS12240 crpG	aspartate 1-decarboxylase *Actinomadura* sp. LD22 aspartate 1-decarboxylase *Actinomadura verrucosospora* aspartate 1-decarboxylase *Actinomadura montaniterrae* putative aspartate-1-decarboxylase precursor *Streptomyces collinus* Tu 365 MULTISPECIES: aspartate 1-decarboxylase Clostridiales CrpG *Nostoc* sp. ATCC 53789	97.04/100 93.3/100 96.3/100 62.5/94 56.14/84 44.74/84	WP_151597223 WP_173091719 WP_151542335 CAN89641 WP_008704365 ABM21575
RB99_01639 Enterobactin exporter EntS ***(rene*P)**	428	entS entS H4W34_005751 RER_27030 RHA1_ro02321 vabS SSMG_02541	enterobactin transporter EntS *Actinomadura montaniterrae* enterobactin transporter EntS *Actinomadura verrucosospora* ENTS family enterobactin (siderophore) exporter *Actinomadura algeriensis* putative siderophore export protein *Rhodococcus erythropolis* PR4 transporter, MFS superfamily protein *Rhodococcus jostii* RHA1 putative siderophore exporter *Vibrio anguillarum* major facilitator superfamily transporter multidrug resistance protein *Streptomyces* sp. AA4 (amychelin chluster)	91.12/100 91.2/100 81.19/98 45.48/92 44.29/97 40.51/99 38.48/92	WP_151542336 WP_173091717 MBE1535918 BAH33411 ABG94127 CAJ45638 EFL06870
RB99_01640 Phenyloxazoline synthase	1124	F9B16_RS23825 F8568_RS30790	amino acid adenylation domain-containing protein *Actinomadura montaniterrae* amino acid adenylation domain-containing protein *Actinomadura* sp. LD22	93.86/99 93.05/99	WP_151542337 WP_151597192

MbtB ***(reneQ)***		ACTIVE_0100 SSMG_02535 gobJ nbtF mbtB	amino acid adenylation domain-containing protein *Actinomadura verrucosospora* non-ribosomal peptide synthetase *Streptomyces* sp. AA4 (amychelin cluster) nonribosomal peptide synthetase *Streptomyces* sp. NRRL F-4415 putative non-ribosomal peptide synthetase *Nocardia farcinica* IFM 10152 Phenyloxazoline synthase MbtB (phenyloxazoline synthetase) *Mycobacterium tuberculosis* H37Rv	92.97/99 59.41/98 57.2/99 53.12/99 48.89/99	WP_173091715 EFL06864 AGE11891 BAD55613 CCP45171
RB99_01641 Ferric enterobactin transport system permease protein FepG	338	ACTIVE_0099 F9B16_RS23830 E1285_RS43350 AMYAL_RS0130245 SSMG_02544 gobO	iron-siderophore uptake system transmembrane protein *Actinomadura verrucosospora* iron chelate uptake ABC transporter family permease subunit *Actinomadura montaniterrae* iron chelate uptake ABC transporter family permease subunit *Actinomadura* sp. 7K507 iron chelate uptake ABC transporter family permease subunit *Amycolatopsis alba* predicted protein *Streptomyces* sp. AA4 (amychelin cluster) ABC transporter *Streptomyces* sp. NRRL F-4415	94.97/100 95.85/99 85.67/99 51.83/97 51.16/93 47.51/88	QKG18465 WP_151542338 WP_132160734 WP_039795885 EFL06873 AGE11896.1
RB99_01642 Ferric enterobactin transport system permease protein FepD	353	F8568_RS34325 F9B16_RS23835 ACTIVE_0098 AMYAL_RS0130240 SSMG_02543 gobP	iron chelate uptake ABC transporter family permease subunit *Actinomadura* sp. LD22 iron chelate uptake ABC transporter family permease subunit *Actinomadura montaniterrae* Fe3+-siderophore ABC transporter permease *Actinomadura verrucosospora* iron chelate uptake ABC transporter family permease subunit *Amycolatopsis alba* predicted protein *Streptomyces* sp. AA4 (amychelin cluster) iron siderophore transporter *Streptomyces* sp. NRRL F-4415	92.9/99 92.35/99 91.78/100 60.84/87 56.97/91 52.6/86	WP_151597222 WP_151542348 QKG18464 WP_020635025 EFL06872 AGE11897
RB99_01643 HTH-type transcriptional repressor AcnR	230	ACTIVE_0097 F9B16_RS23840 F8568_RS34330	TetR family transcriptional regulator *Actinomadura verrucosospora* TetR family transcriptional regulator *Actinomadura montaniterrae* TetR family transcriptional regulator *Actinomadura* sp. LD22	90.74/193 87.33/93 87.78/93	QKG18463 WP_151542349 WP_151597221
RB99_01644 Daunorubicin/doxorubicin resistance ATP-binding protein DrrA	305	ACTIVE_0096 F8568_RS34335 DTB52_RS20675 tsn16 slnTI F583_RS0124810	ATP-binding cassette domain-containing protein *Actinomadura verrucosospora* ATP-binding cassette domain-containing protein *Actinomadura* sp. LD22 ABC transporter ATP-binding protein *Actinomadura madurae* putative ABC transporter, ATP binding component *Streptomyces longisporoflavus* putative ABC transporter ATP-binding protein *Streptomyces albus* ABC transporter ATP-binding protein *Salinispora arenicola*	94.75/100 93.11/100 90.17/96 68.71/96 67.01/94 59.46/98	WP_173091711 WP_151597190 WP_021599067 ACR50788 AEZ53959 WP_019032750
RB99_01645 hypothetical protein	545	F9B16_RS23850 F8568_RS34340 ACTIVE_0095 tsn15 slnTII	ABC transporter permease *Actinomadura montaniterrae* ABC transporter permease *Actinomadura* sp. LD22 ABC transporter permease *Actinomadura verrucosospora* putative ABC transporter, membrane spanning protein *Streptomyces longisporoflavus* putative antibiotic ABC transporter efflux pump *Streptomyces albus*	93.21/100 89.91/100 88.07/100 44.25/93 45.72/96	WP_151542340 WP_151597189 WP_173091709 ACR50787 AEZ53960
RB99_01646 hypothetical protein	48	ACTIVE_0094 E1293_RS47630 F4557_003456	hypothetical protein *Actinomadura verrucosospora* hypothetical protein *Actinomadura darangshiensis* hypothetical protein *Actinomadura catellatispora*	93.75/100 81.25/100 86.67/93	WP_173091707 WP_165978368 MBB4775038
RB99_01647 Toluene-4-sulfonate monooxygenase system iron-sulfur subunit TsaM1	340	F9B16_RS23855 ACTIVE_0093 F8568_RS34345 ORF14 BamIOP4010DRAFT_038 1	aromatic ring-hydroxylating dioxygenase subunit alpha *Actinomadura montaniterrae* Rieske 2Fe-2S domain-containing protein *Actinomadura verrucosospora* Rieske 2Fe-2S domain-containing protein *Actinomadura* sp. LD22 putative methylase *Streptomyces cinnabarigriseus* Rieske (2Fe-2S) domain protein *Burkholderia ambifaria* IOP40-10	94.71/100 94.12/100 94.41/100 41.19/98 35.21/98	WP_151542341 WP_173091705 WP_151597188 CBW54656 EDT06079
RB99_01648 Transcriptional regulator KdgR	281	F9B16_RS23860 F8568_RS34350 ACTIVE_0092 schA27 nbrR5 orf7	helix-turn-helix domain-containing protein *Actinomadura montaniterrae* helix-turn-helix domain-containing protein *Actinomadura* sp. LD22 helix-turn-helix domain-containing protein *Actinomadura verrucosospora* putative transcriptional regulator *Streptomyces* sp. SCC 2136 IclR family transcriptional regulator *Nocardia terpenica* transcriptional regulator *Streptomyces galbus*	92.88/100 90.39/100 91.76/95 60.17/85 32.18/71 31.3/94	WP_151542342 WP_151597220 WP_173091703 CAH10127 AJO72706 ADE22342
RB99_01649 Transcriptional repressor PaaX	319	F9B16_RS23865 F8568_RS34355 ACTIVE_0091	PaaX family transcriptional regulator *Actinomadura montaniterrae* PaaX family transcriptional regulator *Actinomadura* sp. LD22 PaaX family transcriptional regulator *Actinomadura verrucosospora*	93.35/80 93.41/80 89.53/92	WP_151542350 WP_151597219 WP_173091701

		schA31	phenyl acetic acid responsive transcriptional repressor *Streptomyces* sp. SCC 2136	54.83/80	CAH10131.1
RB99_01650 HTH-type transcriptional regulator BetI	206	F9B16_RS23870 ACTIVE_0090 F8568_RS34360 cmxK	TetR family transcriptional regulator *Actinomadura montaniterrae* TetR family transcriptional regulator *Actinomadura verrucosospora* TetR family transcriptional regulator *Actinomadura* sp. LD22 TetR family transcriptional regulator *Myxococcus* sp.	98.53/99 96.60/100 97.07/99 40.1/95	WP_151542343 WP_173091699 WP_151597187 AXM43066
RB99_01651 Oxygen sensor histidine kinase NreB	585	F8568_RS34365 ACTIVE_0088 E1266_RS27640 DTB52_RS20610	sensor histidine kinase *Actinomadura* sp. LD22 sensor histidine kinase *Actinomadura verrucosospora* sensor histidine kinase *Actinomadura* sp. 7K534 sensor histidine kinase *ctinomadura madurae*	88.21/100 88.10/99 72.6/99 42.21/59	WP_151597186 WP_173091695 WP_111831483 ACN29724.1
RB99_01652 Oxygen regulatory protein NreC	224	F9B16_RS48755 F8568_RS34370 AL2_RS24065 MG459168.1:6235..6891 cal2 regC	response regulator *Actinomadura montaniterrae* response regulator *Actinomadura* sp. LD22 response regulator transcription factor *Actinomadura latina* LuxR family DNA-binding response regulator *Streptomyces* sp. ID38640 Cal2 *Streptomyces calvus* regulatory protein C *Actinoplanes friuliensis*	98.21/100 95.98/100 92.86/100 46.61/98 45.91/98 44.95/97	WP_151547073 WP_151597185 WP_067637201 AVV61976.1 ALG65334.1 CAM56776
RB99_01653 Oxygen sensor histidine kinase NreB	622	F9B16_RS48760 ACTIVE_0086 F8568_RS34375 orf26 cal1 regD	hypothetical protein *Actinomadura montaniterrae* signal transduction histidine kinase *Actinomadura verrucosospora* hypothetical protein *Actinomadura* sp. LD22 two-component system sensor kinase *Nonomuraea longicatena* Cal1 *Streptomyces calvus* regulatory protein D *Actinoplanes friuliensis*	94.28/97 90.59/96 90.76/96 38.58/50 35.07/46 33.33/42	WP_151547074 QKG18452 WP_151597184 ACN29724 ALG65335 CAM56777
RB99_01654 Lactose operon repressor	362	F8568_RS34380 F9B16_RS48765 ACTIVE_0085 chaR3 purR Orf(-10)	substrate-binding domain-containing protein *Actinomadura* sp. LD22 substrate-binding domain-containing protein *Actinomadura montaniterrae* LacI family transcriptional regulator *Actinomadura verrucosospora* ChaR3 protein *Streptomyces chartreusis* LacI transcriptional regulator *Micromonospora chalcea* subsp. *Izumensis* LacI family transcriptional regulator *Streptomyces* sp. SCSIO 03032	98.2/92 97.6/92 97.2/88 52.35/82 49.85/93 53.89/59	WP_151597218 WP_151547077 QKG18451 CAH10185 ARW71474 ARP51731
RB99_01655 D-galactonate dehydratase	383	F9B16_RS48770 ACTIVE_0084 F8568_RS34385 F8566_RS12900 orf1178 orf41 sccontig008-48	mandelate racemase/muconate lactonizing enzyme family protein *Actinomadura montaniterrae* mandelate racemase/muconate lactonizing enzyme family protein *Actinomadura verrucosospora* mandelate racemase/muconate lactonizing enzyme family protein *Actinomadura* sp. LD22 mandelate racemase/muconate lactonizing enzyme family protein *Actinomadura rudentiformis* putative dehydratase *Streptomyces kanamyceticus* isomerase *Streptomyces nanchangensis* mandelate racemase/muconate lactonizing protein *Streptomyces chromofuscus*	97.65/100 96.61/100 96.87/100 85.22/98 76.34/96 28.85/90 28.01/95	WP_151547075 WP_173091689 WP_151597183 WP_151560418 BAE95592 ADC45557 AEZ64556
RB99_01656 2-deoxy-scyllo-inosamine dehydrogenase	344	F8568_RS30715 ACTIVE_0083 F8566_RS12895 kanT aprE live	alcohol dehydrogenase catalytic domain-containing protein *Actinomadura* sp. LD22 alcohol dehydrogenase GroES domain-containing protein *Actinomadura verrucosospora* alcohol dehydrogenase catalytic domain-containing protein *Actinomadura rudentiformis* putative dehydrogenase *Streptomyces kanamyceticus* putative 3-amino-2,3-dideoxy-scyllo-inositol 1 dehydrogenase *Streptoalloteichus hindustanus* putative 3-amino-2,3-dideoxy-scyllo-inositol 1-dehydrogenase *Streptomyces lividus*	93.60/100 95.06/100 77.95/96 58.13/96 38.15/91 38.39/94	WP_151597182 QKG18449 WP_151560417 BAE95593 CAI47653 CAG38695

15. References

[1] Harada K.-i., Tomita K, Fujii K, Masuda K, Mikami Y, Yazawa K, Komaki H, Isolation and structural characterization of siderophores, madurastatins, produced by a pathogenic Actinomadura madurae. *The Journal of antibiotics* **2004;***57*:125-135.

DOI: 10.7164/antibiotics.57.125

[2] Tsugawa H, Kind T, Nakabayashi R, Yukihira D, Tanaka W, Cajka T, Saito K, Fiehn O, Arita M, Hydrogen rearrangement rules: computational MS/MS fragmentation and structure elucidation using MS-FINDER software. *Analytical chemistry* **2016;***88:*7946-7958.

DOI: 10.1021/acs.analchem.6b00770

[3] Jung WH, Sham A, Lian T, Singh A, Kosman DJ, Kronstad JW. Iron source preference and regulation of iron uptake in Cryptococcus neoformans. *PLoS Pathog.* 2008;**4:**e45.

[4] Jung WH, Hu G, Kuo W, Kronstad JW. Role of ferroxidases in iron uptake and virulence of Cryptococcus neoformans. *Eukaryot Cell.* 2009;**8:**1511-1520.

[5] Wiebe C, Winkelmann G. Kinetic studies on the specificity of chelate-iron uptake in Aspergillus. *J Bacteriol.* 1975;**123:**837-842.

[6] Raymond-Bouchard I, Carroll CS, Nesbitt JR, Henry KA, Pinto LJ, Moinzadeh M, *et al.* Structural requirements for the activity of the MirB ferrisiderophore transporter of Aspergillus fumigatus. *Eukaryot Cell.* 2012;11:1333-1344.

[7] Wayne P. Reference method for broth dilution antifungal susceptibility testing of yeasts, approved standard. *CLSI document M27-A2.* 2002.

[8] Larkin MA, Blackshields G, Brown NP, Chenna R, McGettigan PA, McWilliam H, Valentin F, Wallace IM, Wilm A, Lopez R, Thompson JD, Gibson TJ, Higgins DG, Clustal W and Clustal X version 2.0. *Bioinformatics* **2007;**23:2947-2948.

DOI: 10.1093/bioinformatics/btm404

[9] Price MN, Dehal PS, Arkin AP, FastTree 2–approximately maximum-likelihood trees for large alignments. *PloS one* **2010;**5:e9490.

DOI: 10.1371/journal.pone.0009490

[10] Afgan E, Baker D, Batut B, van den Beek M, Bouvier D, Čech M, Chilton J, Clements D, Coraor N, Grüning BA, Guerler A, Hillman-Jackson J, Hiltemann S, Jalili V, Rasche H, Soranzo N, Goecks J, Taylor J, Nekrutenko A, Blankenberg D, The Galaxy platform for accessible, reproducible and collaborative biomedical analyses: 2018 update. *Nucleic Acids Research* **2018;**46:W537-W544.

DOI: 10.1093/nar/gky379

[11] Blin K, Shaw S, Kautsar SA, Medema MH, Weber T, The antiSMASH database version 3: increased taxonomic coverage and new query features for modular enzymes. *Nucleic Acids Research* **2020**,49:D639-D643.

DOI: 10.1093/nar/gkaa978

[12] Letunic I, Bork P. Interactive Tree Of Life (iTOL) v5: an online tool for phylogenetic tree display and annotation. *Nucleic Acids Research* **2021;**49:W293-W296.

DOI: 10.1093/nar/gkab301

[13] Röttig, M.; Medema, M. H.; Blin, K.; Weber, T.; Rausch, C.; Kohlbacher, O., NRPSpredictor2—a web server for predicting NRPS adenylation domain specificity. *Nucleic Acids Research* **2011;** *39*: W362-W367.

DOI: 10.1093/nar/gkr323